UNIVERSIDAD NACIONAL AUTÓNOMA DE MÉXICO

PROGRAMA DE MAESTRÍA Y DOCTORADO EN INGENIERÍA
ENERGÍA – SISTEMAS ENERGÉTICOS

CONTRIBUTION TO THE NEUTRONIC ANALYSIS OF BREED AND BURN REACTORS

TESIS
QUE PARA OPTAR POR EL GRADO DE:
MAESTRO EN INGENIERÍA

PRESENTA:
ELÍAS YAMMIR GARCÍA CERVANTES

TUTOR PRINCIPAL
DR. JUAN LUIS FRANÇOIS LACOUTURE, FI-UNAM

MÉXICO, D. F. MAYO 2016

JURADO ASIGNADO:

Presidente:	Dra. Pamela Fran Nelson Edelstein
Secretario:	Dr. Gilberto Espinosa Paredes
Vocal:	Dr. Juan Luis François Lacouture
1 er. Suplente:	Dra. Cecilia Martín del Campo Márquez
2 d o. Suplente:	Dr. Alejandro Núñez Carrera

Lugar o lugares donde se realizó la tesis: CIUDAD DE MÉXICO

TUTOR DE TESIS:

Juan Luis François Lacouture

FIRMA

(Seg u n d a ho j a)

Abstract

The relation between greenhouse emissions and climate change represents a challenge in environmental terms, since an increase in global temperature would have a fatal and irreversible impact on humanity. In this study nuclear power is considered to be part of the solution for the required energy mix due to its low greenhouse emissions and its great advantages over the other technologies.

Specifically the sodium-cooled fast reactors have a fundamental role in nuclear power development, therefore these research programs are briefly discussed to understand the context of these experimental reactors. Future designs performance and safety are also shown.

Added to this, the operation of the sodium-cooled fast reactors could meet the energy demand through the breed and burn philosophy. That is, breeding enough fissile material inside the reactor and burning a quantity of this material avoid the transportation and reprocessing steps in the nuclear fuel cycle, which would simplify largely the back end in the nuclear fuel cycle.

The objective of the current study is to extend the operation of the Advanced Sodium Technological Reactor for Industrial Demonstration (ASTRID) design through a breed and burn strategy named reshuffling without refueling, which would have an impact in economic terms and would maximize fuel utilization. To accomplish this objective an ASTRID-like model is developed in MCNP6 and validated with the existing literature, comparing the reactivity at end of cycle, Doppler constants and sodium void worth. For these three neutronic parameters the results were positive, which led to the conclusion that the developed ASTRID-like model was consistent with the information provided by referenced literature.

A proposed metallic-fueled ASTRID-like reactor is compared with the oxide-fueled design; the first one has more advantages, such as less enrichment required, less reactivity at beginning of cycle and better breeding performance during the simulation.

Finally, in order to extend the operation of the ASTRID design operation, two different reshuffling schemes are analyzed for the ASTRID-like developed models (oxide and metallic). By swapping different zones in the reactor it is found that the reactivity in all models could increase after reshuffling. Specifically it was found that for the oxide-fueled models an operation extension of 1170 days could be achieved, while for the metallic-fueled designs could operate for 2255 days without refueling. In all cases the amount of ^{239}Pu increases, which means that the reactor breeds more than what it consumes, and since the metallic-fueled models have better breeding performance (they bred 66% more than the oxide design), they could operate during longer periods, which was corroborated by the reactor simulations.

It can be concluded that the objective was successfully accomplished since the ASTRID-like design was satisfactorily validated and the reshuffling schemes proved that the extension of the reactor operation could be achieved in all the simulated cases.

Resumen

La relación entre las emisiones de gases de efecto invernadero y el cambio climático representa un reto ambiental, ya que un incremento en la temperatura global tendría un impacto fatal e irreversible para la humanidad. En este estudio se considera a la energía nuclear como parte de la solución para el abastecimiento energético debido a sus prácticamente nulas emisiones de efecto invernadero y a sus ventajas con respecto a otras tecnologías.

Específicamente, los reactores rápidos refrigerados por sodio tienen un papel fundamental en el desarrollo de la energía nuclear, por lo tanto, se presenta una breve descripción de los programas de investigación existentes con el propósito de comprender el contexto de estos reactores experimentales. También se presentan los diseños proyectados al futuro, cuyas características en desempeño y seguridad serán considerablemente mejoradas.

Sumado a esto, la operación de los reactores refrigerados por sodio pueden atender la demanda energética mediante la filosofía de operación de los reactores de quema y cría, que consiste en la cría de suficiente material físil dentro del reactor y quemar una fracción de este material, eliminando los procesos de transportación y reprocesamiento en el ciclo de combustible nuclear, lo que simplificaría en gran medida la parte final del ciclo de combustible nuclear.

El objetivo del presente estudio es extender la operación del reactor ASTRID mediante una estrategia de quema y cría llamada reacomodos sin recarga de combustible, lo que tendría un impacto favorable económicamente e incrementaría la utilización del combustible. Para cumplir con este objetivo, un modelo tipo ASTRID fue desarrollado en MCNP6 para ser validado con la literatura existente, comparando la reactividad al final del ciclo, las constantes Doppler, y el coeficiente por vacíos del refrigerante. Para estos tres parámetros neutrónicos los resultados obtenidos fueron positivos, lo que llevó a la conclusión de que el modelo desarrollado de ASTRID es consistente con la información encontrada en el la literatura de referencia.

Posteriormente, un modelo con combustible metálico de ASTRID es propuesto y comparado con el diseño óxido, teniendo mayores ventajas el primero de éstos, tal como menor enriquecimiento requerido, menor reactividad al inicio del ciclo y mejor desempeño en la cría de combustible durante la simulación.

Finalmente, con el fin de extender la operación del reactor ASTRID, dos esquemas de reacomodos distintos son analizados para los diseños de ASTRID desarrollados (óxido y metálico). Al intercambiar distintas zonas del reactor se observa que la reactividad en todos los modelos podría incrementar después de los reacomodos, y específicamente para los modelos con combustible óxido una extensión de 1170 días podría ser alcanzada, mientras para los casos metálicos podría operar hasta por 2255 días sin recarga de combustible. En todos los casos la cantidad de ^{239}Pu se incrementa, lo que significa que el reactor cría más de lo que consume, y dado que los casos metálicos tienen mejor cría (logró criar 66% más que el caso óxido), los rectores podrían permanecer en operación durante periodos más largos, lo que fue corroborado en las simulaciones.

Puede concluirse que el objetivo fue satisfactoriamente cumplido dado que el diseño del reactor tipo ASTRID fue exitosamente validado y los esquemas de reacomodo probaron que la extensión de la operación del reactor podría lograrse en todos las simulaciones realizadas.

Contents

List of Figures

List of Tables

1. INTRODUCTION

The strong relation between society wellbeing and energy availability implies the development of a strategic plan from which a social benefit could be obtained. Besides, climate change represents a challenge in environmental terms, since an increase in global temperature would have a fatal and irreversible impact in humanity.

During years the energy supply has been given by an energy mix in which oil, coal and natural gas have remained majority for decades. Figure 1.1 shows the world total energy supply by fuel from 1971 to 2013. The world total primary energy supply has increased to more than double since 1973, which increases proportionally the greenhouse emissions (International Energy Agency, 2015). It can also be seen that, despite oil technology reduced its contribution 15% in this period, coal and natural gas gained participation in this energy supply mix.

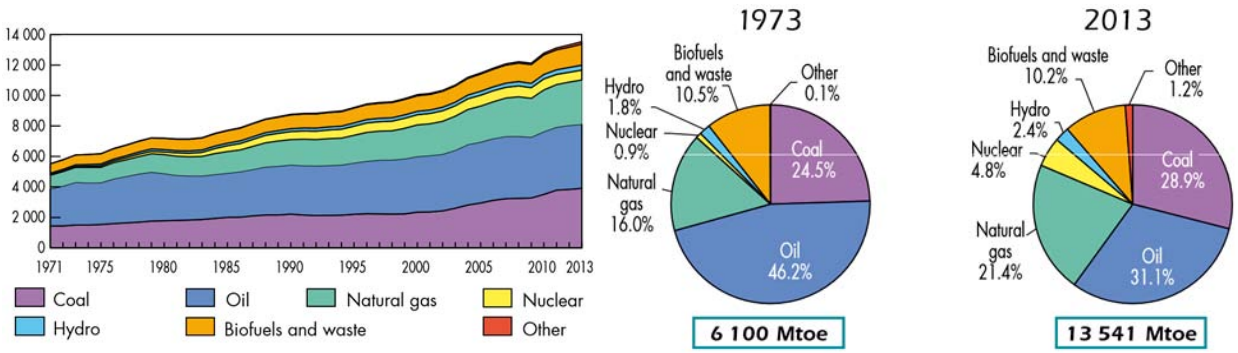

FIGURE 1.1. World total primary energy supply by fuel in Mtoe (left) and shares of these (right) from 1971 to 2013 (International Energy Agency, 2015)

Since most of today's energy comes from fossil fuel sources of energy, waste products are released directly into the air and many of these are greenhouse gases, such that in 2011 CO_2 emissions were 7992 million tons (World Nuclear Association, 2013). Consequences of greenhouse gases are clear; eleven of the twelve years from 1995-2006 rank among the 12 warmest years in the instrumental record of global surface temperature (World Nuclear Association, 2014).

Low carbon dioxide emissions technologies are required in order to limit the climate change and its strong consequences. Although renewable energies are considered as green and environmentally friendly energies, they present disadvantages like the intermittence while producing electricity, plus the non-negligible amount of CO_2 emissions, specifically for the solar technologies. Renewable energies are being developed and researched in order to increase the benefit obtained through these and as a consequence, attain a greater impact on the energy supply mix. Considering this, nuclear power could take place in the energy supply need, because of its low greenhouse emissions and its great advantages compared with other technologies.

In Figure 1.2 it is shown the range of total greenhouse emissions from electricity production chains, in which as expected, fossil fuel sources of energy emit greater amounts of greenhouse gases than the other technologies, whereas nuclear power ranks the lowest greenhouse emitter.

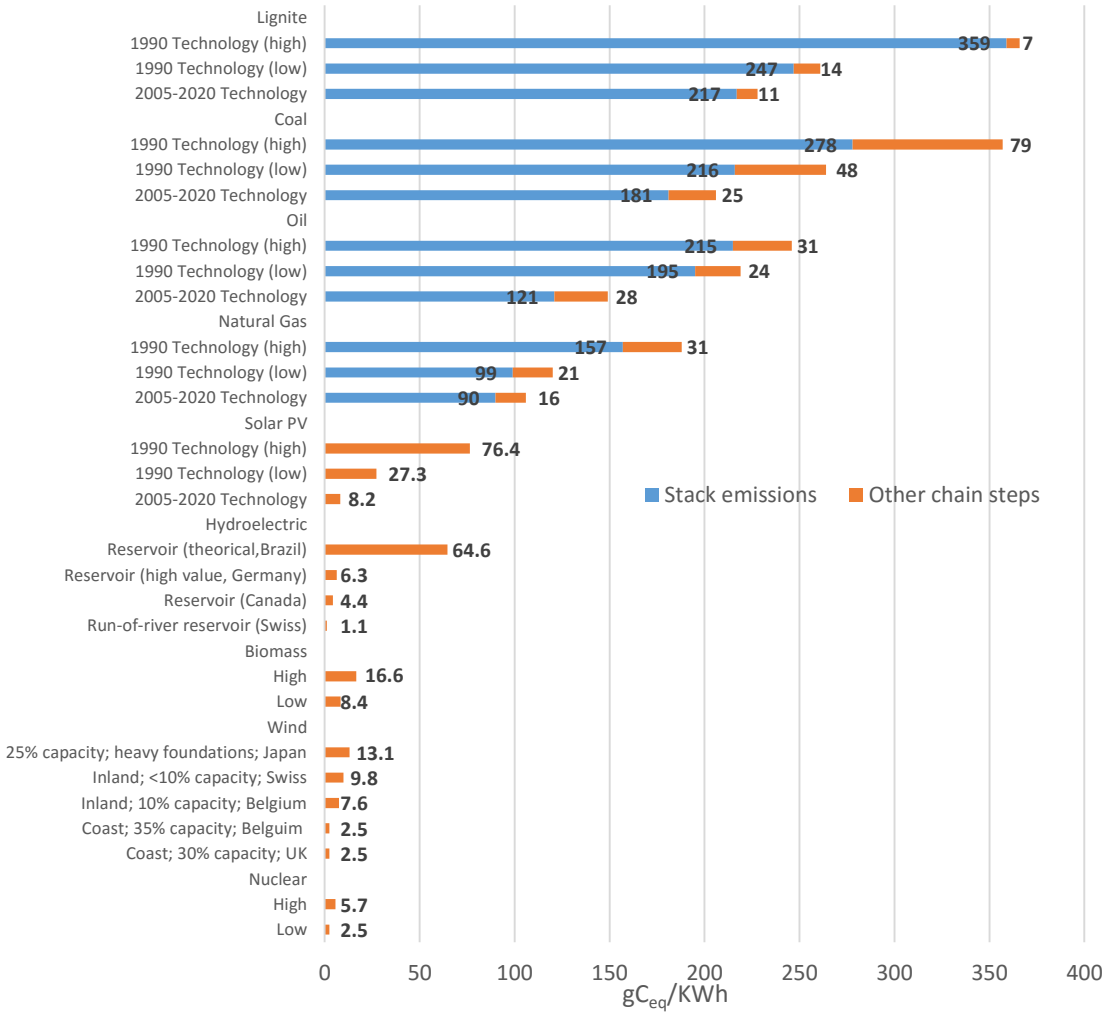

FIGURE 1.2. Range of total greenhouse gas emissions form electricity production chains (Rogner, 2014)

Nuclear technology is preparing a new generation of reactors with designs that incorporate passive safety features and can be also used to distil salt water or hydrogen production (GEN IV International Forum, 2013). It is expected that by 2030's new generation of reactors will be operating: the Generation IV (GEN IV).

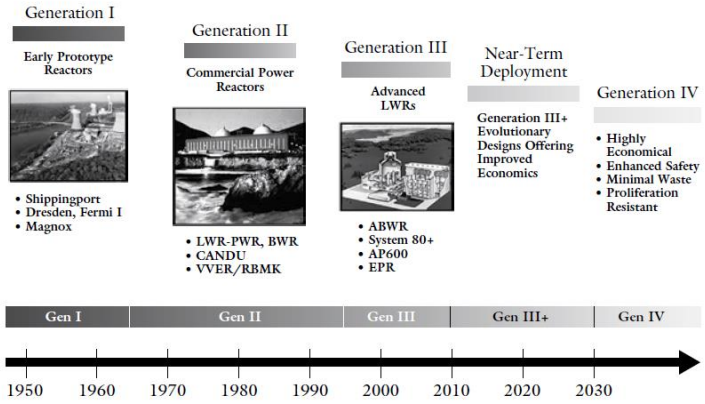

FIGURE 1.3. Evolution of Nuclear power (M. Goldberg & Rosner, 2011).

One of the Gen IV systems chosen to be developed is the "Sodium-cooled Fast Reactor (SFR)" (World Nuclear Association, 2015) that has been developed for decades since 1950's. Unlike the vast majority of reactors currently in operation or in construction worldwide, using only about 1% of natural uranium, sodium fast reactors are able to use more than 80% of the uranium resource. For instance, the current stockpile of depleted uranium available on French territory could feed the needs for electricity production at current rate for thousands of years (Gauché, 2012).

One of the research reactors based on sodium technology is the Advanced Sodium Technological Reactor for Industrial Demonstration (ASTRID), developed in France. The main goals of the ASTRID concept is to demonstrate the operability of an industrial SFR, develop a transmutation program in order to limit the nuclear waste and enhance the safety margins compared to the Gen III reactors.

On the other hand, breed and burn nuclear reactors provide a great pathway for nuclear energy for its simple nuclear fuel cycle and its outstanding operation characteristics. Fuel utilization in sodium fast reactors could be considerably increased due to its different fuel management during its operation, which directly extends the operation of the reactor.

This study is focused in the ASTRID reactor, hence an analysis of its characteristics and neutronic properties is developed through the MCNP6 nuclear code. A particular interest on this study is to develop a breed and burn reshuffling scheme in order to extend the operation of the ASTRID reactor. In summary, the present work is summarized in the following paragraphs:

Chapter 2 describes the Sodium-cooled Fast Reactors and its characteristics. The historical experimental reactors are also presented in this section through the different country irradiation programs, and finally the reactors under development are described.

In chapter 3 the breed and burn nuclear concept essential characteristics are shown, as well the history of the concept and the different B&B research programs, including a brief description of the existing prototypes.

The Monte Carlo method is stated in the chapter 4, in which its methodology is defined as well as its application to this work in the neutron transport equation. Furthermore, the Monte Carlo Nuclear Particle 6 (MCNP6) nuclear code is described, as well as its main capabilities.

The ASTRID-like developed model is validated with the existing literature in the chapter 5, presenting three different neutronic parameters (Keff at End of Cycle, Doppler constants and coolant void worths). In this section a proposed metallic-fueled ASTRID-like is analyzed and compared with the oxide-fueled design.

Chapter 6 describes the proposed reshuffling strategies for the ASTRID model. The obtained results are shown and analyzed, achieving the extension of the reactor's operation for a considerable period of time.

Chapter 7 presents the results analysis and the conclusions on the research, describing the obtained results for the ASTRID-like reactor validation and the studied reshuffling schemes in the developed models.

The chapter 8 presents the used bibliography in the whole research, having papers, book, conferences and reports in this sections.

The last section in this work is an appendix, in which a developed code is presented, which was very useful for the elaboration of the Actinide Inventory. The code was developed in Matlab and requires of two files, “times.txt and Nuclides.txt” in which the required time steps for the Actinide Inventory should be provided as well as the desired isotopes in the Actinide Inventory. This code is able to provide the concentration of the desired isotopes at different time steps and it takes less than 10 seconds to process more than 20000 output lines.

2. SODIUM COOLED REACTORS

Liquid Metal Fast Breeder Reactors (LMFBR) have special characteristics that can be exploited in favor of nuclear power. As its name specify, a LMFBR is cooled by a liquid metal, which could be sodium, lead or mercury. Early prototypes and experimental projects were carried on with these metal elements, and results proved a considerable advantages for nuclear power.

Sodium cooled reactors are of special interests because of the physical properties of this liquid metal, which makes it a better choice compared with the mercury and lead. This chapter discusses the sodium reactor main characteristics, history and future programs related to these reactors.

2.1. Sodium-cooled Fast Reactors description

The fundamental reaction from which heat is obtained in a Sodium-cooled Fast Reactors (SFR) is the nuclear fission. First discovered by Otto Hahn and Fritz Strassmann in 1939 (Murray & Holbert, 2015), the nuclear fission consist in the absorption of an incident neutron in a transient nucleus that eventually decays by splitting the nuclide into lighter nuclei called fission products.

In order to split the nuclide of an element a specific energy is required, called the binding energy, which is a measure between the difference of the mass nucleus and the individual masses of the protons and neutrons that constitute it. A quantity of energy of about 210 MeV is released per fission. Table 1 shows the partial amounts that constitute the energy released per fission.

TABLE 1. Energy partial amounts per nuclear fission (European Nuclear Society, 2003).

Energy partial amounts	**Emitted energy (MeV)**
Kinetic energy of fission products	175
Kinetic energy of fission neutrons	5
Energy of the gamma radiation during fission	7
Energy of beta and gamma radiation during decay of radioactive fission products	13
Energy of neutrinos	10
Total	210

In a nuclear reactor a chain reaction can be sustained, since during the fission process a quantity of neutrons is released, being these available to produce another fission in other nuclides. Depending on the neutron energy and the nuclide, different quantity of neutrons are emitted as shown in Figure 2.1

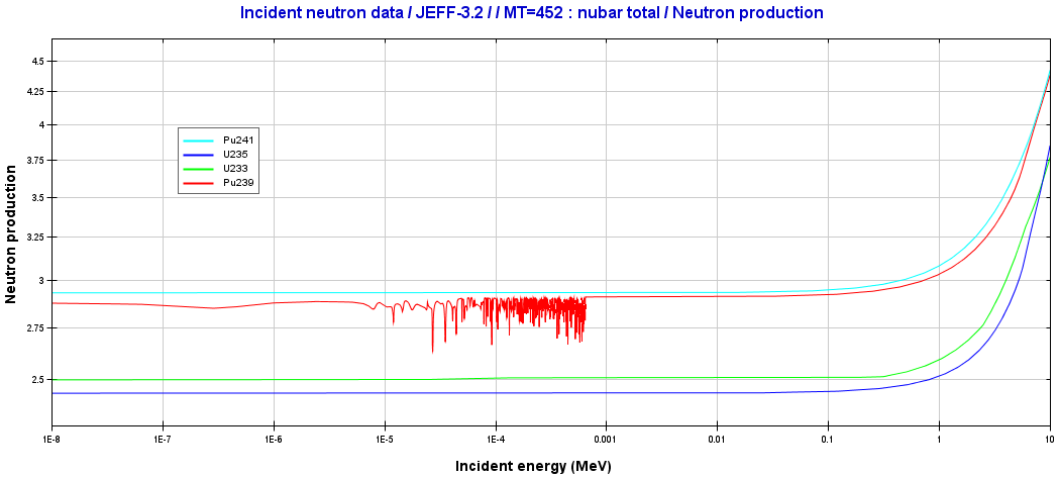

FIGURE 2.1. ν_T, average total (prompt and delayed) number of neutrons released per fission event for ^{233}U, ^{235}U, ^{239}Pu and ^{241}Pu

The neutrons are the essential component in a nuclear reactor, having these different interactions in a SFR. For instance, the elastic and inelastic scattering have a considerable impact in the reactor physics. In an inelastic scattering reaction, the incident neutron is first absorbed by the nucleus to form a compound nucleus, which eventually decays by reemitting a neutron and leaving the nuclide in an excited state. The elastic scattering involves first the absorption of the incident neutron, followed by the reemission of the neutron with the target nucleus returning to its ground state. In contrast to the inelastic scattering, the kinetic energy is conserved in elastic events *(Duderstadt & Hamilton, 1976)*.

Generally in each collision the neutron energy decreases, although if this energy is small enough, the upscattering phenomena may be presented, which is the gain of neutron kinetic energy through these collisions. Depending the collided nuclide, a different energy loss is presented; Table 2 presents the different slowing down power for different elements.

TABLE 2. Slowing-down properties of major constituent materials of SFR (Yang, 2011).

	Scattering cross sections, σ_s (b)	**Atom density $\left(\frac{1}{barn \cdot cm}\right)$**	**Slowing down power $\xi\Sigma_s$ (cm^{-1})**
TRU	4.0	3.2E-03	1.1E-04
U	5.6	5.6E-03	2.7E-04
Zr	8.1	2.6E-03	4.6E-04
Fe	3.4	1.9E-02	2.3E-03
Na	3.8	8.2E-03	2.7E-03
O	3.6	1.4E-02	5.8E-03
H	11.9	2.9E-02	3.5E-01

Through scattering, moderation can be achieved in a nuclear reactor, such as in the light water reactors (LWR), in which water (H_2O) is the moderator and the coolant at the same time. Sodium, due its thermal and neutronic properties, is a good coolant but not a good moderator as seen in Table 2. Added to the sodium neutronic properties, the absence of a moderator element in a SFR permit a meager moderation of the neutrons in the nuclear reactor, reason why fast spectrum reactions can be achieved.

Hence, the neutron spectrum depends mainly on the neutronic properties of the coolant, the structural material and the matrix fuel. Figure 2.2 presents a comparison between neutron spectra corresponding to a SFR and a pressurized water reactor (PWR). Since a PWR is a thermal nuclear reactor, its neutron spectrum tends to increase in the interval between 1E-02 and 2E-01 eV, unlike a SFR in which its neutron spectrum is located in the interval between the 1E+04 to 1E+07 eV.

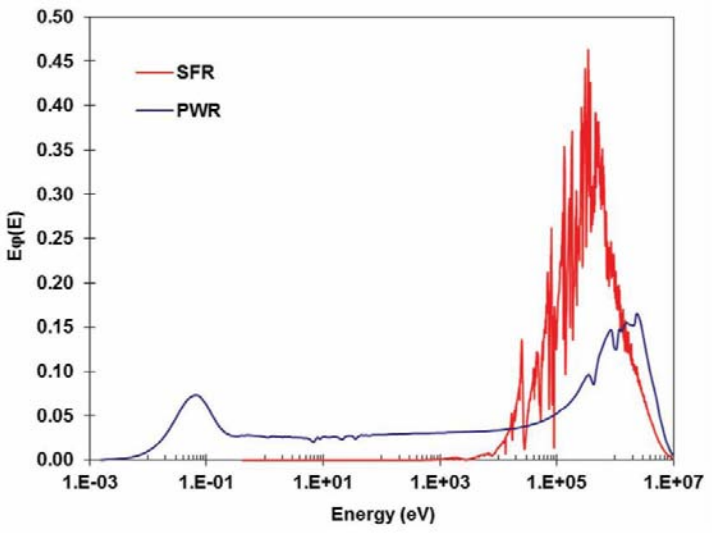

FIGURE 2.2. Neutron Flux Spectra of Thermal (PWR) and Fast (SFR) Reactors *(Yang, 2011)*

Another important reaction is radiative capture, since it removes neutrons from the chain reaction. In this reaction the incident neutron is first absorbed by a nucleus to form a compound nucleus of mass number A+1, and then this nucleus decays by emitting a cascade of high-energy gammas (Duderstadt & Hamilton, 1976).

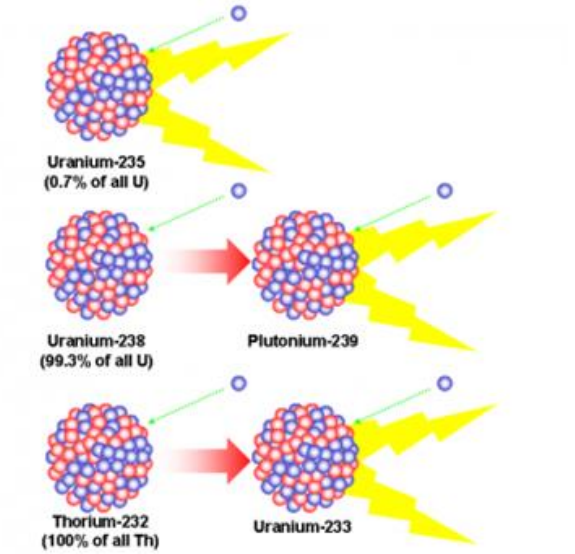

FIGURE 2.3. Breeding nuclear reactions (Sorensen, 2011)

Through this reaction the transmutation of elements can be done, since in every fission there is a release of more than one neutron, therefore the emitted neutrons besides of producing other fissions and maintain the chain reaction, can be absorbed by fertile nuclei causing them to transmute into a higher isotope. A great capability of the SFRs, related to the fast neutron spectrum, is the breeding conversion of the fertile material into fissile material, such as the conversion of ^{238}U to ^{239}Pu or ^{232}Th to ^{233}U. A good management of fertile and fissile materials, through a successful breeding program would extend the energy provided by the uranium fuel reserves for thousands of years (Gauché, 2012).

Although there are different reactions in a SFR, the breeding process has a particular role in these reactors, since taking advantage of this process it may enhance the fuel utilization with breed and burn operation, as it will be described in chapter 3.

There are different kinds of nuclear fuels that enable breeding at different ratios, depending on its neutronic characteristics. One of the most common fuel in nuclear power is the oxide nuclear fuel which consists on a sintered pellet (ceramic) of Uranium or Mixed-Oxide fuel. The containing matrix in this fuel is de oxygen, and as a consequence an intrinsic neutron moderation of neutrons reduces the spectrum energy. Irradiation experience has been gained in the Fast Flux Test Facility (FFTF) and in international experimental reactors in France, Russia and Japan (Basak, 2009).

Metallic nuclear fuel is another type of nuclear fuel that has been under research for decades mainly in the US with the EBR-II and FFTF. Binary (U-Zr) or ternary (U-Pu-Zr) metal-alloy full-length slugs are manufactured where zirconium is the fuel matrix, which enables a harder spectrum in a SFR (Basak, 2009). Nitride and Carbide are other nuclear fuels that have less irradiation experience, but remain active in experimental irradiation programs. A brief description of the advantages and disadvantages of nuclear fuels are presented in table 3.

TABLE 3. Nuclear fuel advantages and disadvantages for SFRs *(Basak, 2009)*.

Fuel	Advantages	Disadvantages
Oxide	- Proven burnup >25 at % - Industrial scale fabrication & irradiation experience. - High melting temperature. - Good stability at high temperature for TRU	- Poor thermal conductivity. - Powder processing route of fuel fabrication is associated to the problem of radio toxic dust hazard. - Intrinsic moderation of neutrons.
Metallic	- Hard spectrum - High thermal conductivity - Proven to 20 at % in EBR-II - Simplified fabrication, involving melting and casting, avoiding the problem of radiotoxic dust hazard.	- Low melting temperature. - Volatility of Am. - Large swelling rate requires large sodium bonded pellet clad gap. - Alpha contaminated Na waste.
Carbide	- Hard spectrum. - High thermal conductivity. - Proven to 18 at %	- Pyrophoric (must be handled and fabricated in inert gas atmosphere). - Powder processing route of fuel fabrication is associated to the problem of radio toxic dust hazard. - High vapor pressure of AmC (vaporizes at <1500 K)
Nitride	- Hard spectrum. - High thermal conductivity. - Test fuel pins have demonstrated proven burn up of 20 at % - High solubility rate in nitric acid.	- Pyrophoric (must be handled and fabricated in inert gas atmosphere). - Powder processing route of fuel fabrication is associated to the problem of radio toxic dust hazard. - Larger pellet clad mechanical interaction. - Production of ^{14}C. - To avoid dissociation of AmN, temperature of fuel fabrication should be below 1800 K

In a SFR there are different components that constitute the reactor. The basic element on it is the fuel pin, which is composed by nuclear fuel surrounded by a cladding. Due to the fuel swelling during its irradiation, a mechanical interaction increases between the cladding and the nuclear fuel, which is reduced by a gap between these; for the oxide fuel a low density gas while for the metallic fuel a sodium gap is found. A separation between fuel pins is done by the spacing wire to facilitate coolant flow, which is helicoidally distributed along the fuel pin.

A certain number of fuel pins are arranged within an assembly, in which coolant flows through each and every subassembly to remove the heat generated in it. Each assembly is mounted on a grid plate, which forms a common inlet plenum from which the coolant flows through the individual assemblies (Raj, Chellapandi, & Vasudeva, 2015). Fast reactors assemblies commonly have a hexagonal geometry as shown in Figure 2.4, where the fuel lattice and the fuel assembly of a fast reactor are presented.

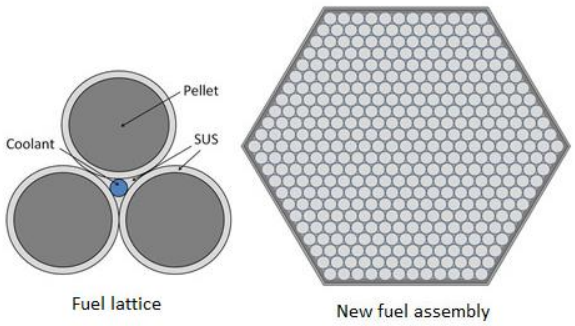

FIGURE 2.4. Fuel lattice and fuel assembly (horizontal cross section) of a SFR (Oka, Inoue, & Yoshida, 2013).

Another important elements in a SFR are the regulation and safety control rods, through which the reactivity control and the reactor shutdown are performed. This elements are strategically positioned in the reactor to ensure the reactor's security. The conjunction of the fuel assemblies and control rods comprise the reactor core, through which sodium flows upwards removing the heat generated by the nuclear fuel.

Thus, the heated sodium is passed through a heat exchanger, in which a secondary sodium loop removes the heat via an intermediate heat exchanger and eventually transfers it to a power generation loop. Two different configurations that meet these characteristics are well known nowadays: the pool and the loop design (Waltar, Todd, & Tsvetkov, 2012).

In the loop configuration the primary coolant is allowed to leave the reactor vessel, and the intermediate heat exchanger (IHX) is located in the containment area outside the vessel, while in the pool design the primary coolant and the IHX are kept within the reactor vessel. Figure 2.5 shows the schematic view of the pool and loop SFRs configurations.

The loop configuration has reliability improvements such as the ease of the loop isolation and maintenance on the IHX. In this design the primary vessel is surrounded by a guard vessel and for safety matters it requires a double-walled piping in areas outside the vessel (Judd, 2014). This design has been preferred in Japan as will be seen in the following section.

The pool configuration has a larger reactor vessel, which reduces the impact of a primary pipe break or leak. As in the loop design, the pool configuration has a primary vessel surrounded by a guard vessel. This configuration has been selected mainly in the United States, France, Russia, S. Korea, China and India (U.S. Department of Energy, 2015). For both designs, a power generation loop is required, in which heat removed by sodium is transferred to generate a steam that eventually generates electricity by flowing through a turbine.

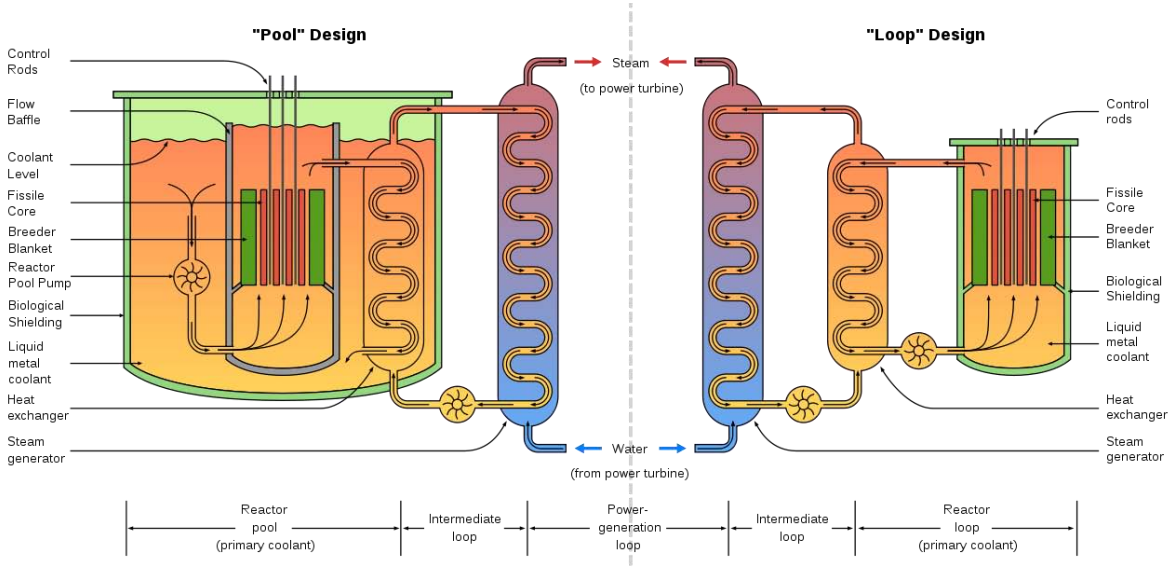

FIGURE 2.5. Schematic diagrams of pool and loop SFR configurations (Graevemoore, 2008).

Different SFRs around the world have been developed in different experimental programs, through which irradiation and operation experience has been gained in different countries. It is worth to describe the most successful programs and experimental reactors, as shown in next section.

2.2. Program history

The Sodium-cooled Fast Reactors have been developed for decades since 1950, when different countries around the world began research programs in which sodium reactors were technologically proved. This section discuss about the irradiation programs developed by different countries in which the United States, France, Japan and Russia are very notable.

2.2.1. Sodium-cooled Fast Reactors in the United States.

The United States started to gain experience in fast neutron reactors after the Second World War. Military efforts took into account the sodium nuclear reactor technology to be implemented in submarines under the supervision of the Admiral Hyman G. Rickover, but it was abandoned due to the experienced trouble with leaks in the steam generators. Meanwhile the first liquid metal reactor of the world was developed in 1945, called *Clementine* with 25 KW_t mercury-cooled built at Los Alamos (Cochran, et al., 2010).

Although the first fast nuclear reactor in the world was not sodium-cooled, the following developed reactor named LAMPRE-I, used the sodium as coolant because its thermal and chemical characteristics. LAMPRE-1 achieved criticality in 1961, and was intended to operate at 20 MW_{th}, but after the inadequate behavior of some core materials at high temperature the design was reduced to 1 MW_{th}. Finally, after a very brief operation, LAMPRE-I was shut down in mid-1963 (Cochran, et al., 2010).

Experimental Breeder Reactor-I

On November 19, 1947, this reactor was authorized and developed by the Argonne National Laboratory (ANL), which designed and built the second sodium-cooled fast nuclear reactor in the United States. Also known as "Chicago Pile 4" and "Zinn's Infernal Pile", the EBR-I was the first fast neutron reactor designed to both, breed plutonium and to produce electric power, achieving first criticality on December 20, 1951 (The American Society of Mechanical Engineers, 1979).

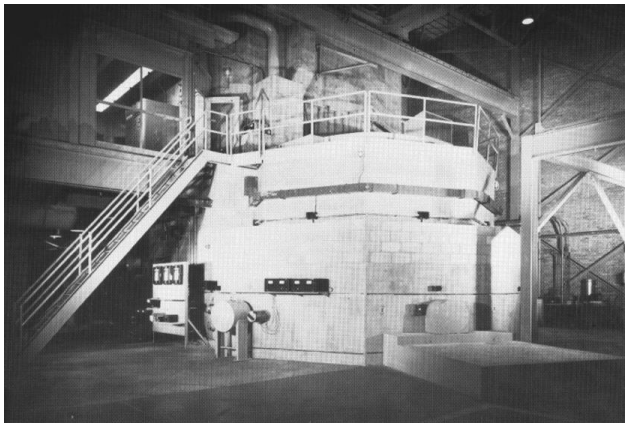

FIGURE 2.6. Interior of the Experimental Breeder Reactor I (The American Society of Mechanical Engineers, 1979).

Unfortunately, the EBR-I was designed with a positive prompt power coefficient of reactivity, and during an experiment on November 29, 1955, the core had a partial meltdown of 40-50 percent. The damaged core was removed and repaired and it operated until December 30, 1963, when it shut-down (IAEA Nuclear Energy Series, 2011).

Experimental Breeder Reactor-II

The Experimental Breeder Reactor II (EBR-II) is probably the most successful fast reactor in the United States due to its irradiation program. Sodium-cooled pool type, the EBR-II was a 62.5 MW_{th} nuclear reactor designed by the ANL and constructed at the National Reactor Testing Station, in June 1958 (IAEA Nuclear Energy Series, 2011).

EBR-II demonstrated the operation of a SFR as a power plant, having as a specific feature a Fuel Condition Facility that enabled reprocessing and recycling of fuel, reason why it changed its approach from a demonstration plant to an irradiation facility in 1967. The EBR-II became the demonstration facility for the Integral Fast Reactor (IFR), which was a concept that proved inherent safety through two different tests. IFR project was canceled three years before completion in 1994 (Koch, 2008).

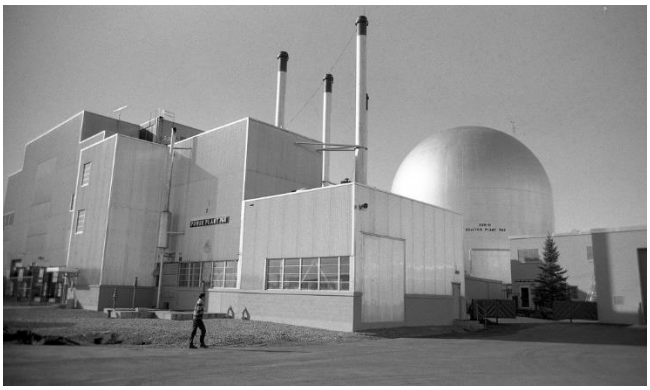

FIGURE 2.7. Experimental Breeder Reactor II (Argonne National Laboratory, 2012).

During thirty years the EBR-II remained active for the research and technology demonstration, until September 1994 when it was shutdown. EBR-II dismantling comprehended the draining of the primary and secondary sodium loops, besides the defueling of the reactor, which consists in conditioning the spent fuel in acceptable forms for disposal in a national geological repository (Koch, 2008).

The Fast Flux Test Facility

The Fast Flux Test Facility (FFTF) was authorized in July 1967 with a loop-type sodium-cooled nuclear fast reactor design of 400 MW_{th}. The construction of the FFTF was completed in 1978, achieving its first criticality in 1980 and started serving as a test facility in 1982. The main purpose of this reactor was to demonstrate the operation of a medium scale sodium-cooled nuclear reactor, and test the required technology towards a large scale sodium cooled fast reactor (Cochran, et al., 2010).

FIGURE 2.8. The Fast Flux Test Facility (Binus, 2003).

Several tests concerning safety and operation were done in this reactor until 1993, when the usefulness of this reactor decreased, and as a consequence, it was decided to deactivate it. Despite several efforts to find a new mission for the FFTF, none of them was consolidated, so that it remained waiting for a justification to be tested again. (Cochran, et al., 2010)

2.2.2. Sodium-cooled Fast Reactors in France.

France developed different sodium-cooled nuclear reactors that will be seen in this section. Since the ending of the Second World War, France pursued the construction of nuclear weapons using plutonium, therefore a reprocessing plant began operating in Marcoule in 1958, named UP1 (*Usine de plutonium 1*) (IAEA Nuclear Energy Series, 2011).

Later, in 1965 the *Harmonie* facility started to test the neutron irradiation behavior and in 1966 different breeder core configurations were studied in the facility Masurca, both of them in Cadarache. In 1966 the second reprocessing plant UP2 (Usine de plutonium 2) was developed for separating plutonium in a gas-graphite reactor fuel (Schneider, 2009). These facilities were the predecessors to the most known French reactors; Rapsodie, Phénix and Superphénix described below.

Rapsodie

The first experimental sodium-cooled reactor in France, called Rapsodie, started its construction in 1962 and went critical on 28 January 1967. It was first designed with a nominal capacity of 20 MW_{th}, but after a core redesign in 1970, the power was adjusted to 40 MW_{th}. It operated with that power until 1980, when it was reduced to 22 MW_{th} in order to minimize the thermal stress causing cracks in the reactor vessel. Rapsodie was designed with a commercial approach, with a loop-type configuration. The mean duration of the reactor runs was 80 days, and the fuel reached up to 100 GWd/T (Cochran, et al., 2010).

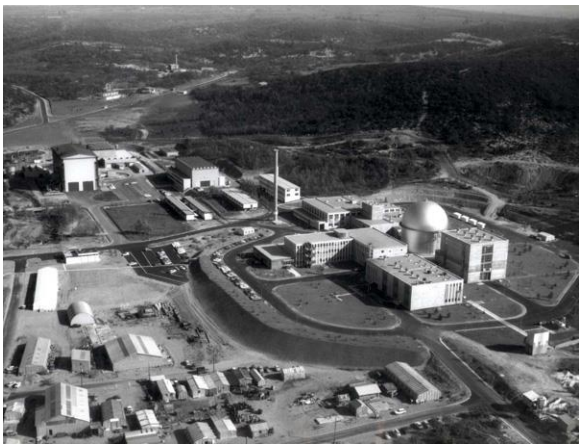

FIGURE 2.9. Rapsodie Nuclear Reactor (CEA, 1967).

During its operation, this reactor suffered two leaks, but none of them had fatal consequences. Rapsodie reactor operated until April 1983, when its shutdown became permanently. Currently, Rapsodie is under dismantling, which considers the sodium drain of the core, the fuel discharge and the confinement of the vessel (CEA, 2012).

Phénix

In 1968 the construction of Phénix began in Marcoule and on August 31, 1973 achieved its first criticality (Schneider, 2009). Phénix was a pool-type reactor of 563 MW_{th} that was connected to the electrical grid with a power of 250 MW_e. The mean length of reactor runs was 90 days and it achieved burnups up to 150 GWd/T.

FIGURE 2.10. Phénix Nuclear Reactor (Bérenger, 2012).

After remarkable operational record, in 1980 Phénix experienced several unexplained reactivity transients that had potential safety implications, and as a consequence, the reactor was shut-down between 1991 and 1994. Although it was restarted for short periods, in June 2003, the National Safety Authority (ASN) authorized the restart of Phénix for six refueling periods with a restriction in the nominal power, it had to be decreased form 233 MW_e to 130 MW_e. In 2009 Phénix was shut down, and currently is in the dismantling stage, whose duration will be about 30 years (IAEA Nuclear Energy Series, 2011).

Superphénix

Superphénix was the successor of Rapsodie and Phénix, which also was a pool-type sodium-cooled of 2900 MW_{th} and 1200 MW_e. The objective of this design was to build the first commercial-size plutonium-fueled fast breeder reactor of the world, but unfortunately, this reactor experienced a great opposition from scientist community (Schneider, 2009). It achieved its first criticality in 1985, but there were many administrative and operational issues around this project, such as a major sodium leak in the fuel tank, and due to the impossibility of repairing it, it took 10 months to develop a different method to load and discharge fuel from the reactor core.

Added to this, the drastically decreased nuclear power interest, the Superphénix struggled in its operation to the point its lifetime load factor was less than 7%. On 1997, when the project seem to regain direction again, due to a core reconfiguration and the implementation of a research program into transmutation, the incoming Prime Minister decided to abandon Superphénix, decision that became official on 2 February 1998. The dismantling started in 1999 and by 2008, the fuel has been discharged and transferred to the storage facility on site, and the turbine hall has been emptied (Cochran, et al., 2010).

FIGURE 2.11. Superphénix Nuclear Reactor (Forget, 2007).

2.2.3. Sodium-cooled Fast Reactors in Japan.

The fast breeder reactor program in Japan was published in 1956, when the Japan Atomic Energy Commission decided the importation of LWR technology from the United States. This program planed the construction of an experimental breeder reactor during the 1970 decade, and the commercial breeder design by the late 1980s (Cochran, et al., 2010).

Joyo

Joyo was the first fast reactor in Japan, located in Ōarai, Ibaraki. Sodium-cooled, the Joyo had a nominal power of 50 MW_{th} when it achieved criticality in 1977, then in 1979 power was increased to 75 MW_{th} and finally was again increased to 100 MW_{th} in 1982. Joyo was an irradiation test facility that analyzed different fuels and material behavior for future Japanese reactors, such that it accomplished 70,000 hours of operation (Ohira & Uto, 2012).

FIGURE 2.12. Joyo Nuclear Reactor (Japan Nuclear Cycle Development Institute , 2001).

For thirty years Joyo operated approximately 27% of the time, until in 2007 it suffered an incident that forced its irradiation program stop for 7 years, when the replacement of damaged elements would be done.

Monju

Monju was developed in parallel that Joyo did, but it was in 1994 when it reached its first criticality mainly because Monju's construction was delayed. Monju is a 714 MW_{th} loop-type sodium-cooled fast reactor developed in Tsuruga Nuclear Power Plant, Fukui Prefecture (IAEA Nuclear Energy Series, 2011).

FIGURE 2.13. Monju Nuclear Reactor (Japan Nuclear Cycle Development Institute, 2001).

Probably the most known event about Monju is the serious sodium leak presented on December 8, 1995, which caused fire that damaged a thermocouple attached to the secondary loop. Despite there was no release of radioactivity and no injuries were reported, the social and political response to this incident delayed the repair and restart of Monju, mainly because the Power Reactor and Nuclear Fuel Development Corporation (PNC) tried to cover-up the accident. Although Monju was then restarted in May 2010, another accident in August 2010 shut-down the reactor, condition in which it remains nowadays.

2.2.4. Sodium-cooled Fast Reactors in Russia.

Russian SFRs have gained experience since the 1950's decade, and their research program in these reactors has been successful. In 1949, when Russia was still the Soviet Union, the physicist Alexander Leypunsky presented a report with the idea of developing reactors that could produce more fissile material than they consumed, so in November 1949 the government launched the development of the first fast reactor program (Cochran, et al., 2010).

BR-5/10

The main goal of BR-5 was to demonstrate the feasibility of creation and operation of sodium cooled fast reactor, as well as the fulfillment of testing different nuclear fuels and structural materials. It achieved its first criticality in Obninsk 1959, and the maximum achieved burnup was 6.1% in plutonium dioxide.

In 1971 it was necessary to reconstruct the BR-5 into BR-10, which increased its nominal power from 5 MW_{th} to 8 MW_{th}. In BR-10 different research was done, analyzing failed fuel pins, mass transfer and distribution of different impurities and nuclides in the primary circuit.

The research program for BR-10 included the development of purification of coolant oxides and radioactive cesium and the development of technologies for removal of non-drainable sodium residues from the circuit by vacuum distillation.

In 2002, BR-10 was stopped and nowadays is under decommissioning, taking advantage of its present situation there is a development of technological processes proposed for SFR decommissioning (Buksha, 1996).

BOR-60

BOR-60 played an important role in justification further developed designs and technical proposals of SFRs. It achieved its criticality in 1969, and its licensing was extended until 2014. This reactor was used for isotope production as well as to analyze different behavior of different fuels and structural materials. It achieved more than 225000 hours in critical condition which is a considerable experience in a research program.

One of the great advances in this reactor was the steam generator tests, being these successful programs since there were no leaks in both steam generators for 19-years operation (Buksha, 1996).

BN-Reactors

The BN-Reactors are a Russian sodium-cooled fast reactors developed by the company OKBM Afrikantov. Four different designs were developed by this company named BN-350, BN-600, BN-800 and BN-1200. These reactors have a commercial focus, and the objective of these was to develop technological strategies towards a SFR proposal.

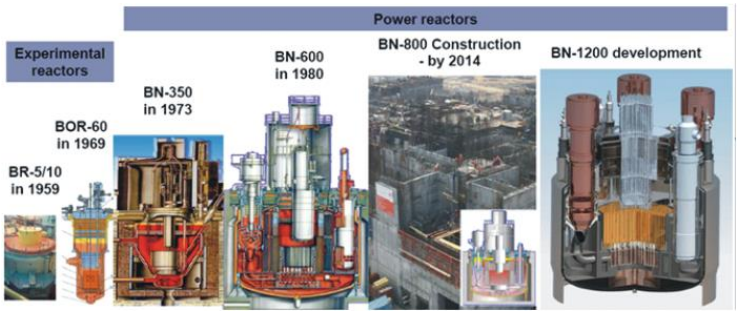

FIGURE 2.14. Russian Sodium-cooled Nuclear Reactors (Hozzászólás, 2013).

BN-350 is the first prototype constructed, achieving its criticality in 1972. The loop-type nuclear reactor experienced large number of leakages mainly in the steam generators, but after ensuring the reliability of the steam generators the design was improved taking a transition from vessel-type to sectional-modular steam generators. The gained experience in BN-350 provided the basis for the BN-600 development.

BN-600 is probably the most successful Russian project because the correctness decisions taken in its design. Actually it operated as a commercial reactor, achieving an average load factor equal to 73.82%. It was a pool-type sodium-cooled nuclear reactor of 600 MW_e which achieved its first criticality in 1980. For nearly 30 years it operated and produced more than 110 billion kWh of electric power (Buksha, 1996).

The newest reactor in this type is the BN-800, with an 880 MW_e entered on operation in December 2015. One of the major objectives in this reactor is the demonstration of closed nuclear fuel cycle. BN-1200 is the prototype reactor to be developed for the 4^{th} generation, with a power pf 1200 MW_e.

2.3. Future and development of SFRs

The development of SFRs has not stopped during time, such that different countries around the world continue with SFR programs that include TRU recycling and waste management that minimize the environmental impact. The future SFRs have specific improvements on safety matters, and the fuel utilization could be enhanced by using these reactors. This sections gives a brief description of the most popular SFRs in current development.

2.3.1. PRISM

The Power Reactor Innovative Small Module (PRISM) is a modular nuclear reactor, sodium cooled with an electric power 311 MW_e. It is being developed in the United States by General Electric and Hitachi. The conception of the PRISM nuclear power plant comprehends two reactors per turbine and a total of six reactors per site for a total of 1866 MW_e. Fuel for PRISM nuclear reactor would be fabricated on site which is a great advantage in the fuel cycle (Hitachi & GE, 2007).

There are three different designs for PRISM reactor: the first is a breeder design, this means that produces more fissile isotopes than the ones that it consumes. The second is a breakeven reactor in which the consumption of fissile isotopes is equivalent to the fissile isotopes it produces. The last configuration of this reactor is a burner design, which is very notable mainly for the capability of burning transuranic (TRU) elements.

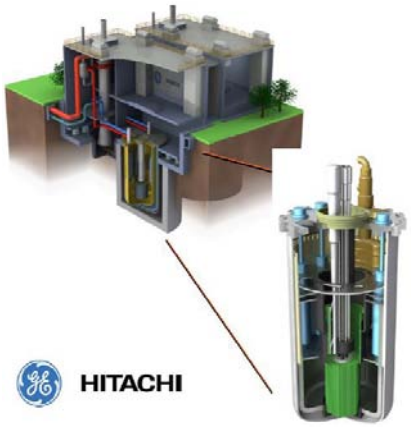

FIGURE 2.15. PRISM Nuclear Reactor (Hitachi & GE, 2007).

Its design has passive safety characteristics like the passive heat decay and the passive accommodation of ATWS. Since it is a modular reactor, the initial investment is much lower compared with the conventional reactors (Hitachi & GE, 2007).

2.3.2. Toshiba 4S Design

The Super-Safe, Small and Simple Reactor (4S) is a design being developed by Toshiba in Japan. It is a pool-type sodium-cooled fast reactor with two different electrical outputs, 10 and 50 MW_e. This metal fueled reactor has thirty years lifetime without on-site refueling, achieving 34 GWd/T average burnup for the 10 MW_e nominal power and 90 GWd/T burnup for the 50 MW_e electrical output (Toshiba Corporation, 2013).

FIGURE 2.16. Toshiba 4S Design (Toshiba Corporation, 2013).

It is not considered as a breeder reactor since there are not blankets in its design, but despite this, the energy available during its whole operation, considering its dimensions and critical mass, represents great advantages compared to other SFR designs (Dugdale, 2010).

2.3.3. Japan Sodium-cooled Fast Reactor

The Japan Sodium-cooled Fast Reactor (JSFR) is a design developed by the Japan Atomic Energy Agency (JAEA). Its development would be divided in two stages, the first is the demonstration of a SFR design of 1765 MW_{th}, and in the second phase a commercial reactor of 3530 MW_{th} will be tested (JAEA, 2006).

This concept also incorporated the TRU recycling which would reduce the environmental burden. The Fuel Assembly with Inner Duct Structure (FAIDUS) will be incorporated in the JSFR bringing a superior performance for discharge molten fuel after a severe accident. Unfortunately, this project has been suspended since the Fukushima-daiichi accident (Ohki, 2012).

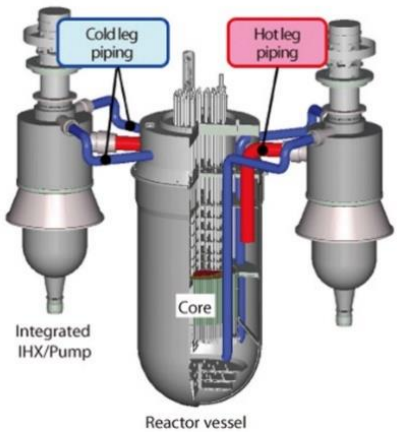

FIGURE 2.17. JSFR Nuclear Reactor (JAEA, 2006).

2.3.4. BN-1200

The BN-1200 is a Russian pool-type sodium-cooled nuclear reactor, which is the next generation of the well-developed BN-reactors. With a thermal capacity of 2800 MW_{th}, the BN-1200 objective is to enhance the safety up to the level that GEN IV requires.

In 2014 the BN-1200 design was determined and validated for the power unit and the reactor is currently being constructed in Beloyarsk. The BN-1200 program includes the technical and economical improvements in the reactor power unit to the level of the Russian VVER of equal power (Shepelev, 2015).

The BN-1200 is probably the most advanced design into a commercial approach, mainly because of the gained experience in the BN-350, BN-600 and BN-800 reactors.

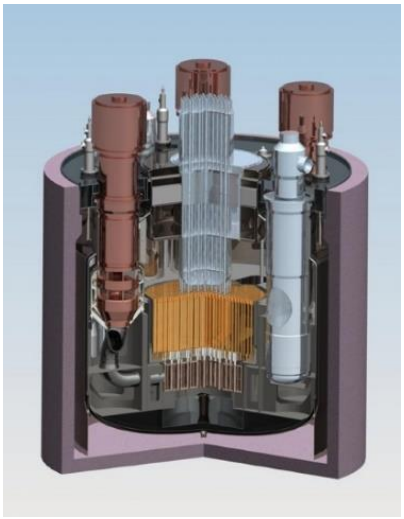

FIGURE 2.18. BN-1200 Nuclear Reactor (ENERGO, 2015).

2.3.5. Prototype Fast Breeder Reactor

Prototype Fast Breeder Reactor (PFBR) is an Indian project developed in Kalpakkam with the priority of demonstrate the techno-economic viability of fast breeder reactors on an industrial scale. The PFBR is a pool-type sodium-cooled reactor with an electrical power of 500 MW and a thermal power of 1250 MW. The PFBR is fueled with mixed oxide fuel (MOX) and it uses depleted uranium in the blankets. It is designed to do refueling every 185 Effective Full Power Days (EFPD) expecting a total of 100 GWd/T (Dravid, 2010).

FIGURE 2.19. The PFBR Nuclear Reactor (Heard, 2011).

Being the first of its kind in India, the PFBR construction has already finalized and it is expected to achieve criticality in April 2016. Given the successful development of this project, the Indian government is looking forward to construct six more fast breeder reactors once that the PFBR reaches one year of operation (Bennett & Coleman, 2015).

This project has generated much controversy because some scientists believe that only a recreated model of Rapsodie has been developed, which is an old design developed by France as stated in the section 2.2 (Jesudasan, 2013).

2.3.6. The Advanced Sodium Technology Reactor for Industrial Demonstration

The Advanced Sodium Technological Reactor for Industrial Demonstration (ASTRID) is a sodium-cooled pool type fast nuclear reactor of 1500 MW_t. The ASTRID project seems to be a promising project that could join into the commercial fast nuclear reactors, since the main objective of this project is to demonstrate the operability of an industrial scale reactor, and to accumulate experience of the tested technology towards the industrial deployment of the GEN IV (CEA, 2012).

In the ASTRID project, oxide nuclear pellets ($UPuO_2$) will fuel reactor, and a closed nuclear fuel cycle will be tested in order to ensure the economic competitiveness with other energy sources. The minor actinide transmutation program in ASTRID includes the manufacture of these isotopes contained in pellets to perform transmutation experiments in the reactor, centering on the behavior analysis of the complete subassembly, which would determine the feasibility to reduce the quantity of nuclear waste.

Into the irradiation program the qualification of different materials is considered, such as the absorbers (B_4C), the cladding (AIM1), the wrapper tube (EM10), the reflector subassemblies and the lateral neutron shielding (SiC, MgO, $MgAl_2O_3$, or $B_4{}^{11}C$) (Chenaud, et al., 2013).

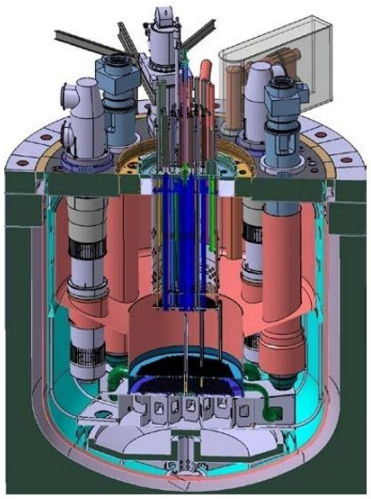

FIGURE 2.20. ASTRID nuclear Reactor (Saez, et al., 2013).

Since the present study is focused in the ASTRID project, a wider description of this reactor will be shown in section 5.1 in order to comprehend the characteristics and advantages that this design has.

3. BREED AND BURN REACTORS

The breed and burn reactor is a nuclear reactor designed to burn part of the bred material without reprocessing fissile isotopes. Great advantages could be obtained in the nuclear power industry by their implementation, specifically on the uranium utilization.

This chapter is centered on the breed and burn reactor concept characteristics as well as the concept evolution during time. Different prototype reactors are shown in the last section of this chapter.

3.1. Essential characteristics

The Breed and Burn (B&B) reactors breed fissile isotopes from fertile ones (that could be depleted or natural uranium or even thorium), and then it fissions a considerable fraction of the bred fissile isotopes (plutonium-239, plutonium-241 or uraium-233).

In the B&B reactors, the fuel is characterized in two different zones: the ignition and the breeding zones. The ignition zone has enriched fuel (uranium or plutonium) in order to produce enough neutrons that could provoke other fissions or even interact in the transmutation process in the breeding zone. The breeding zone is the section in which the production of new fissile material is done; hence, the fissions take place in this zone when breeding has advanced. The B&B reactors require a reflector that decreases the leakage probability, avoiding a considerable loss of neutrons and increasing the probability of sustaining a chain reaction (Di Sanzo & Greenspan, 2012).

The fuel cycle of a B&B reactor operated with depleted uranium (stoked as residual material from enrichment plants) is greatly simplified (since breeding and burning of nuclear fuel take place inside the reactor) compared with the fuel cycle of a conventional Light Water Reactor (LWR), where the front-end covers the operations from the mining of uranium to the manufacture of fuel assemblies for loading into the reactors and the back-end covers the operations concerned with spent fuel that leaves reactors, as shown in Figure 3.1

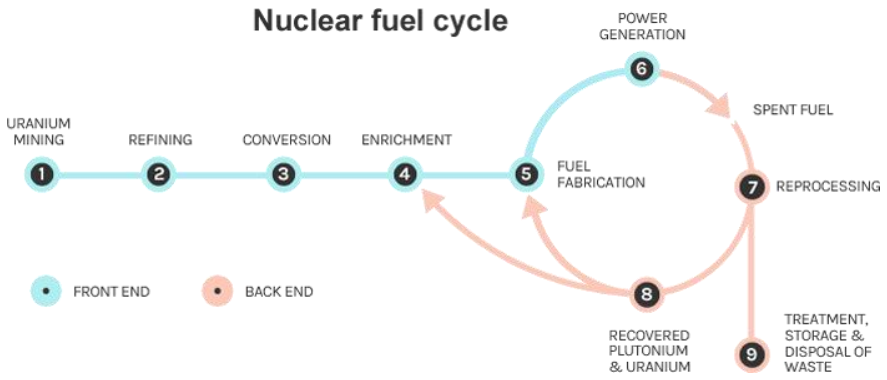

FIGURE 3.1. Nuclear Fuel Cycle of LWRs (World Nuclear Transport Institute, 2012).

As stated, the fuel cycle in the B&B reactors is highly simplified because the necessity of mining, and processing of fresh fuel is eliminated. Since in the B&B reactors the breed and burn take place in the same reactor, there are no refueling procedures, hence the spent fuel is discharged only at the end of the operation of the B&B reactor, which decreases the spent fuel transportation expenses and avoids the reprocessing of spent fuel, which is a considerable economical advantage (Ellis, et al., 2010). Figure 3.2 presents the simplification of the B&B reactors fuel cycle.

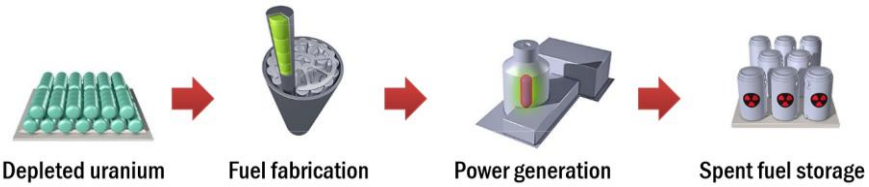

FIGURE 3.2. Nuclear Fuel Cycle of the B&B Reactors (Ellis, 2011).

There are different strategies in the burnup of the nuclear fuel in the B&B reactors; one of them is the spawning method proposed by Greenspan. It consists in burning the nuclear fuel at its minimum sustainable burnup, and once the fuel has reached this level, it could be considered as the starter fuel in a brand new B&B reactor. Taking this operation mode in the B&B reactors, the installed electrical capacity can increase in an exponential mode. Figure 3.3 shows a schematic of the spawning mode in B&B reactors.

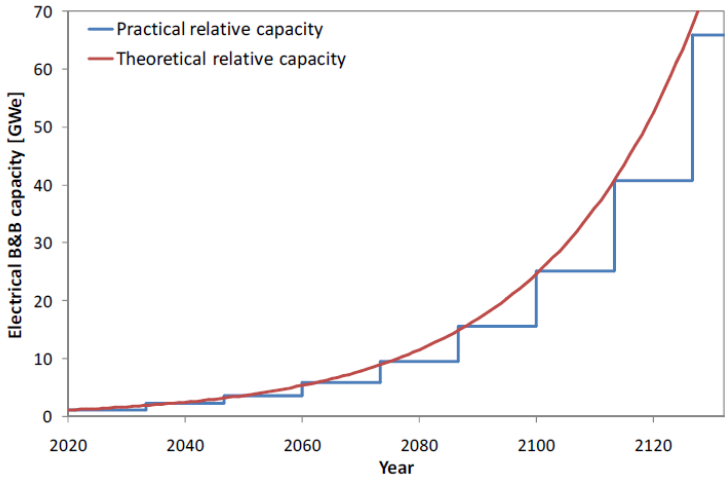

FIGURE 3.3. Electrical capacity evolution due to one large B&B reactor deployed in 2020 and operated in spawning mode (Greenspan, 2012).

There are two different breed and burn concepts: the Traveling Wave Reactor (TWR) and the Stationary Wave Reactor (SWR), being these two the current breed and burn concepts developed.

In TWR concept the breeding and burning process can be seen as the superposition of two waves (breeding and burning) that advances through the reactor, starting in the ignition zone. The conventional TWR has a cylindrical shape, with the ignition zone at one end of it and the breeding zone adjacent to the ignition zone. As said before, neutrons emitted from fissions in the ignition zone, besides of causing more fissions, are captured by the fertile material in the breeding zone to later turn into new fissile material.

The burning wave starts in the ignition zone, while the breeding begins to take place in the contiguous breeding zone to the ignition zone. As the breeding of fissile isotopes is done in the breeding zone, the burning wave starts to travel along the reactor, as shown in Figure 3.4.

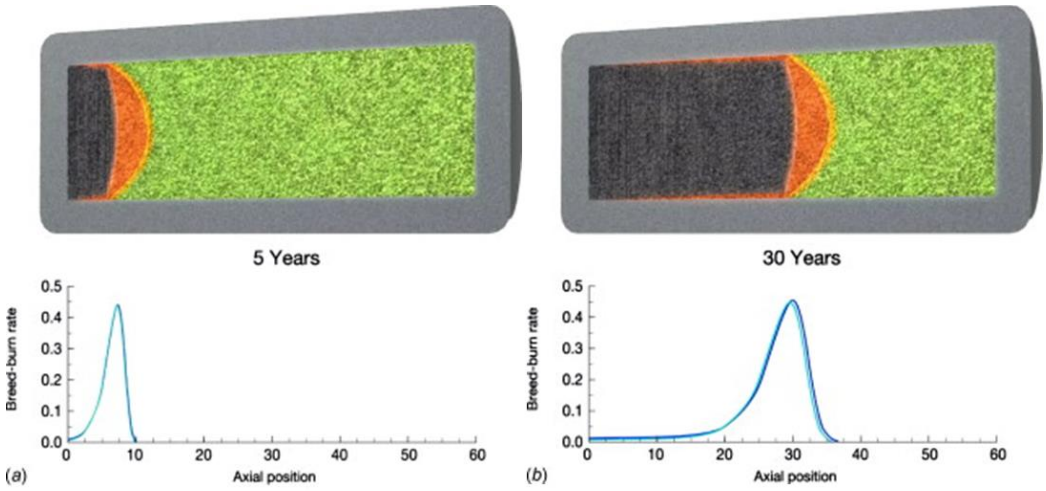

FIGURE 3.4. TWR breed and burn waves at 5 years (a) and 30 years (b) (Weaver, Gilleland, Ahlfeld, Whitmer, & Zimmerman, 2010).

One of the advantages of the TWRs is that it could operate during years depending on the reactor's dimensions and the fuel composition. Theoretic approximations show that it would operate up to 200 years, but due to material limitations, it could operate for 60 years. One particular complication in these reactors is the heat removal, since the power is generated in different axial distance depending on the time.

The SWR design has different performance in the burning and breeding compared with the TWR. In a SWR the fissions and the transmutation take place in the whole reactor at the same time. In a SWR the core has a conventional geometry, fuel is placed radially and power density is typical of a fast reactor through entire life.

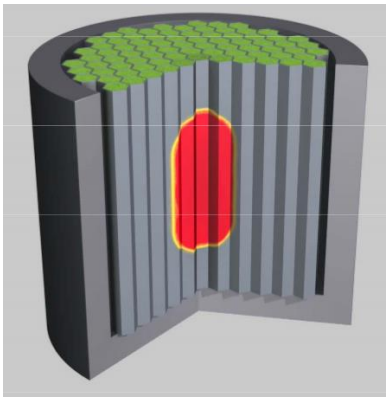

FIGURE 3.5. SWR breed and burn core (Ellis, 2011).

Unlike the TWRs, the SWRs have a conventional geometry that facilitates the heat removal in the reactor, reason for which the SWR appear to be the most feasible B&B concept thanks to the proved technology and tested materials in the experimental SFRs, as shown in section 2.2.

The B&B reactors have different fuel cycles, a brief description of them is discussed in this section. It is to notice that in these fuel cycles the limit is imposed by the materials, specifically the fuel swelling and the cladding constrains impede the extended operation of the B&B reactors.

The once–through fuel cycle is one of the B&B fuel cycles, and it consists in introducing the nuclear fuel in the reactor, burn it and eventually discharge and store the spent fuel. This is the most simple fuel cycle in a B&B reactor since there's no reshuffling or reconditioning process is required.

The melt-refining process fuel cycle extend the reactor operation by reconditioning the fuel: fuel clad is replaced, volatile and gaseous fission products are released, and after the fuel recast, it is reloaded in the core. Burnup is extended in this fuel cycle and the nuclear waste is considerably reduced.

Fuel reshuffling is a technique that enables the extension of operation of the fuel reactors, in which different reshuffling schemes favor the breeding in different zones of the reactor. This fuel cycle is a particular interest in this study.

Due to LWR operation for decades, the amount of depleted uranium "waste" has increased; this allows the performance of B&B reactors, in which several tons of depleted uranium may be used as breeding zone (Weaver & et al., Extending the Nuclear Fuel Cycle with Traveling-Wave Reactors, 2009). Given this scenario, and due to the nuclear fuel cycle of a B&B reactor, it is desirable to use this kind of reactors using the different strategies in the burnup of the nuclear fuel, in which it may be possible to increase the uranium utilization to >95% (Greenspan, 2012), as it can be seen in Table 4.

TABLE 4. Estimated uranium utilization limits and energy value of depleted uranium when used in B&B and in LWR (Greenspan, 2012).

Mode of operation	*Uranium utilization*	*Relative U utilization*	*No. of years at present supply*
LWRs- reference	0.6%	1	0
(a) Subcritical BB blanket; no reconditioning	10%	20	400
(b) SWR; 20% average discharge burnup	20%	40	800
(c) SWR; 1 reconditioning @ 20%	40%	80	1600
(d) SWR or TWR ; with fuel reconditioning >1	50%	100	2000
(e) Fast reactor with continuous recycling	>95%	>190	3900

*SWR: Stationary Wave Reactor.

As shown in Table 5, the years of energy supply that could provide the B&B reactors bring a unique horizon to the nuclear power, with more competitiveness in safety, economics and resources utilization. The B&B reactors have great advantages since its technology offers a path forward to an emissions-free, proliferation resistant global energy supply with maximized resource utilization. In the pursuit of these interests, different researchers had developed different prototypes that fit the B&B description, being these developed since the early nuclear power era, in 1958.

3.2. Development of the Breed and Burn concept

In order to comprehend the research background of the B&B reactors a brief description of the developed projects is presented in this section, which provides the basis to understand the B&B evolution designs and the countries implicated in its analysis.

The breed and burn concept was first mentioned in 1958 by S. M. Feinberg and A. Kunegin at the United Nations International Conference of Atoms for Peace, in which unenriched fuel is moved around the core to sustain fission. Further breed and burn analysis was done by Klaus Fuchs and H. Hessel in 1961, in which chemical fuel treatment was not considered (Qvist, 2013).

It was until 1979, when a new breed and burn concept was presented by Fischer et al: The Fast Mixed Spectrum Reactor (FMSR), developed in the Brookhaven National Laboratory (BNL) in collaboration with the Massachusetts Institute of Technology (MIT). The FMSR will be described in section 3.3.4. Also in 1978 Driscoll, Atefi and Lanning developed studies on oxide and thorium-fueled TWR at the MIT, describing this concept in the article “An evaluation of the Breed/Burn Fast Reactor Concept” (Waltar, Todd, & Tsvetkov, 2012).

In 1984 the publication “Problems of development of fast reactors self-provision without fuel reprocessing” by J. S. Slesarev, V. A. Stukalov and S. A. Subbotin provided a new SWR design.

In 1988 L. P. Feoktistov presented an analysis of a concept of a physically safe reactor with two publications: “Neutron-fission wave” ”Variant” of safe reactor”. Research continued in 1992 with V. Goldin and the mathematical modeling of B&B reactors.

In 1995 Seifritz, in Germany, demonstrated that burnup could be propagated through a neutron absorber medium in the article “Non-Linear Burn-up Waves in Opaque Neutron Absorbers”. Meanwhile in the United States a gas-cooled thorium-fueled TWR was proposed in 1996 by E. Teller, M. Ishikawa and L. Wood, through the article “Completely Automated Nuclear Power Reactors for Long-Term Operation”

A year later, in 1997, Gregory Toshinsky analyzed a SWR core design and published the LMFBR Operation in the Nuclear Cycle Without Fuel Processing, Advanced Reactor Safety Topical”. In 1999 Akhiezer et al. published “Propagation of a Nuclear Chain Reaction in the Diffusion Approximation” where nuclear chain reaction in a cylindrical breeder medium was studied for critical and subctitical regimes, and in “Slow Nuclear Burning” the propagation of the nuclear fission wave is studied.

One of the most known B&B reactors is the Constant Axial shape of Neutron flux, Nuclide Densities and power shape during Life of Energy production (CANDLE) which is a TWR, proposed by Sekimoto et al. in 2000. In this year Hugo Van Dam published “Burnup waves” study in which the propagation of burnup waves was presented. In 2003 Fomin and Pilipenko developed theorical studies on TWRs with the article “Some aspects of Slow Nuclear Burning”.

In 2005, Xue Cheng and Maschek worked on the nuclear buckling effects for TWRs. In this year Yarsky, Hejzlar and Driscoll developed a SWR design in the MIT. In parallel, Ehud Greenspan et al. developed SWR core studies in the UC Berkeley University.

B. Gaveau analyzed in 2006 the nuclear bucking effect for SWR. In this year TerraPower (named Intellectual Ventures by that time) started developing commercial sodium-cooled SWR designs.

Finally in 2010 Y. Kim et al. started developing for the Korean Institute of Science and Technology (KAIST) a TWR design, and General Atomics started developing commercial B&B designs, research where the Energy Multiplier Module was proposed.

3.3. Existing prototypes

In this section the different developed B&B prototypes are presented, and briefly described. It is to notice that none of the developed B&B prototypes has ever been constructed and tested, however, the experience gained in the experimental SFRs enable the feasibility of the shown B&B designs.

3.3.1. The SWR research

The SWRs have been developed since the early 1960's and since then different researchers started a conceptual development of B&B reactor designs. The SWRs prototypes enhance the resources utilization and deals with the proliferation issue with a feasible outlook to its implementation. This section presents in a briefly manner the main characteristics of the SWRs prototypes.

3.3.1.1. Fuchs and Hessel first Standing Wave Reactor design

In 1961 Klaus Fuchs and H. Hessel studied a natural uranium B&B reactor without chemical reprocessing. The abstract of its publication is shown below:

> *"The advantages of a breeder reactor which operates without chemical processing of the fuel elements are evident. A rough calculation is given to demonstrate the principal possibilities of such a reactor and to calculate the obtainable burnup of the natural uranium, which is limited, on the part of the neutron physics, essentially by the absorption in the fission products and construction materials. Two cases are considered: a heterogeneous reactor in which the fuel elements move continuously through the reactor and are removed finally; and a homogeneous reactor in which the breeder material and fission material form a homogeneous solution. Natural uranium was continuously fed in and a corresponding fraction of the homogeneous mixture was removed. (J.S.R.)"* (Fuchs & Hessel, 1961)

3.3.1.2. The Fast Mixed Spectrum Reactor

It was in the late 1970s when the first SWR was analyzed by Fischer et al. in the BNL in collaboration with the MIT. The FMSR has been a reference in the B&B reactors since many of the principles employed in the present day were developed in this reactor, like fuel assemblies reshuffling strategies and venting of the fission gas in the metallic fuel. Figure 3.6 shows the FMSR schematics.

Fissile and blanket fuels are loaded into the fast and thermal cores zones respectively. Then fissile material is bred in the thermal zone during core operation. As sufficient fuel is bred and after the driver fuel assembly has reached its discharge burnup, the core is shuffled.

During the shuffling process, the burned driver fuel assemblies are discharged, and the bred fuel assemblies are shuffled into the fast core zone. Then fresh depleted uranium blanket assemblies are charged into the thermal core zone. The core is then restarted. It is noted that during the breeding phase, a sufficient irradiation time of the blanket fuel in the thermal zone is required to ensure favorable breeding before it is moved into the fast core zone.

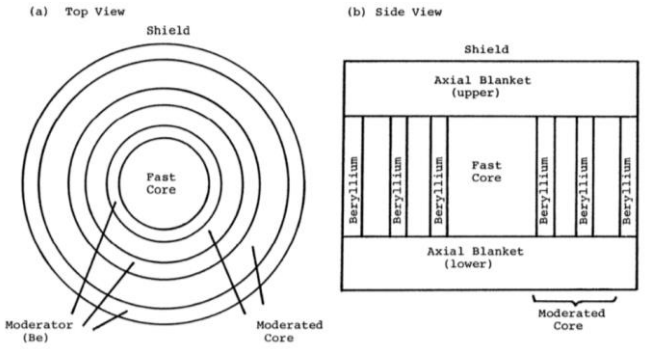

FIGURE 3.6. The FMSR concept (Qvist, 2013).

The FMSR core design has 240 assemblies in the fast zones and 168 assemblies in the thermal zone for a total of 408 assemblies. Axially the FMSR is divided in three zones, lower axial blanket, active core and upper axial blanket. The FMSR is a 3000 MW_t design, and it offered non-proliferation characteristics and good utilization of uranium resources (Fischer & Cerbone, 1979).

3.3.1.3. Slesarev and Toshinsky designs

In 1984 Slesarev and Toshinsky developed a SWR design that considered a high burnup without chemical waste reprocessing. The abstract of their publication is shown below.

> "Conceptual options for fast reactors operation with conditions of fuel self-provision without subsequent chemical waste reprocessing are considered. It is shown that such a regime can be realized for a number of dense fuels, supposed the feasibility of deep fuel burnups. Requirements for the burnup depth are appreciably mitigated when hardening a neutron spectrum or at a low enrichment feeding. The use of such fast reactors with low-enriched fuel feeding is equal to both solution of the problems on significant improvements of the conventional reactors fuel balance (PWR) and putting into practice the industrial reprocessing of irradiated fuel. The design of fast reactors of the mentioned type is stated to make it possible to obtain time reserves and means for developing an economical reprocessing of fuel or even to quit with it totally." (Slesarev, Stukalov, & Subbotin, 1984)

3.3.1.4. The MIT gas-cooled B&B reactor

In September 2005 the MIT designed and analyzed a B&B gas-cooled fast reactor (GFR). The GFR fits perfectly the B&B neutronic parameters, such as the ultra-hard neutron spectrum. The MIT's GFR concept comprehended two practical reactor designs: The "demonstration concept" and the "advanced concept".

The demonstration concept has a highly neutronically $U^{15}N$ fuel in a hexagonal array. The core is helium cooled coupled to a steam Rankine power conversion. The fuel in this reactor is manufactures using advanced vibration compaction techniques.

The advanced design would operate without the expensive $U^{15}N$, instead carbide fuel substitutes it. Since higher heavy metal loading are needed an innovative The Tube-in-Duct (TID) fuel assembly was proposed, which meet the large heavy metal loading required in a B&B nuclear reactor. Figure 3.7 presents a schematics of the TID assembly (Driscoll, 2005).

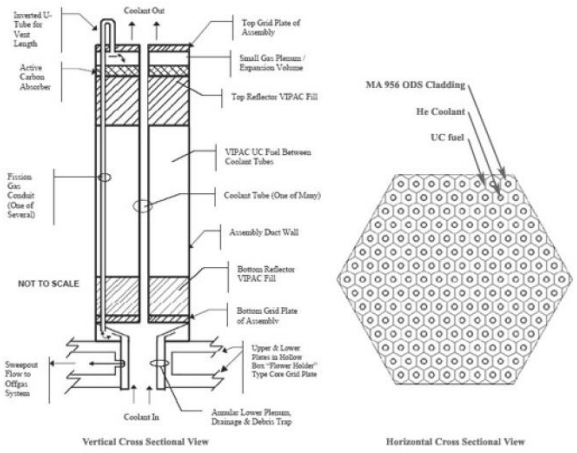

FIGURE 3.7. TID Conceptual Diagram (Driscoll, 2005).

3.3.1.5. The University of California Berkeley Standing Wave Reactor Research

The research made at the University of California (UC) Berkeley University has given wide results in B&B reactors. Core design, safety and cycle characteristics of SWRs operating on a once-through fuel cycle or with limited separations using melt-refining process. The SWR have been exhaustedly analyzed, from minimum attainable burnup in breed and burn reactors to full analysis of SWRs cores including safety, neutronic and innovative burnups.

One of the most interesting designs is a prolate (cigar like) shape SFR, for which the majority of the neutron leakage is in the radial direction which enables a subcritical blanket surrounding the core to breed fissile material. Figure 3.8 shows the prolate SFR B&B design.

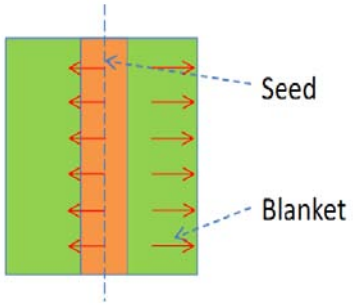

FIGURE 3.8. A proposed core having "cigar shape" surrounded by a blanket (Greenspan, 2012).

3.3.1.6. The Ultra-Long Life Fast Reactor

The Ultra-Long Life Fast Reactor (ULFR) is a sodium-cooled fast reactor concept with a once-through fuel cycle. Since previous irradiation tests proved an acceptable behavior of molybdenum-based metallic fuel, the ULFR incorporates it to increase the heavy metal loading in the core.

The ULFR consists of 342 driver assemblies, 144 internal blanket assemblies, and 174 radial blanket assemblies. The burn zone propagates inwardly due to the different enrichments in the inner (9%), middle (11%) and outer core (13%), while depleted uranium fuel with ^{235}U content of 0.25% is loaded into the internal, axial and radial blankets (Kim & Taiwo, 2010).

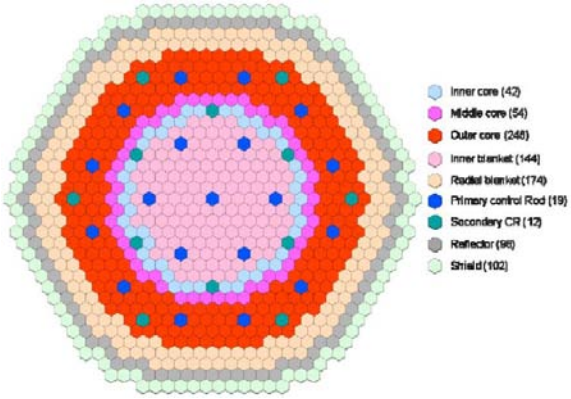

FIGURE 3.9. Map core of the ULFR (Kim & Taiwo, 2010).

Current studies attribute several benefits to the ULFR; these include capital and operational cost reductions, low proliferation risk, and effectively holding LWR spent fuel without disposal until technologies for a closed nuclear fuel cycle are developed and deployed.

3.3.1.7. Sustainable Sodium Cooled Fast Reactor

The Sustainable Sodium-cooled Fast Reactor (SSFR) primary purpose is to develop a sustainable sodium-cooled fast reactor using depleted uranium (DU) feed only; as in the FMSR design. Since the fissile content of depleted uranium is insufficient to make the fast reactor core critical, the core requires fissile material initially. The core however becomes sustainable eventually due to the utilization of bred plutonium.

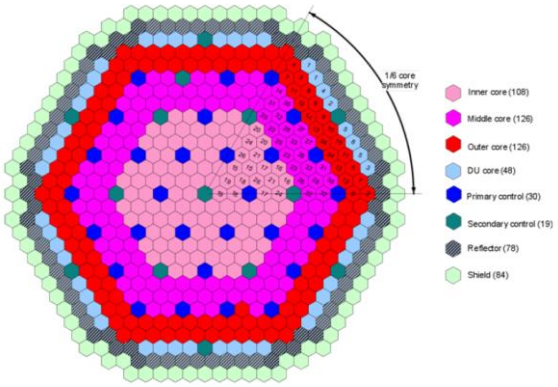

FIGURE 3.10. Radial Core Layout of SSFR (Kim & Taiwo, 2010).

The SSFR adopts a conventional sodium-cooled fast reactor concept, it does not have a thermal zone, as the FMSR. In addition, since a cylindrical core geometry was used in the FMSR feasibility study by BNL (Fischer & Cerbone, 1979) and hence a multi-batch fuel movement was not modeled explicitly, the evaluation for the SSFR has been done using the hexagonal-Z core configuration for more detailed evaluation. The results of the two systems are however expected to be similar.

3.3.2. TWR research reactors

Different TWRs prototypes have been developed because its unique mode of operation and advantages. Its long life operation bring nuclear power to a renewed pathway that offers competitiveness in economic matters. In this section a description of the main prototypes is shown.

3.3.2.1. The Teller et al. Traveling Wave Reactor

The TWR was first introduced by E. Teller, M. Ishikawa and L. Wood in 1996. It consisted on a cylindrical shape thorium fueled with an ignition zone at one end and it was surrounded by graphite neutron reflector. This design also considered desirable the operation of this reactors deep underground, with minimal access to biosphere provided, and in case of accident, coolant conduits could be emplaced so as to be compatible with multiple, redundant emergency single-actuation passage-closure. Figure 3.11 presents a plane section of the Teller et al. TWR reactor core.

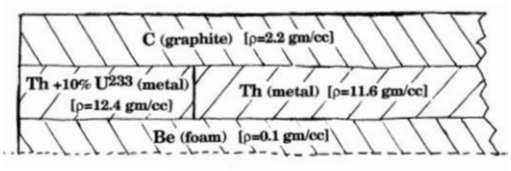

FIGURE 3.11. A diametral plane section of a typical Teller. TWR reactor core (Teller, Ishikawa, & Wood, 1995).

3.3.2.2. The CANDLE concept

The Constant Axial shape of Neutron flux, Nuclide Densities and power shape during Life of Energy Production (CANDLE) was proposed by Hiroshi Sekimoto in 2010. The CANDLE concept is a quite traditional TWR, having a starter ignition zone highly enriched at one end. Depleted uranium will eventually bred enough fissile material in the contiguous zone to the starter fuel until enough fissile isotopes enable the reactor's power to travel along the depleted zone.

FIGURE 3.12. Conceptual drawing of CANDLE (Kim & Taiwo, 2010).

The burn fuel (called also ashes) can be discharged and fresh depleted uranium can be loaded so that the reactor could provide energy as long as depleted uranium is available in the reactor. The CANDLE concept have been analyzed with different coolants, including lead and sodium. Figure 3.12 provides a schematic of the CANDLE concept (Kim & Taiwo, 2010).

3.3.2.3. The Energy Multiplier Module

The Energy Multiplier Module (EM^2) is currently developed by General Atomics, and it would reduce capital investment and power cost by 30% compared to ALWRs. The EM^2 has a nominal power of 500 MW_{th}, 45% efficiency with passively safe characteristics (Rawls, 2010). It has a once-through fuel cycle and consumes and reduces used nuclear fuel inventory. With the EM^2 the need for uranium enrichment is significantly reduced. Figure 3.13 shows the core composition and arrangement of the EM^2.

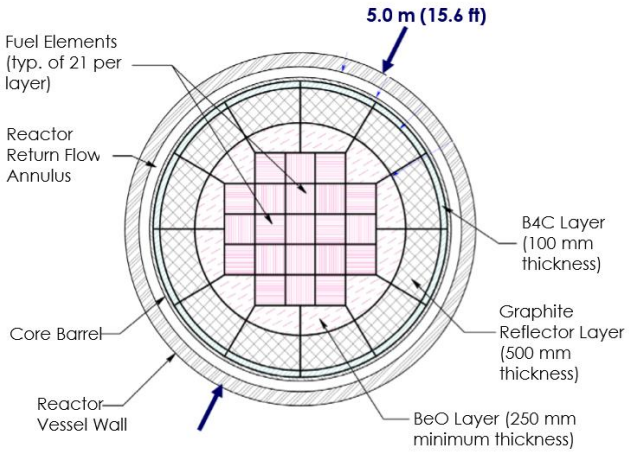

FIGURE 3.13. EM^2 core composition and arrangement (Rawls, 2010).

EM^2 reduces the risk of weapons material proliferation through an enhanced fuel utilization that reduces the spent fuel inventory. The EM^2 employs a closed fuel cycle without the use of conventional reprocessing. It would operate for about 30 years without reshuffling or refueling.

4. MCNP6 CODE DESCRIPTION

The Monte Carlo method is a statistical sampling technique that over the years has been successfully applied to a vast number of scientific problems. Although Monte Carlo calculations are costly, they give a result of which the accuracy is exactly known and the calculation costs can be adjusted to meet the required precision.

This chapter discusses the Monte Carlo method and its implementation in the nuclear applications. Particularly, the Monte Carlo N-Particle 6 (MCNP6) is of special interest because its utilization in the current study.

4.1. The Monte Carlo method

4.1.1. Fundamental principle of the Monte Carlo method

The solution of many problems can be expressed in terms of an integration of a function. Despite the major interest is obtain a numerical value from such expressions, it may be difficult or tedious to obtain analytically. For integrals of the form:

$$I = \int_{\Omega} f(x)dx \qquad (4\text{-}1)$$

being Ω the domain of integration, the integral I can be related to an expectation of a random variable with respect to some probability measure. For probability measures of a random variable X that have a density $\rho(x)$ the expectation can be expressed as:

$$E\big(f(X)\big) = \int_{\Omega} f(x)\rho(x)dx \qquad (4\text{-}2)$$

This integral can be expressed in terms of an expectation in a number of different ways. One general approach is to use a density having the feature that $\rho(x) > 0$ whenever $f(x) \neq 0$.This gives that (Atzberger, 2004):

$$I = \int_{\Omega} f(x)dx = \int_{\Omega} \frac{\big(f(x)\big)}{\big(\rho(x)\big)}\rho(x)dx \qquad (4\text{-}3)$$

$$= E\left(\frac{f(X)}{g(X)}\right) = E\big(g(X)\big) \qquad (4\text{-}4)$$

where$g(X) = \left(\frac{f(X)}{g(X)}\right)$. In the case of a domain of integration Ω is finite, random variable X uniformly distributed on Ω with density $\rho(x) = \frac{1}{|\Omega|}$ to obtain:

$$I = \int_{\Omega} f(x)dx = \int_{\Omega} \frac{f(x)}{\frac{1}{|\Omega|}} \frac{1}{|\Omega|} dx \qquad (4\text{-}5)$$

$$= |\Omega| E\big(f(X)\big) \qquad (4\text{-}6)$$

The utility of expressing the integral in terms of an expectation derives from the Law of Large Numbers[1], which states that for a collection of independent identically distributed random variables $\{X_i\}_{i=1}^{\infty}$

$$E\big(g(X)\big) = \lim_{N\to\infty} \frac{1}{N} \sum_{i=1}^{1} g(X_i) \qquad (4\text{-}7)$$

This offers a way to estimate the numerical value of *I* (Atzberger, 2004):

- Generate N random variates $\{X_i\}_{i=1}^{N}$with distribution $\rho(x)$ on Ω.
- Approximate the expectation using the Law of the Large Numbers $I \approx \frac{1}{N}\sum_{i=1}^{1} g(X_i)$

4.1.2. Precision and accuracy of the Monte Carlo Method

Since the Monte Carlo method is an esthocastic method it has uncertainties related to the calculated results. There are confidence intervals that indicate the precision in the Monte Carlo, being these stronly related to the standart deviation of the calculation. Thus, it is more convinient to have larger confidence intervales with the less possible standart deviation, using variance reducition techniques.

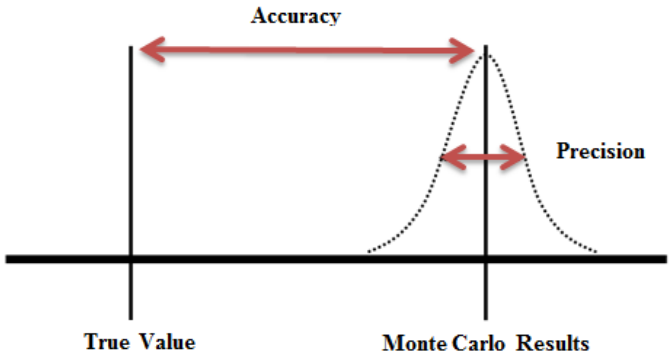

FIGURE 4.1. Schematic diagram of the definition for accuracy and precision (Saidi, Sadeghi, & Tenreiro, 2013).

[1] The law of large numbers is a theorem that describes the result of performing the same experiment a large number of times, being this consistent with the frequency interpretation of probability. This law make statements about the convergence of a sequence of experiments ($\bar{X}_n$) to an expected value. Usually two major categories are distinguished: *Weak Laws* versus *Strong Laws*. The Strong Laws deal with probabilities involving limits of $\bar{X}_n$, while the weak laws deal with limits of probabilities involving $\bar{X}_n$ (Verhoeff, 1993).

The confidence intervals are valid only if the physical phase space is adequately sampled by the Monte Carlo calculation. There are several factors that can affect the precision in these calculations, such as the variance reduction techniques and the number of histories simulated. Generally uncertainty or error caused by the statistical fluctuation of the x_i, refers to the precision of the results and not to the accuracy. Accuracy is a measure of how close the sample mean, is to the true mean (Saidi, Sadeghi, & Tenreiro, 2013). Figure 4.1 shows a schematic diagram of the definition for accuracy and precision.

The accuracy of the Monte Carlo method can be estimated as:

$$error = \left| \frac{1}{N} \sum_{i=1}^{N} g(X_i) - I \right| \qquad (4\text{-}8)$$

$$\approx \left| \frac{\sigma_g}{\sqrt{N}} \eta(0,1) \right| \qquad (4\text{-}9)$$

where

$$\sigma_g^2 = \int_{\Omega} (g(x) - I)^2 \rho(x) dx \qquad (4\text{-}10)$$

And $\eta(0,1)$ denotes a standard normal random variable with mean zero and variance 1. The last approximation was obtained by using the *Central Limit Theorem*[2], which states that for a sum of independent and identically distributed random variables Y_i with mean μ and finite variance σ^2:

$$\frac{\sum_{i=1}^{N} Y_i - N\mu}{\sigma\sqrt{N}} \rightarrow \eta(0,1), as\ N \rightarrow \infty \qquad (4\text{-}11)$$

The error converges asymptotically at a rate $\frac{1}{\sqrt{N}}$ independent of the dimensionality of the problem considered (Atzberger, 2004).

4.1.3. Monte Carlo method applied to the transport equation

The Monte Carlo method can also be applied to obtain an approximation to the solution of the transport equation. The history of neutrons is reproduced in this method, recreating the different interactions of this particle with the medium, since there are strongly related to probability distributions functions.

It is worth to mention that the Monte Carlo method is based on statistics, reason for which, there is not a unique solution, but a confidence interval around the exact solution. To reduce the range around the exact solution, a large number of history particles is required to be traced, which directly increases considerably the calculation time (François, 2008).

[2] This theorem says that the sum of mutually independent random variables, can be is well-approximated by a certain type of continuous function known as a normal density function.

The neutron's history starts with birth, by fission or any external source, and finishes with the absorption or leakage of the system. Between these determinant events, the neutron experiences different interaction that are registered in the neutron's history. We shall now consider an originated particle in A with energy, direction and known coordinates, as seen in Figure 4.2. This particle travels a distance S_0 until a scattering event happens, changing its direction and energy that can be inferred through statistical calculations (François, 2008).

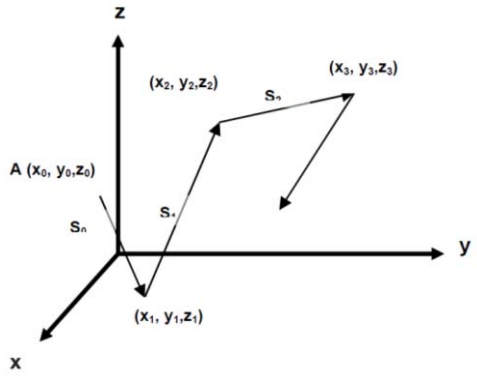

FIGURE 4.2. Path of a particle through a medium (François, 2008).

It is fundamental to trace each particle by knowing its spatial coordinates, energy and spherical direction, being these enough to define the state of α, where:

$$\alpha \equiv \alpha(x, y, z; E; \theta; \phi) \qquad (4\text{-}12)$$

Thus, the neutron history comprehends every collision like a succession of states $\alpha_0, \alpha_1, \ldots, \alpha_n$, where the k-th state is:

$$\alpha_k \equiv \alpha_k(x_k, y_k, z_k; E_k; \theta_k; \phi_k) \qquad (4\text{-}13)$$

There are mathematical procedures to determine the position of the next collision, as well as the energy and particle direction. Consider that ***s*** is the distance that travels the particle without colliding and Σ_t being the macroscopic cross section. The probability of the particle not interacting with the medium is given by $e^{-\Sigma_t s}$, and the probability that a particle would have a collision is $\Sigma_t ds$, therefore, the probability function that describes the particle interactions between **s** and **s+ds** is given by equation 4-14.

$$\Sigma_t e^{-\Sigma_t s} ds \qquad (4\text{-}14)$$

From equation 4-14 **s** can be randomly determined, then the collision coordinates can be obtain as shown in equation 4-15

$$\begin{aligned} x_{i+1} &= x_i + s_i(\sin\theta_i \cos\phi_i) \\ y_{i+1} &= y_i + s_i(\sin\theta_i \sin\phi_i) \\ z_{i+1} &= z_i + s_i(\cos\theta_i) \end{aligned} \qquad (4\text{-}15)$$

The relation between the physic event and the random number is fundamental in this method, and it can be done by a probability function *p(x)*, which describes the relative frequency of the random variable *x* comprehended in a determined interval. This probability function can also be defined as the probability of the random variable in analysis to be within the interval *(x, x+dx).*

A function probability is given by expression:

$$prob(x < X < x + dx) = p(x) \qquad (4\text{-}16)$$

Where p(x) is the probability of an interaction within the interval *(x, x+dx)* and if x occurs in an continuous interval:

$$prob(a < x < b) = \int_a^b p(x)dx \qquad (4\text{-}17)$$

It is due to this expressions that the Monte Carlo method can be applied to the integro-differential transport equation, which can be seen as the balance of three different mechanisms (Papadakis, 2010):

- Net neutron current incoming and outgoing of the volume ΔV.
- Absorption or scattering events that causes the neutron to lose its energy and change its direction.
- Neutron emission in the volume ΔV due to scattering from other energies and directions and fission neutrons and external sources.

Then, the balance can be stated as follows:

$$\begin{aligned}(Increase\ in\ N) = (emitted\ neutrons) - (lost\ outgoing\ neutrons\ from\ \Delta V) \\ - (lost\ neutrons\ due\ absorption\ or\ scattering)\end{aligned} \qquad (4\text{-}18)$$

Equation *4-18* can be mathematically expressed as shown in equation *4-19,* which is valid for a given volume system V.

$$\begin{aligned}&\frac{1}{v(E)}\frac{\partial\varphi(\vec{r},E,\hat{\Omega},t)}{\partial t} + \hat{\Omega}\cdot\nabla\varphi(\vec{r},E,\hat{\Omega},t) + \Sigma_t(\vec{r},E)\varphi(\vec{r},E,\hat{\Omega},t) \\ &= \int_{4\Pi} d\hat{\Omega}' \int_0^{\infty} dE'\Sigma_s(\vec{r},E'\to E,\hat{\Omega}'\to\hat{\Omega})\varphi(\vec{r},E',\hat{\Omega},t) + s\,(\vec{r},E,\hat{\Omega},t)\end{aligned} \qquad (4\text{-}19)$$

where:

t	Time
E	Energy
$\vec{r}$	Position vector
$\hat{\Omega}$	Unit vector in direction of motion
$\Sigma_t(\vec{r},E)$	Macroscopic total cross section
$s(\vec{r},E,\hat{\Omega},t)$	Source term
$\Sigma_s(\vec{r},E'\to E,\hat{\Omega}'\to\hat{\Omega})$	Double differential scattering cross section
$\varphi(\vec{r},E,\hat{\Omega},t)d\vec{r}dEd\hat{\Omega}$	Angular neutron flux

4.2. MCNP6 characteristics

The Monte Carlo N-Particle (MCNP) code is developed by Los Alamos National Laboratory, and is a general purpose code that can be used for neutron, electron or coupled neutron/photon/electron transport. The applications in which it is often used are radiation protection, radiation shielding, radiography, medical physics, nuclear criticality safety, decontamination and decommissioning and fission reactor design, being the latter the central application of this code in this study.

This code uses a nuclear data library based in particular cross-section evaluations such as the Evaluated Nuclear Data Files (ENDF). It also treats an arbitrary three-dimensional configuration of materials in geometric cells bounded by first- and second-degree surfaces.

In reactor physics MCNP application an input must be elaborated in which geometry must be defined through cells and surfaces, then, different materials can fill the defined cells. Accurate and explicit models can be made in the MCNP6 at different levels, in which very complex designs can be well simulated.

Criticality calculations can be estimated by averaging a number of neutron histories with the MCNP6 code. The effective multiplication factor (k_{eff}) in the MCNP code is given by the number of generated neutrons via fission per cycle divided by the evaluated neutrons histories in the current cycle. The associated error in the estimation of the k_{eff}, usually decreases proportionally according the number of cycles of k_{eff}, hence, It is required a large number of cycle in order to achieve a good estamation.

In the MCNP6, the k_{eff} is estimated by the expression 4-20 (François, 2008).

$$keff = \frac{1}{N}\sum_{i=1}^{N} k_i \qquad (4\text{-}20)$$

In summary, a sequence of randon numbers is used to produce a random distribution of quantities that simulate the analysis problem. An example of how the Monte Carlo method is used to obtain the multiplication factor is shown below (François, 2008):

1. Determine the neutron position at the beginning of the first cycle.
2. Utilize a random number to assign the neutron energy.
3. Utilize the next random number to determine the neutron cosine direction.
4. Determine the localization of the next collision with the next random number. Notice that the neutron traveled distance directly depends of the material cross section.
5. Verify the new position of the neutron in order to determine if the particle has leaked from the system, if that occurs, it adds one element to the leaks and starts over the step 1.
6. Determine the occurred interaction, each interaction has a cross section that assigns the occurrence probability:
    a) If scattering interaction happens, the neutron energy after the scattering must be determined using the next random number.
    b) If absorption occurs, turn to step 1 and start over the step 1 with a new neutron.

c) If a fission occurs, determine how many neutrons are produced (using code libraries) and determine the total number of produced neutrons in the cycle. It should be determined the position of the fission generated neutrons to start up the next cycle.

This process should be repeated as required in order to obtain a proper calculation.

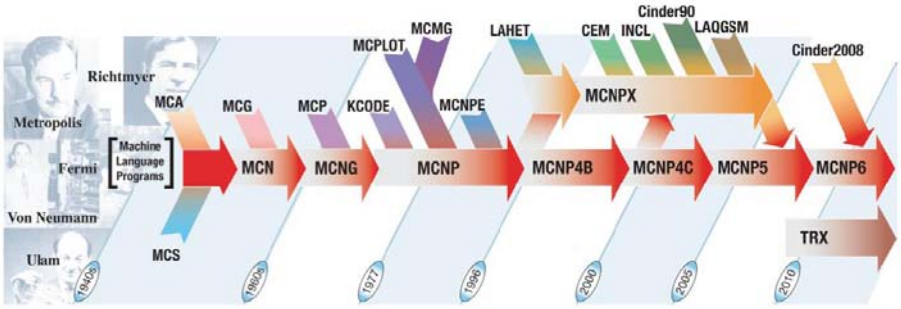

FIGURE 4.2. MCNP history (Brown, Kiedrowski, & Bull, 2013)

Different versions of MCNP have been developed as seen in Figure 4.3. In this study, the sixth version of the MCNP code (MCNP6) is used, which includes the MCNPX and MCNP5 best features (Brown, Kiedrowski, & Bull, 2013):

- All MCNP5-1.60 capabilities (mpI+threads)
- All MCNPX 2.7.0 capabiliies (mpi)
- Adjoint-weighted perturbation estimators
- CINDER 2008 decay & depletion
- High energy protons and magnetic fields, for proton radiography
- Unstructured mesh, for linking ABAQUS
- Structures mesh, for liking PARTISN

The MCNP6 code has been one of the most concurred computational tools due to its wide application, and in particular, in reactor physics is considered a reference code. Despite its calculation cost requires too much time, the obtained results are considerably accurate.

The MCNP6 has a depletion burnup subroutine called CINDER90, which is a FORTRAN program with a data library used to calculate the inventory of nuclides in an irradiated material. Nuclide inventory code in CINDER90 follows the conversion of a nuclide to a different nuclide by a particle absorption and/or radioactive decay. Figure 4.4 depicts the Monte Carlo linked depletion process.

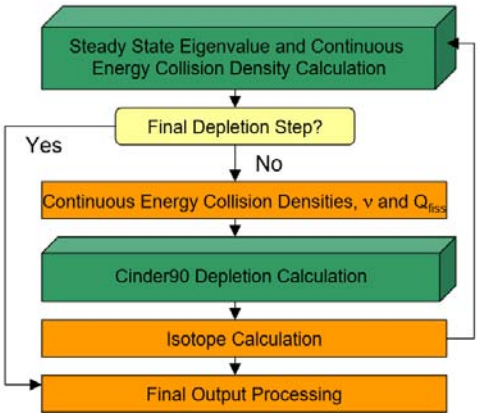

FIGURE 4.3. Monte Carlo Linked Depletion Process (James & McKinney, 2007).

The depletion equation that uses the CINDER90 code uses time-dependent fluxes, interaction rates, and nuclide number densities to determine the time-dependent nuclide inventory. The depletion equation is shown in equation 4-31.

$$\frac{dN_A}{dt} = -\lambda_A N_A - \left[\sum_g \sigma_{a_g}^A \phi_g\right] N_A + \lambda_B \lambda_B + \left[\sum_g \sigma_{\gamma_g}^C \phi_g\right] N_C \qquad (4\text{-}21)$$

where

$-\lambda_A N_A$ is the loss due to radioactive decay of A

$-\left[\sum_g \sigma_{a_g}^A \phi_g\right] N_A$ is the loss due to neutron capture by A

$\lambda_B \lambda_B$ is gain due to decay of B to A

$\left[\sum_g \sigma_{\gamma_g}^C \phi_g\right] N_C$ is the gain to transmutation of C to A via neutron capture

Since the time-dependent flux also is dependent on the time-dependent nuclide density, thus making the depletion equation nonlinear. CINDER90 deals with this nonlinear equation through the predictor-corrector method, by setting the time-dependent flux as a constant value over the burn step, then a "predicted" value of number densities, fluxes, and interaction rates is calculated for a time step duration. Values are corrected by redepleting the system over the same time step, incorporating the new calculated fluxed and interaction rates.

Parallel processing is one of the major trends in computing technology, mainly because of its faster processing for iterative calculations. Fortunately, the MCNP6 has implemented this resource in the computational calculations, which saves great amount of time in comparison with the sequential programming.

5. ASTRID REACTOR SIMULATION

The simulations concerning the ASTRID nuclear reactor are discussed in this chapter, starting with a description of the model main characteristics, which are the basis of the developed models.

The ASTRID developed model is validated with the result provided by the European Benchmark on the ASTRID-like low-void-effect core characterization, presented in the ICAPP conference in Nice, France, on May 2015.

Once the ASTRID model was validated, a metallic-fueled ASTRID design is proposed and compared with the conventional oxide-fueled ASTRID concept, remarking the different capabilities of each models. Simulations were performed with MCNP6 and simulations were performed with a hundred active cycles of 15000 neutrons for a total of a million and a half neutron histories.

5.1. Model characteristics

The ASTRID nuclear reactor was first introduced in section 2.3.6, in which a general description of the nuclear reactor is given. In this section a technical description is provided with the purpose of understanding the main characteristics of the ASTRID reactor.

There are two different concepts for the ASTRID nuclear reactor. The first is a conventional SFR design, where a seed is surrounded by fertile blankets while in the peripheral zone reflector and neutron shielding subassemblies are placed.

The second ASTRID's design is the low void effect core or CFV concept (CFV: *Cœur à Faible effet de Vidange sodium*). This evolutionary design presents a large gain on the total sodium void effect because of the presence of a sodium plenum zone, an absorbing zone in upper shielding and an internal fertile zone in the core geometry. Figure 5.1 depicts the ASTRID configuration through the different zones in the reactor.

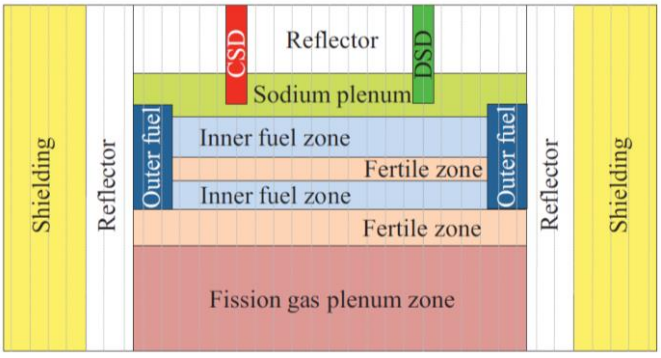

FIGURE 5.1. Heterogeneous structure of the low-void-effect (ASTRID-like) core (Bortot, et al., 2015).

A pre-conceptual ASTRID CFV design has been developed mainly by CEA, AREVA and EDF (Chenaud, et al., 2013); study from which the dimensions and characteristics of the reactor are taken. Some basic parameters are shown below in Table 5.

TABLE 5. Main ASTRID parameters

Parameter	CFV-V1
Number of fuel sub-assemblies (Inner zone / Outer zone)	291 (177 / 114)
Number of pins per sub-assembly	217
S/A pitch (cm)	17.611
Sodium inter-assembly gap thickness (cm)	0.473
Inner zone / outer zone fissile height (cm)	60 / 90
Inner fertile zone / lower axial blanket (cm)	20 / 30
Inner zone / outer zone Na plenum (cm)	40 / 30
Circumscribed diameter of the core (cm)	340
Enrichment (PuO_2)	21.6 %
Nominal thermal power (MW)	1500

The behavior during transients is one of the interesting features of this reactor, such as the unprotected loss of flow (ULOF), unprotected loss of heat sinks (ULOHS), condition involving control rod withdrawal (CRW) or the total loss of power transient, where the CFV concept has proved a valuable safety improvement.

Different CFV ASTRID versions are currently developed at CEA, where the main purpose of these designs ensure the safety characteristics that are the principal concern in a sodium-cooled fast reactor. A CFV2 design has been conceived, wherein the amount of fuel pins has been increased per subassembly and the duct wall thickness and the inter-assembly gap was optimized.

In the current study the first CFV version is analyzed, firstly by developing a heterogeneous ASTRID model as described in this section. Then, a proposed metallic-fueled ASTRID design is shown in order to compare the different capabilities of these.

5.2. Model elaboration

The developed ASTRID model was done taking into account the characteristics given in the European Benchmark on the ASTRID-like low-void-effect core characterization, presented in the ICAPP conference in Nice, France, on May 2015.

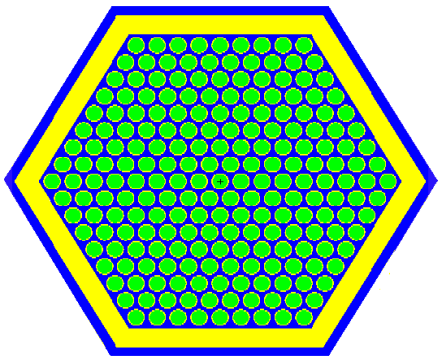

FIGURE 5.2. Assembly cross-section of the ASTRID nuclear reactor.

The construction of the model was done taking into account the parameters shown in Table 5. It is to notice that some reactors parameters were not available during the input elaboration, same that were inferred. Figure 5.2 shows the subassembly cross-section, composed by 217 pins, the duct and the sodium inter-assembly gap thickness.

Different zones were considered in the ASTRID model, such as the fission gas plenum zone, the fertile zone, the fissile zone, the sodium plenum and the reflector and neutronic protection. Figure 5.3 shows a description of the distribution of these zones in the reactor, all surrounded by sodium.

In order to accomplish our study objective, the different temperatures in the reactor materials were taken into account in our ASTRID model. Table 6 gives the different temperatures at which our model was built.

TABLE 6. Temperatures in the reactor materials.

	Temperature (K)
Fuel in fissile zone	1500
Fuel in fertile zone	900
AIM1 cladding	750
Sodium coolant	750

In Figure 5.3 it is possible to observe the axial distribution along the reactor, in which a gas plenum is placed at the bottom of the design. A lower fertile zone blanket, an intermediate fissile zone, an intermediate fertile blanket, followed by a fissile area and a sodium plenum, composes the inner fuel zone, while a fissile region and the sodium plenum comprise the outer fuel zone.

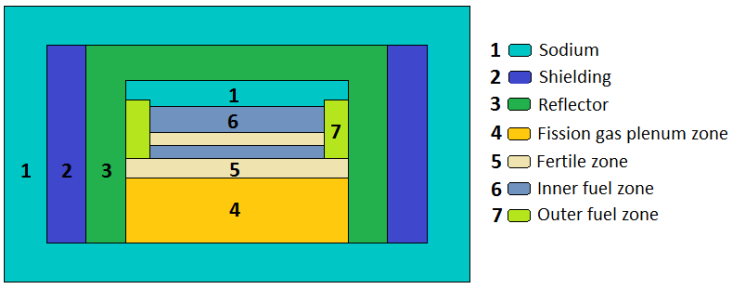

FIGURE 5.3. Axial nuclear reactor core cross section.

The radial configuration is shown in Figure 5.4 for the oxide ASTRID-like model. The inner zone is located in the center of the reactor composed of 177 fuel subassemblies (4 diluent assemblies), 6 safety rods and 12 control rods. In the developed model control and safety rods are supposed completely extracted. The outer zone encloses the inner zone with 114 fuel subassemblies. Reflector subassemblies enclose the outer fuel zone, with a total of 216 subassemblies, and around the latter, the shielding subassemblies which are 354.

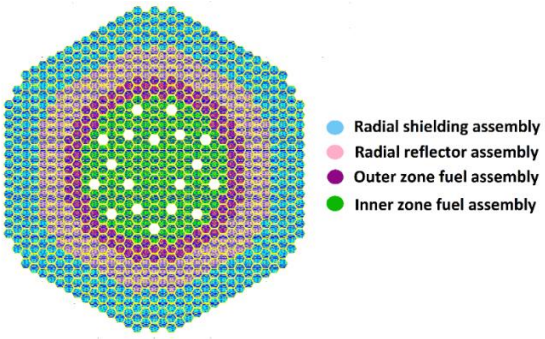

FIGURE 5.4. ASTRID core map.

5.3. Oxide-fueled ASTRID results

In order to validate our ASTRID model, three different parameters are compared to the obtained values on the European Benchmark on the ASTRID-like low-void-effect core characterization, presented in the ICAPP conference in Nice, France, on May 2015 (Bortot, et al., 2015), in which ten participating institutions provided quantitative information about neutronic parameters and safety coefficients.

In this paper three different neutronic parameters are presented for the ASTRID developed model: Keff at End of Cycle (EoC), Doppler constants and coolant void worths. These parameters were obtained using MCNP6 nuclear code, with JEFF-3.2 cross sections library. Since CIEMAT also used MCNP6, a specific comparison with this participant will be done.

Simulations were performed with a hundred active cycles of 15000 neutrons for a total of a million and a half neutron histories, five different time steps (0, 65, 165, 265, 365 days) and TIER 2, which is a selected daughter products in the chain depletion.

5.3.1. Keff at End of Cycle (EoC)

One cycle of operation was simulated with the parameters described in Table 5. In Figure 5.5, the effective multiplication factor is presented, which is within the expected value, since it has a very close approximation to other institutions results.

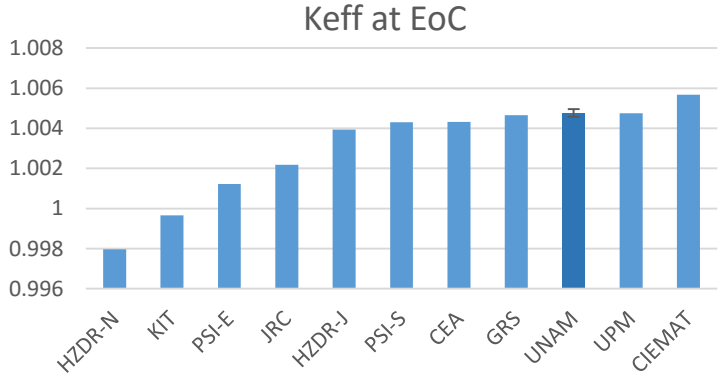

FIGURE 5.5. Effective neutron multiplication at EoC.

A 90 pcm difference is registered when comparing our result with the reported by CIEMAT. Less than 100 pcm difference is achieved for six of the ten benchmark participants, while the larger difference is found to be -681 pcm when comparing with HZDR-N, whose value is far from all the participants.

5.3.2. Doppler constants[3]

Four different cases are analyzed in this section: for the first two cases involving the fissile fuel temperature perturbations, a decrease from 1500 K to 1200 K (K_{D1}) and an increase from 1500 K to 1800 K (K_{D2}) are presented, while for the fertile zone temperature perturbations, a decrease from 900 K to 600 K (K_{D3}) and an increase from 900 K to 1200 K (K_{D4}) are considered.

Large discrepancies are found between the Doppler constant values obtained by the benchmark participants, which it is more significant for stochastic codes, possibly due to an insufficient statistics[10]. The four cases are compared in Figure 5.6, in which the benchmark participant's results, and average value (dashed line) are also shown.

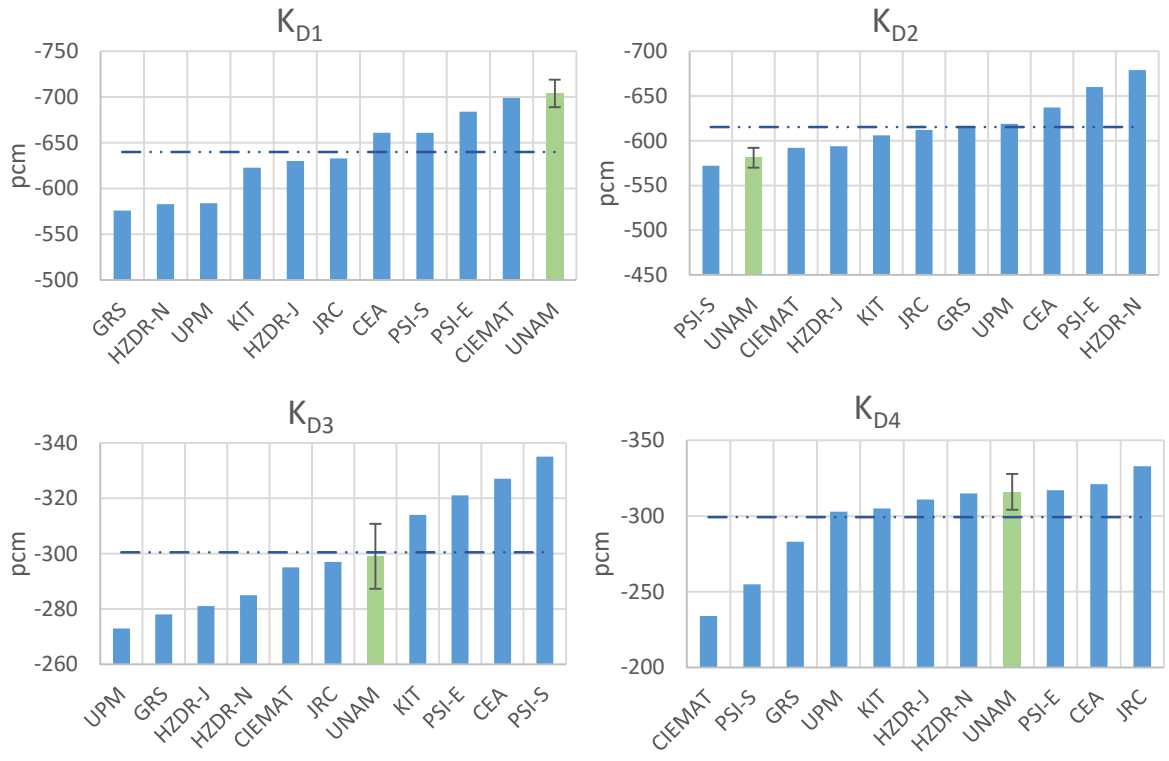

FIGURE 5.6. Doppler constants.

[3] Doppler constant is defined as $K_D = T\frac{dk}{dT}$ and it was determined by solving the integral $\rho_D = K_D \int_{T_1}^{T_2} \frac{dT}{T}$, which results in $K_D = \frac{\rho_D}{ln\left(\frac{T_2}{T_1}\right)}$

It is to be noticed that the obtained Doppler constants in these simulations are within the range of the benchmark participants for three of the four cases (K_{D2}, K_{D3} and K_{D4}), and only K_{D1} is 5 pcm out of range.

Given that CIEMAT used MCNP6.1 too, a particular similitude between the values obtained by this institution and the obtained in this paper is found. For cases K_{D1} and K_{D2} slightly differences of 5 and 4 pcm are respectively achieved, while an 11 pcm discrepancy is found in case $K_{D3.}$ The larger discrepancy was identified in case K_{D4}, in which an 82 pcm variation was registered.

In general terms it can be said that the Doppler constants were successfully determined, since the obtained values have only a small difference compared with those reported by the benchmark participants.

5.3.3. Coolant void worth

Since the main characteristic of this reactor is to obtain a negative reactivity for coolant void, this section represents a fundamental concept of the CFV ASTRID design. Three different divisions of the core are defined, which are: above the inner zone, above the outer zone and all fuel regions. With these three regions, five different scenarios were studied and presented in this section.

Benchmark participants divided the core in: lower fissile region of inner zone (Lower IF), inner fertile region of inner zone (IB), upper fissile region of inner zone (Upper IF), fissile region of outer zone (OF), above inner fissile zone (above IF), above outer zone fissile (above OF).With various combinations of these sections, nine different scenarios were analyzed.

Five of these nine scenarios were studied in this work: Figure 5.7 shows the corresponding schematics of the presented scenarios.

S1: Above inner zone.

S2: Above outer zone.

S3: Above inner and outer zone.

S4: Inner and outer zone.

S5: Above inner and outer zone and inner and outer zone.

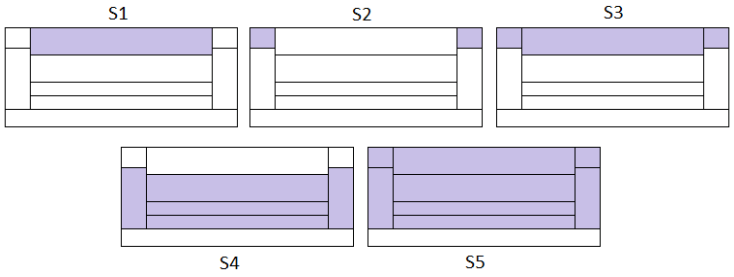

FIGURE 5.7. The five different scenarios on coolant void worth.

The five analyzed scenarios match with the benchmark reported results. The lack of numerical results from the benchmark participants led us to perform a graphical comparison shown in Figure 5.8, in which benchmark participant results (color lines) has been directly taken from the European Benchmark on the ASTRID-like low-void-effect core characterization and the results obtained in this work are presented in dashed lines in the same figure. Figure 5.8 also presents the reactivity effect in each analyzed scenario.

As expected, scenarios where sodium plenum void is involved, a negative reactivity effect is registered, whereas fuel regions voiding have a large positive effect. An interesting finding is that the total voiding in the reactor has a negative reactivity effect, which is the main objective of this design.

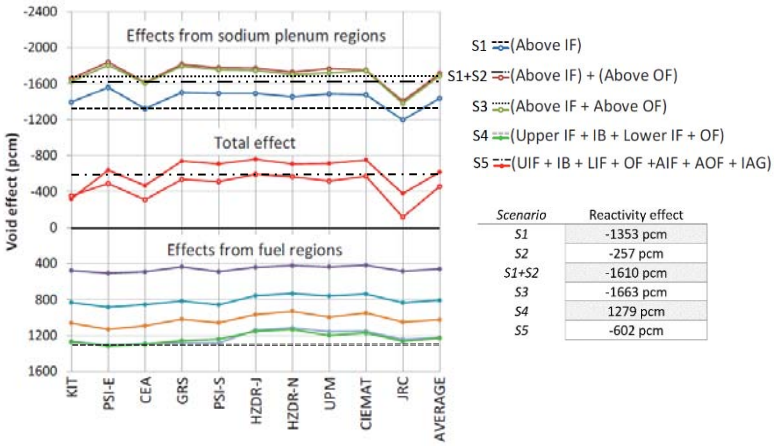

Scenario	Reactivity effect
S1	-1353 pcm
S2	-257 pcm
S1+S2	-1610 pcm
S3	-1663 pcm
S4	1279 pcm
S5	-602 pcm

FIGURE 5.8. Coolant void worth comparison.

Benchmark participants obtained an average reactivity effect of -1600 pcm and 1200 pcm (Bortot, et al., 2015) from voiding of plenum regions and average fuel voiding, respectively, which is very similar to the results obtained in this work for scenario 3 (-1663 pcm) and 4 (1279 pcm) respectively. The obtained values do not differ largely from those of CIEMAT, in average, these values were within the range reported by the institutions, which lead to a positive conclusion in the validation of our ASTRID model.

5.4. Metallic-fueled ASTRID-like reactor description

There are considerable advantages in using metallic fuel in SFRs. One advantage of using metallic nuclear fuel is that it is possible to achieve a harder neutron spectrum than in the oxide nuclear fuel, mainly because of the lack of moderation of the matrix (Zr). It also has a simplified fabrication, involving melting and casting processes, which avoids the problem of radiotoxic dust hazard.

Metallic and oxide nuclear fuel have different thermo-physical properties, such as a larger density in the metallic fuel, lower melting temperature and larger thermal conductivity (Judkins & Olsen, 1979). Metallic fuels have demonstrated acceptable performance and reliability up to 10 at% burnup, reason why it is considered as a good candidate to be implemented in sodium-cooled fast reactors (Sofu, 2015) . Irradiation experience has been gained mainly in the United States (EBR-II and FFTF) (Sofu, 2015).

In this section a metal-fueled ASTRID design is presented in order to observe the different advantages in using this kind of reactor. In the next section a comparison between the oxide and metallic fueled ASTRID-like reactors is done, regarding their different behavior in the presented neutronic properties.

The developed metallic nuclear fuel rods have the fuel slug distributed in an annular distribution. It also has a large fission gas plenum below the fuel slug to accomplish high burnup as well as a low density gas gap that mitigates the fuel swelling. Figure 5.9 depicts the assembly cross-section and the fuel rod of the metallic-fueled ASTRID nuclear reactor.

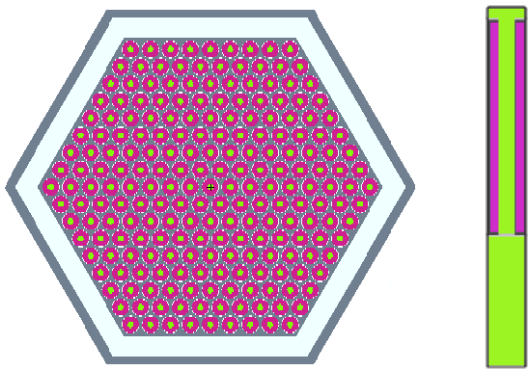

FIGURE 5.9. Assembly cross-section (left) and fuel rod (right) of the metallic-fueled ASTRID nuclear reactor.

The metallic model was built with the purpose of having the same reactivity at the end of cycle that the oxide design used in the ASTRID benchmark, and as a consequence, the enrichment of the metallic fuel was found to be 17.3%. Different enrichments were used in each fuel, mainly because of the isotopic density increases in the metallic fuel, therefore, the oxide fuel enrichment was as specified in Table 5 and the metallic enrichment is 17.3% in plutonium. Depleted uranium was used in the fertile zone with zirconium as matrix (U-10Zr).

Table 7 gives the nuclide fraction assigned to the fissile material and to the fertile material for both, oxide (MOX) and metallic (UPuZr) nuclear fuel.

TABLE 7. Nuclide fraction of the oxide and metallic fuel.

	MOX (UO_2-21.6PuO_2)		**Metallic fuel (U-17.3Pu-10Zr)**	
	Fissile Zone	Fertile Zone	Fissile Zone	Fertile Zone
U-235	0.005293405	0.002203745	0.00523152	0.00225
U-238	0.729901718	0.879294343	0.72136848	0.89775
Pu-238	0.00567151	-	0.0048552	-
Pu-239	0.10431519	-	0.089301	-
Pu-240	0.05448696	-	0.0466446	-
Pu-241	0.0214707	-	0.0183804	-
Pu-242	0.01660941	-	0.0142188	-
O/Zr	0.062251119	0.118501912	0.1	0.1

Metallic fuel rod dimensions are taken from the Nuclear Fuel Fabrication and Refabrication Cost Estimation Methodology done by the Oak Ridge National Laboratory (Sofu, 2015). The cladding is composed with HT-9 martensitic steel alloy (Chen, 2013).

It is to notice that metallic fuel temperature was simulated at 1200 K instead of 1500 K for the fissile zone, because of the higher thermal conductivity of metallic fuel (Sofu, 2015).

Simulations were performed with a hundred active cycles of 15000 neutrons for a total of a million and a half neutron histories, five different time steps (0, 65, 165, 265, 365 days) and TIER 2, which is a selected daughter products in the chain depletion.

5.5. Comparison between metallic and oxide fueled ASTRID-like reactors

In this section a comparison between the developed oxide and metallic design is done in order to highlight the differences and advantages of each model. A metallic proposed design was selected in because its breeding capabilities could enhance the fuel utilization. Despite the oxide fuel has gained lot of operation experience, the metallic fuel has neutronic and thermophysical advantages that make this fuel preferable for SFRs.

5.5.1. Keff during one cycle.

The effective neutron multiplication factor (Keff) behavior during one cycle of operation is shown in Figure 5.10, where it is possible to see that both fuel types: metallic and oxide, achieve one year of operation (365 days) as it was expected.

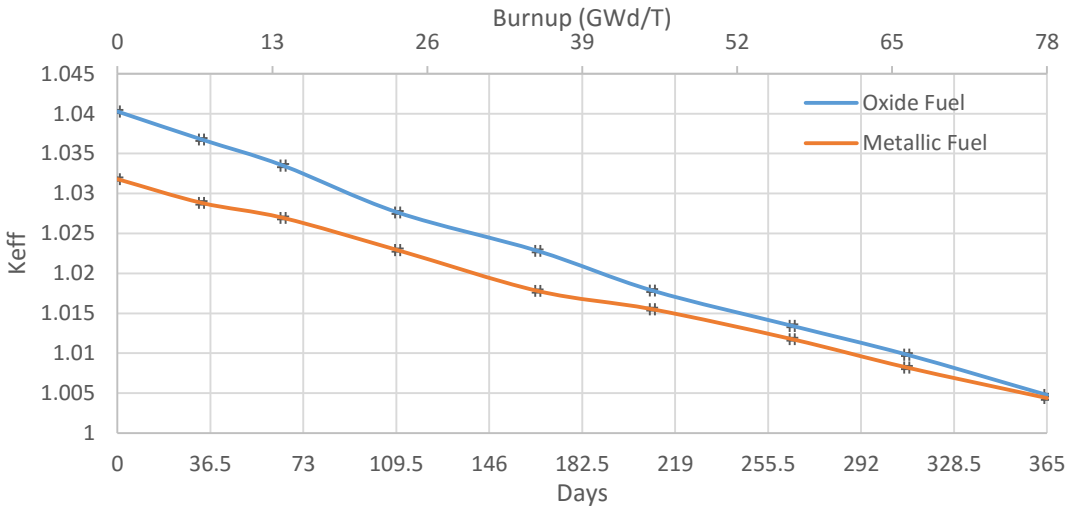

FIGURE 5.10. Keff during one cycle of operation.

The Keff difference between oxide and metallic models at the beginning of the cycle decreases as the simulation goes on, and the difference at the end of the cycle is 39 pcm. The Keff difference decreases (different slope of the Keff vs burnup curve) mainly because of the different breeding capability between the oxide and the metallic fuel, since, as it will be shown afterwards (Figure 5.16), the breeding capability (^{239}Pu) is higher in the metallic fuel.

5.5.2. Doppler constants

Four different Doppler constants are analyzed in this section, two of them concerning the fissile fuel temperature perturbations for the oxide design: a decrease from 1500 K to 1200 K (K_{D1}) and an increase from 1500 K to 1800 K (K_{D2}), while for the metallic model a decrease from 1200 K to 900 K (K_{D1}) and an increase from 1200 K to 1500 K (K_{D2}) is considered.

The fertile zone temperature perturbations consist of a decrease from 900 K to 600 K (K_{D3}) and an increase from 900 K to 1200 K (K_{D4}) for both models. Figure 9 shows a comparative chart of the obtained values for oxide and metallic models.

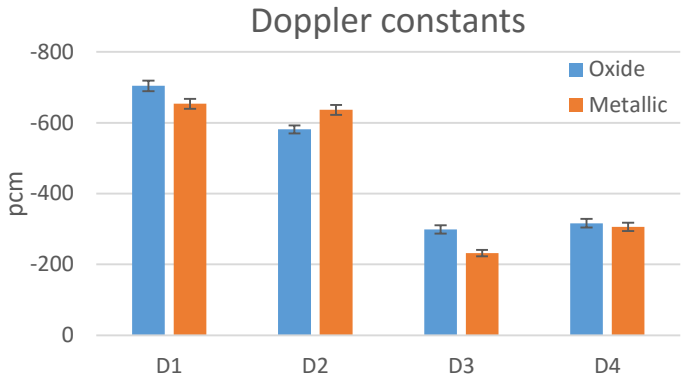

FIGURE 5.11. Doppler constants comparison for oxide and metallic models.

5.5.3. Coolant void worth

Five different scenarios are presented in this section, which are the same as presented in section 4.1.3. Figure 5.13 presents the coolant void worth comparison between oxide and metallic fueled ASTRID models.

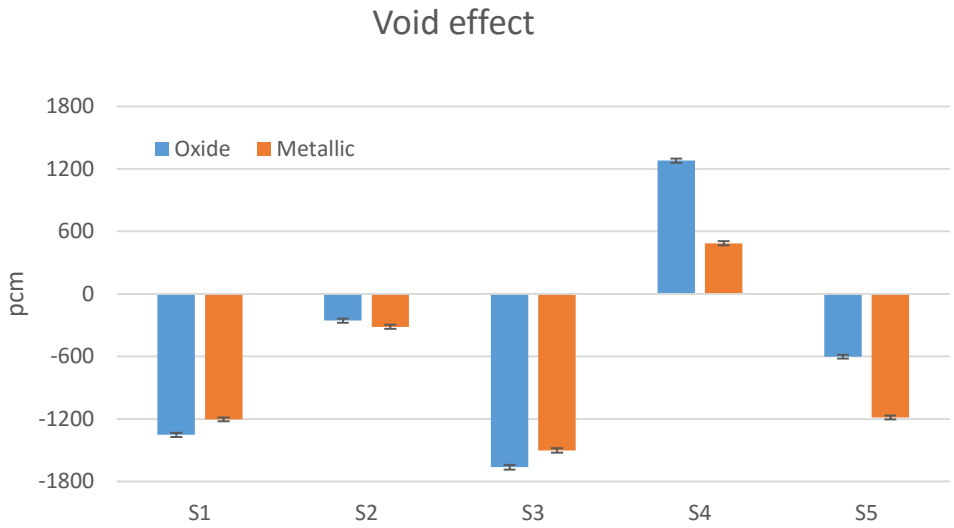

FIGURE 5.12. Coolant void worth comparison for oxide and metallic models.

Similar behavior on the void effect was obtained in comparison with the oxide model, negative reactivity effect on the total voiding of the reactor was achieved (S5: -1187 pcm) as shown in Figure 5.13, whereas a positive reactivity was registered in the fuel regions voiding (S4: 486 pcm).

Less reactivity effect is found for the metallic model in the scenarios S1, S3 and S4, while in the scenarios S2 and S5 the reactivity effect is higher in this model. It should be empathized that the coolant void worth for the whole reactor is more negative in the metallic model than in the oxide design, in which coolant void above the outer fuel zone contributes in this result, which is corroborated in scenario 2.

5.5.4. Actinide Inventory

Actinide inventory for the oxide fueled ASTRID design is presented in Figure 5.14, divided in two different charts. It is possible to observe the isotopic consumption in the fissile zone and the isotopic production, due to the breeding process, in the fertile material. An interesting finding is the ^{239}Pu amount available after the end of the simulation in the fissile and the fertile zones.

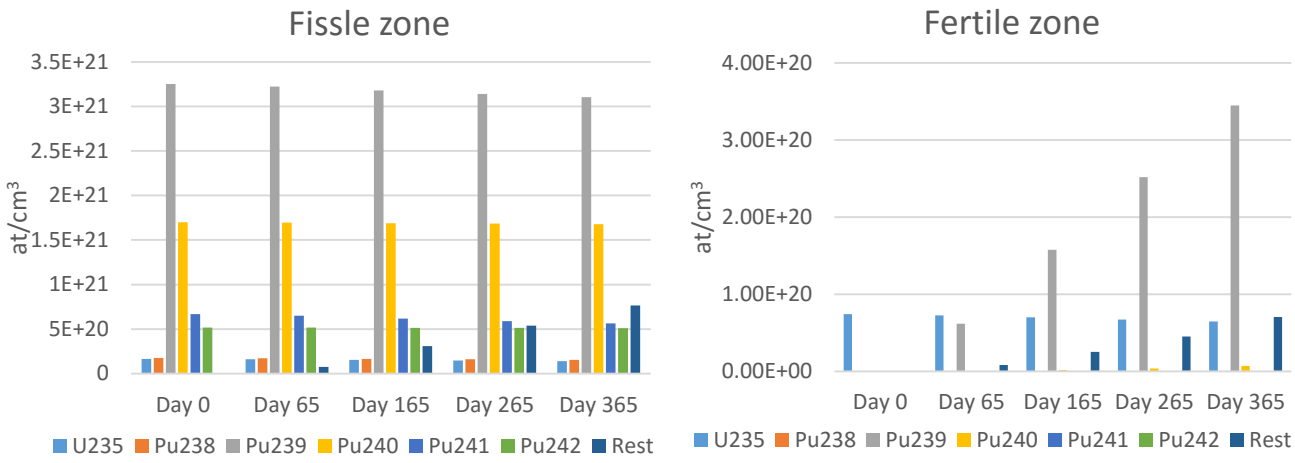

FIGURE 5.13. Actinide inventory for the oxide fueled ASTRID design.

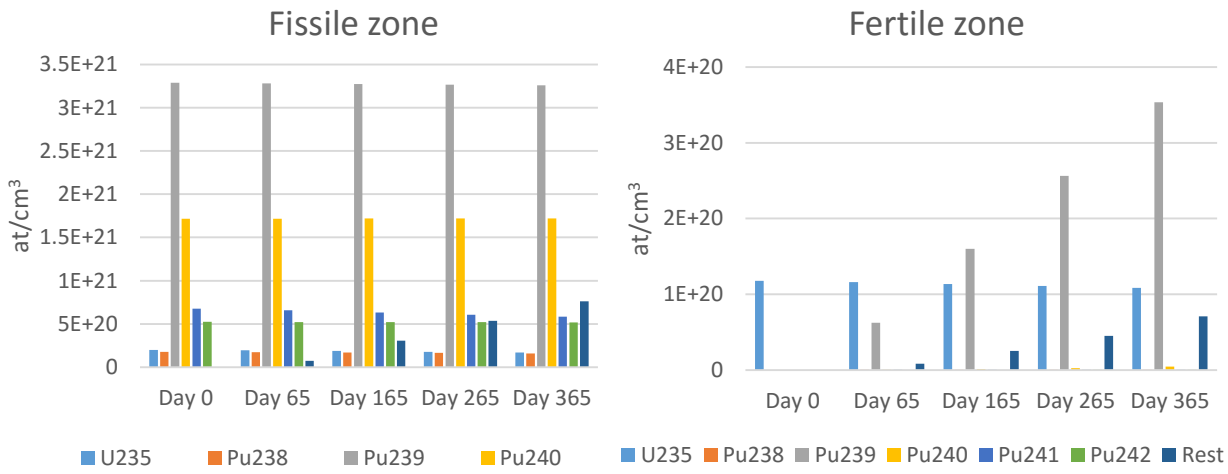

FIGURE 5.14. Actinide inventory for the metallic fueled ASTRID design.

Actinide inventory for the metallic fueled ASTRID design is presented in Figure 5.15. It is possible to observe the consumption of ^{239}Pu in the fissile zone, but it is to be noticed that there is a considerable remaining amount of this isotope in the fissile zone. Breeding in fertile zone of ^{239}Pu was successfully achieved since an increasing inventory of this isotope is presented during the simulation.

5.5.5. Plutonium inventory

In order to analyze with greater detail the breeding capability of each model, ^{239}Pu inventory is presented in this section. Consumption of isotope ^{239}Pu in the fissile zone for both cases is shown in Figure 5.16 (left). Oxide model has a steeper slope than the metallic fueled design in the fissile zone.

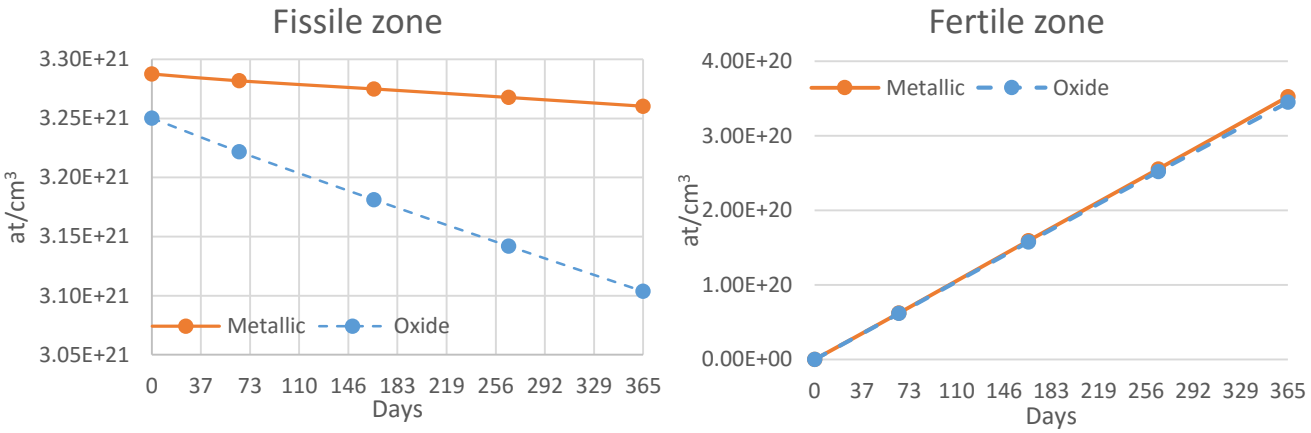

FIGURE 5.15. Plutonium inventory fir fissile (left) and fertile (right) zone in oxide and metallic models.

Given that the oxide and the metal fuels differ on the containing matrix, an implicit slightly higher moderation of the oxide fuel produce a slightly softer neutron spectrum (see Figure 5.17), being this the main reason why the fertile zone of the metallic design breeds a little bit more ^{239}Pu.

Although zirconium scattering cross section is higher in the fast spectrum, the oxide scattering has a greater impact in the moderation, since per collision, the neutron loses more energy with the oxide than with the zirconium (Yang, 2011).

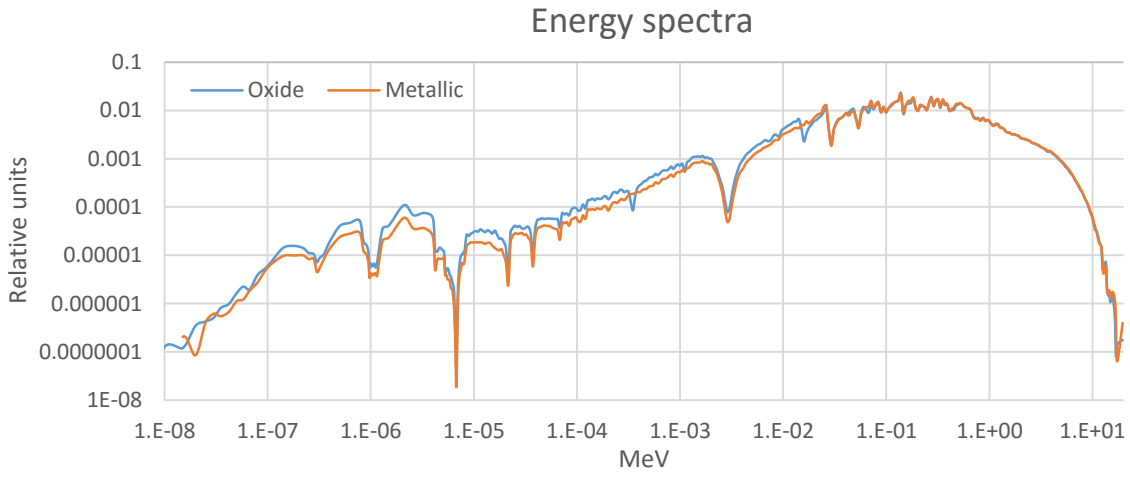

FIGURE 5.16. Comparison of metallic and oxide neutron spectra.

Finally, the total ^{239}Pu inventory in both zones (fissile and fertile) is presented in Figure 5.18. While consumption of ^{239}Pu is done mainly in the fissile zone, breeding increases the amount of this isotope. For both cases the quantity of plutonium increases as the simulation goes on, having more plutonium than the initial. Metallic model achieved 4% more ^{239}Pu than the conventional oxide design because of the neutron spectrum of the metallic case allows breeding to be higher, thus, a better management of plutonium could be performed with this design.

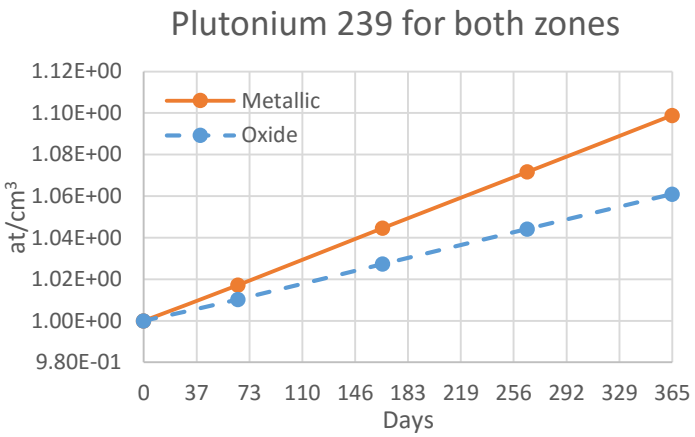

FIGURE 5.17. Plutonium inventory in fissile and fertile zones.

6. ASTRID BREED AND BURN NUCLEAR REACTOR

In the current section a proposed breed and burn ASTRID-like reactor is analyzed. With reference to what was presented in sections 5.5.4 and 5.5.5, it was shown that a considerable amount of ^{239}Pu remained in the core after the end of the first cycle. This led to the interest of analyzing the possibility of extend the operation of the reactor under a breed and burn reshuffling scheme. Two different reshuffling schemes were developed for the oxide and metallic fueled ASTRID-like reactors that are presented in this section.

6.1. Breed and Burn Reshuffling scheme

As shown in Figure 6.1, the ASTRID-like model developed consists of four different radial zones, being the neutronic shielding and the reflector the outer ones. As explained in section 5.1, the ASTRID core design has an outer fissile fuel zone, as well as an internal fertile blanket.

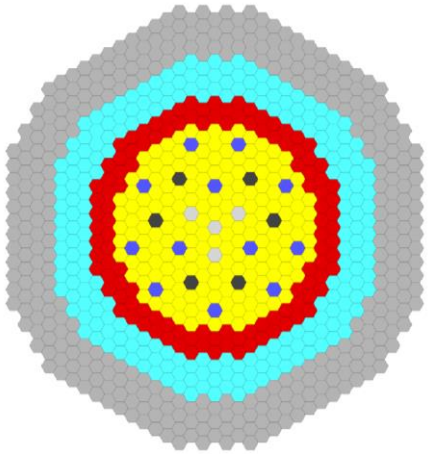

FIGURE 6.1. Map core of the ASTRID reactor.

It is shown in section 5.5.4 the inventory of fissile isotopes at the end of first cycle, and in section 5.5.5 a specific analysis of the ^{239}Pu inventory was done in order to observe the evolution of this isotope. Regarding this analysis, it was concluded that a considerable amount of ^{239}Pu remains in the core, and that through a reshuffling scheme the operation of the reactor may be extended.

It is important to mention that at present, in the ASTRID design there is a fuel residence time of 1440 EFPD (Vasile, 2012), with four fuel batches and a reload of 1.15 tons of plutonium per year (Chenaud, et al., 2013). In the current analysis a reshuffling scheme is proposed in order to determine the possibility of extending the operation of the reactor without loading fresh fuel.

In order to simulate the reshuffling scheme, in MCNP6 six different zones of the reactor core were defined, as depicted in Figure 6.2, in which the description excludes the reflector and the neutronic protection of the core. Two different sections comprehend the fissile zone: the outer ring shown in red color, and the intermediate ring shown in orange color. Fertile zones are shown in green, blue and yellow color.

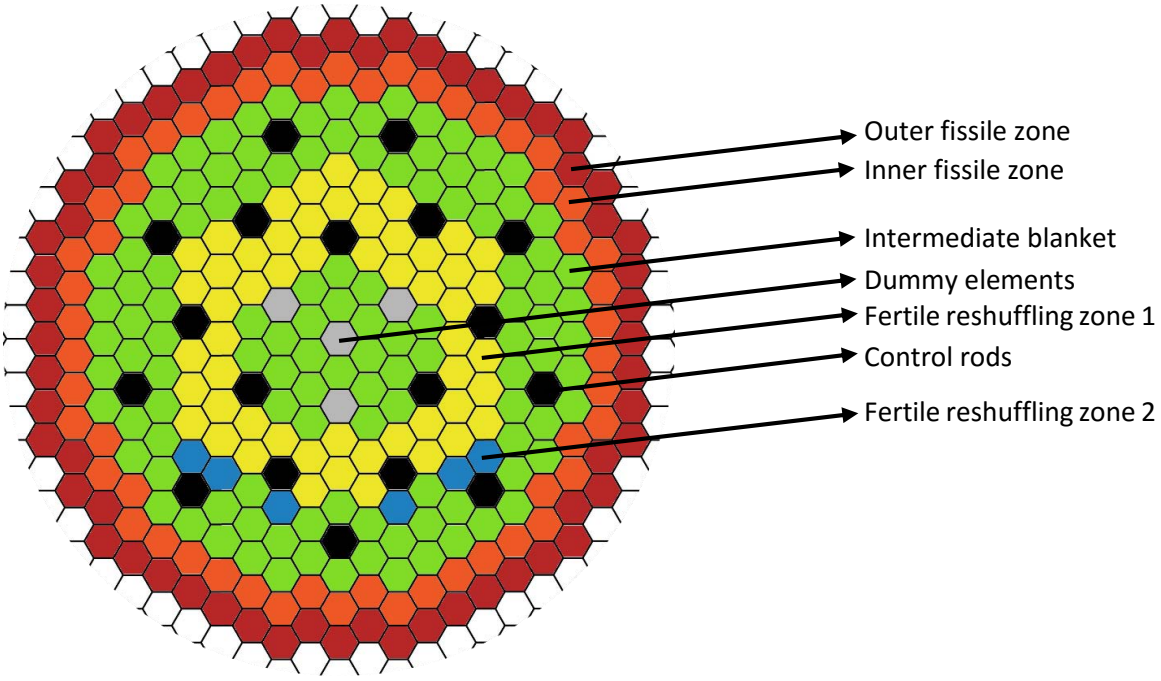

FIGURE 6.2. Map core of the ASTRID reactor with reshuffling scheme.

Two different reshuffling schemes were developed for the ASTRID model in order to observe the impact on reactivity. For both reshuffling schemes the first cycle has a duration of 365 days, after that two different fuel cycles are proposed in each scheme.

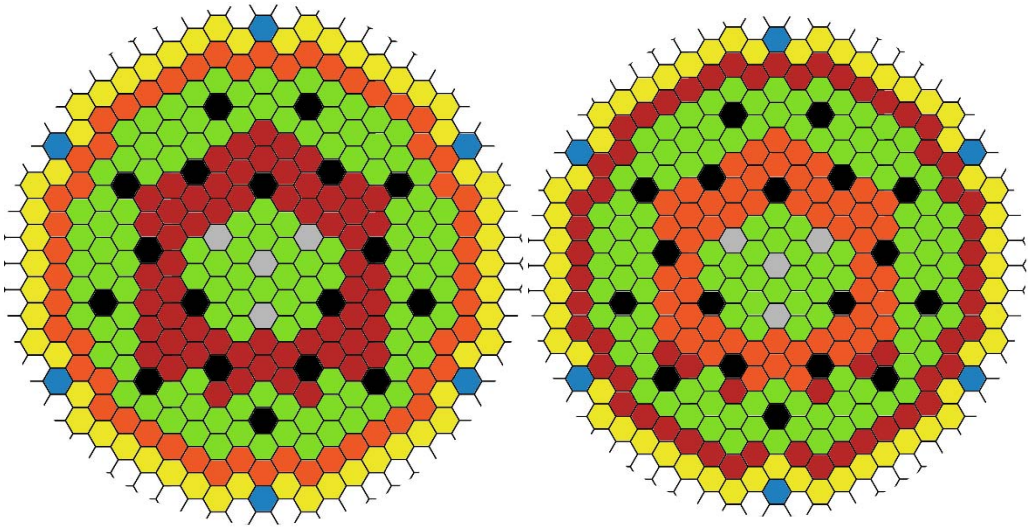

FIGURE 6.3. Map core for the fuel cycles 2 (left) and 3 (right) of the reshuffling scheme 1.

The reshuffling scheme 1 (RS1) consists in swapping the outer fissile zone with the fertile reshuffling zone 1 and 2. The reactivity after swapping these zones should increase during a cycle, the reactor is then operated until its reactivity decreases near to the critical state. After this intermediate cycle, a second reshuffling is suggested by swapping the outer fissile zone (in red color) with the inner fuel zone (in orange color). The position of the fertile reshuffling zone 2 is filled with the outer fissile zone too.

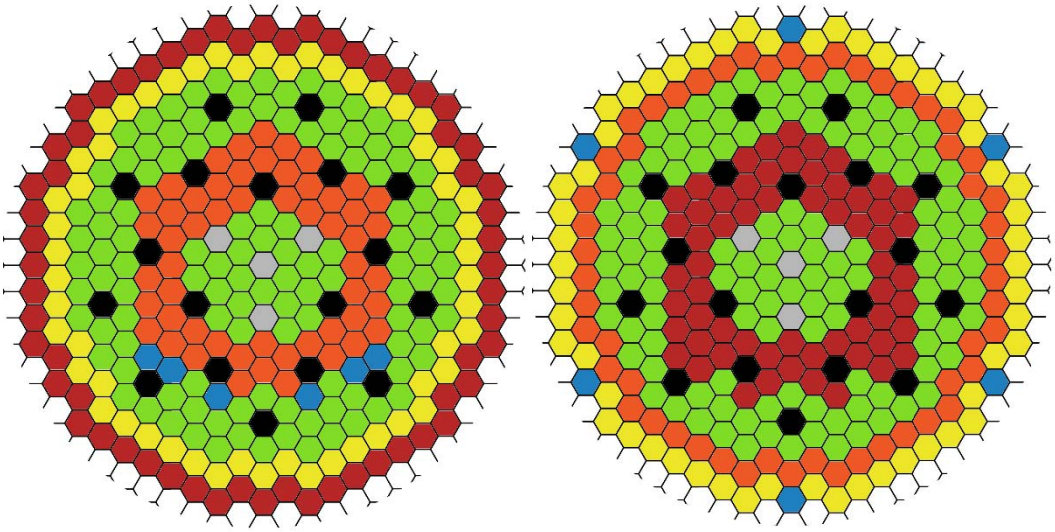

FIGURE 6.4. Map core for the cycles 2 (left) and cycle 3 (right) of the reshuffling scheme 2

The reshuffling scheme 2 (RS2) swaps the inner fuel zone (in orange color) with the reshuffling fuel zone 1 (in yellow color). Then, the reactivity of the reactor increases and during one fuel cycle this core configuration enables the reactor to be operating until it decreases near to the critical state. In order to continue the operation of the reactor with a third cycle, it is necessary to place the reshuffling fuel zone 1 (in yellow color) in the outer fissile zone (in red color), the inner fissile zone (in orange color) should return to its position and the outer fissile zone (in red color) needs to be set in the reshuffling zone 1. Figure 6.4 depicts the map core for the reshuffling scheme 2.

6.2. The ASTRID-like reshuffling schemes results

In the present section the results involving the ASTRID-like breed and burn reshuffling schemes are shown. Since there are two different ASTRID-like models, that is the oxide and the metallic designs, these reshuffling schemes are tested in every model.

At this time it is convenient to mention that a bug was found during the simulations in MCNP6. This bug has been detected by Los Alamos National Laboratory and it is a trouble with the SWAP card, which enables the reshuffling task. When using the SWAP card in the parallel MPI simulation mode, the SWAP card is simply ignored, reason for which this simulations where done in a sequential execution. Due to this bug and to the costing simulation time, the neutrons per cycle were reduced, and the effective cycles were increased. Simulations in MCNP6 were performed with 250 active cycles of 4000 neutrons for a total of a million histories. The first cycle was set to 365 days for all the simulations, and different duration of reshuffling cycles were determined. TIER 2, which is a selected fission products model in chain depletion calculation, was set in all of the simulations.

6.2.1. Oxide fueled ASTRID-like reshuffling analysis

The criticality for the reshuffling scheme 1 of the oxide-fueled model is shown in Figure 6.5. It is clearly appreciated that after the end of the first cycle, when the reactivity has dropped near to a critical state, the reshuffling is done, and as a consequence of this, the reactivity of the reactor increases and even exceeds with 707 pcm the reactivity value at BOL.

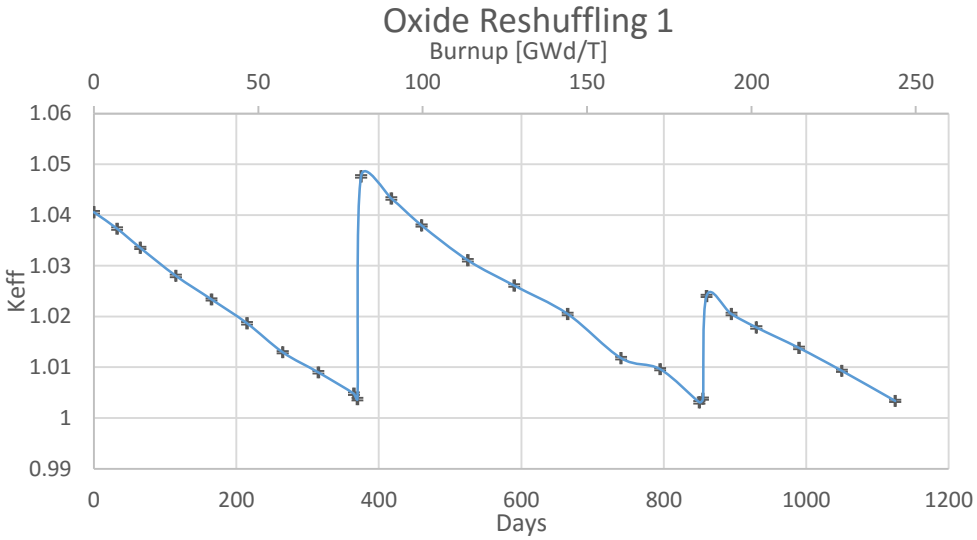

FIGURE 6.5. Keff of the ASTRID-like oxide-fueled model with reshuffling scheme 1

After the first reshuffling in the core, the reactivity drops with a stable slope reaching 490 days of operation, and after this time the reactor reactivity drops close to the critical state. Reshuffling two is simulated at that time, and reactivity again rises for another cycle of 270 days. Reactivity during this cycle decreases until the day 1125 when it ends its operation. It is found that with the same fuel that was loaded at the beginning of the simulation, the reactor could extend its operation for 760 days. Although the reshuffling enabled the reactor to operate for at least two more years, it should be said that the operation in this reactor did not covered the fuel residence time considered in the irradiation program of the ASTRID reactor, which is of 1460 days. It was found that the reactor operating under reshuffling scheme 1 could extend its operation more than 3 times the first cycle duration and it reaches a burnup of 240 [GWd/T].

An interesting analysis is to track the actinide inventory during the simulation. Figure 6.6 shows the fissile and fertile zone of the ASTRID design for the whole simulation, including the two reshuffling strategies. For the fissile zone, the predominant isotope of the fuel mixture is the ^{239}Pu, which is consumed as the reactor operates during its cycles. The fertile zone in this design very clearly shows the breeding capability of ^{239}Pu. The amount of ^{239}Pu at the End of the First Cycle is doubled by the end of the first reshuffling cycle, and it increases almost 40% by the end of the second reshuffling. By the end of the simulation, the amount of ^{239}Pu bred in the fertile zone is comparable with one third of the initial amount of ^{239}Pu in the fissile zone, which is not negligible since highly enriched fuel is placed in the fissile zone.

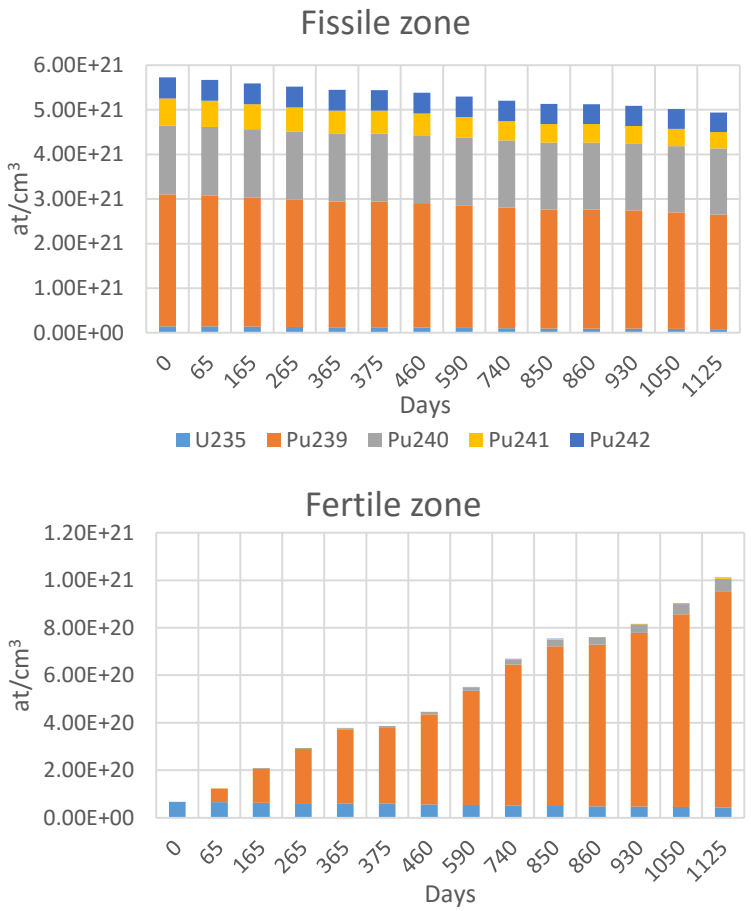

FIGURE 6.6. Actinide inventory of the fissile and fertile zones for the oxide-fueled design and reshuffling scheme 1

Figure 6.7 depicts the actinide inventory for the reactor, where it can be seen that the amount of ^{239}Pu at the end of the simulation increases, ^{240}Pu remains with its concentration constant, fissile isotopes ^{235}U and ^{241}Pu decrease its concentration while ^{242}Pu slightly decreases during the simulation.

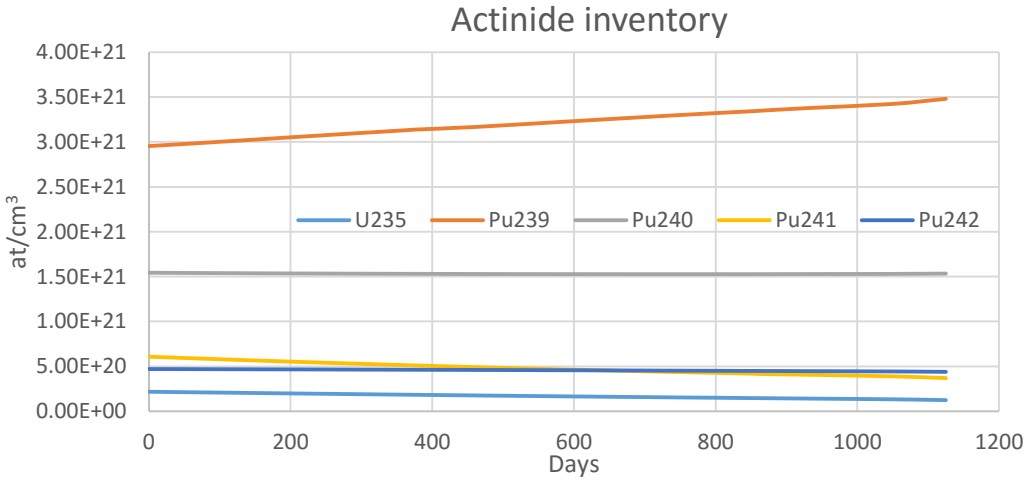

FIGURE 6.7. Actinide Inventory for the oxide-fueled design and reshuffling scheme 1

Criticality for the reshuffling 2 of the oxide-fueled design is shown below in Figure 6.8. After the end of the first cycle, the reactivity has dropped near the critical state of the reactor, then, the first reshuffling begins. The criticality rises when the reshuffling in the reactor is done, achieving 596 pcm less reactivity than the presented at the BOL. Reactivity drops near the critical state after 365 days of simulation, then, the second reshuffling is done and reactivity increases again with 769 pcm less than the reactivity at BOL. Reactor can be in operation during 440 days besides the 730 days achieved in the previous cycles, for a total of 1170 days.

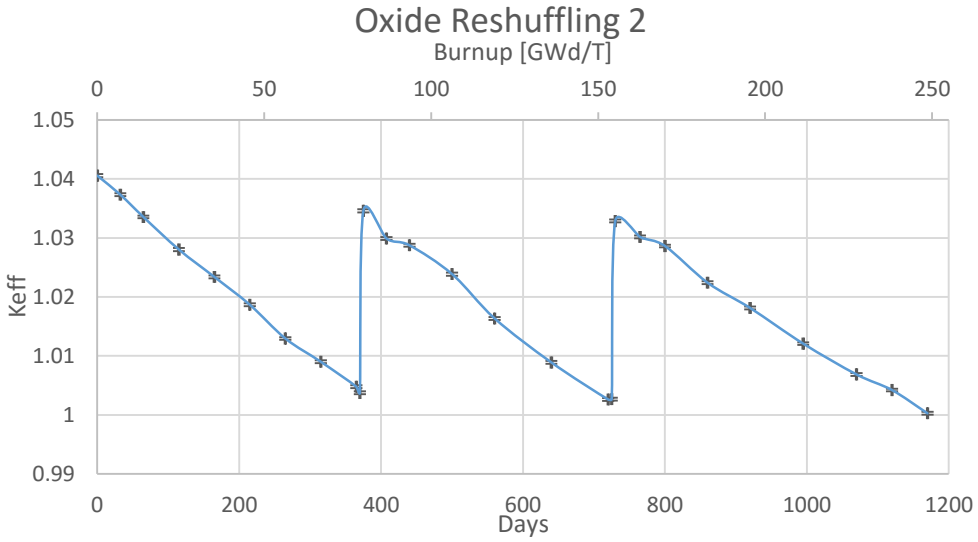

FIGURE 6.8. Keff of the ASTRID-like oxide-fueled model with reshuffling scheme 2

It was shown that the operation of the reactor could be extended for 805 days through the reshuffling scheme 2, and 45 days more than the reshuffling scheme 1. The achieved burnup in this simulation was 250 [GWd/T], which is a considerable value. It can be said that the reshuffling scheme 2 is preferred over the reshuffling strategy 1, not only because it lasts more time in supercritical state, but also because after the reshuffling its reactivity has less severe increases.

Despite the reactor extended its operation with the reshuffling scheme 2 for a total of 1170 days, the reactor did not covered the fuel residence time considered in the irradiation program of the ASTRID reactor (1460 days), mainly because this irradiation program takes into account the reload of fresh material every 365 days. This reshuffling scheme enabled the reactor to extend its operation for more than three times the first cycle duration.

The actinide inventory of the fissile and fertile zones is presented in Figure 6.9. As in the description for reshuffling scheme 1, the predominant isotope in the fuel composition for the fissile zone is the ^{239}Pu, which is consumed during the simulation of the reactor. Despite the concentration of ^{240}Pu is considerably small, the consumption of this isotope is notable, being reduced near to the half of its initial concentration either by fission or by absorption. In the fertile zone, ^{239}Pu is bred successfully to a point that by the end of the simulation the amount of this isotope available is one third of the initial concentration in the fissile zone.

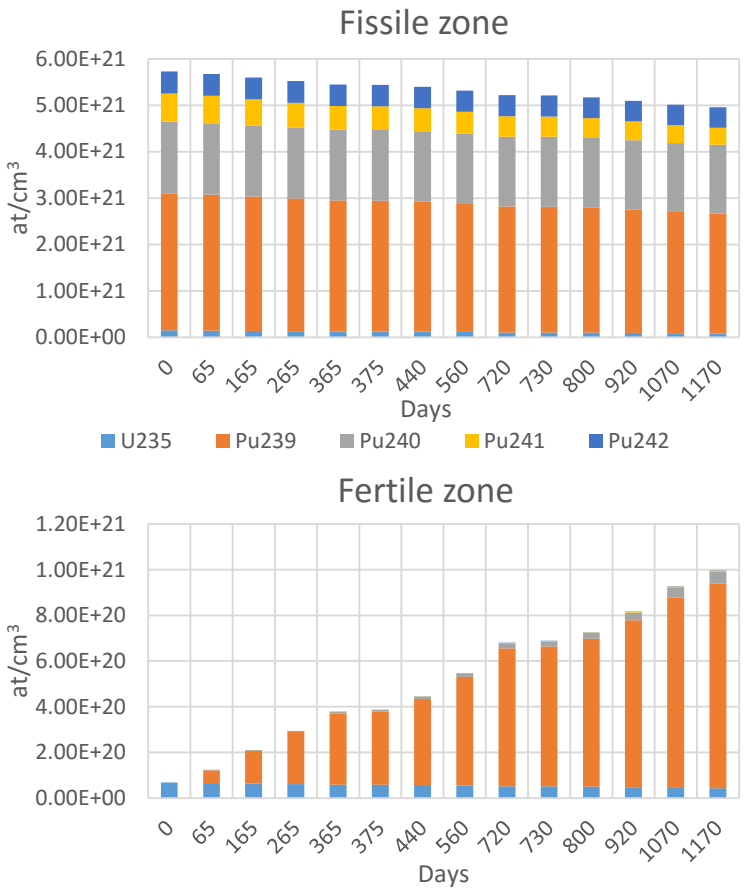

FIGURE 6.9. Actinide inventory of the fissile and fertile zones for the oxide-fueled design and reshuffling scheme 2

Figure 6.10 shows the actinide inventory of the reactor, in which, despite the consumption of the ^{239}Pu in the fissile zone, the bred ^{239}Pu in the fertile zone not only compensates the isotope concentration, but increases the total amount of ^{239}Pu, which enables the extension of the reactor operation. Fissile isotopes ^{235}U and ^{241}Pu are consumed, while ^{240}Pu seem to remain constant during the simulation.

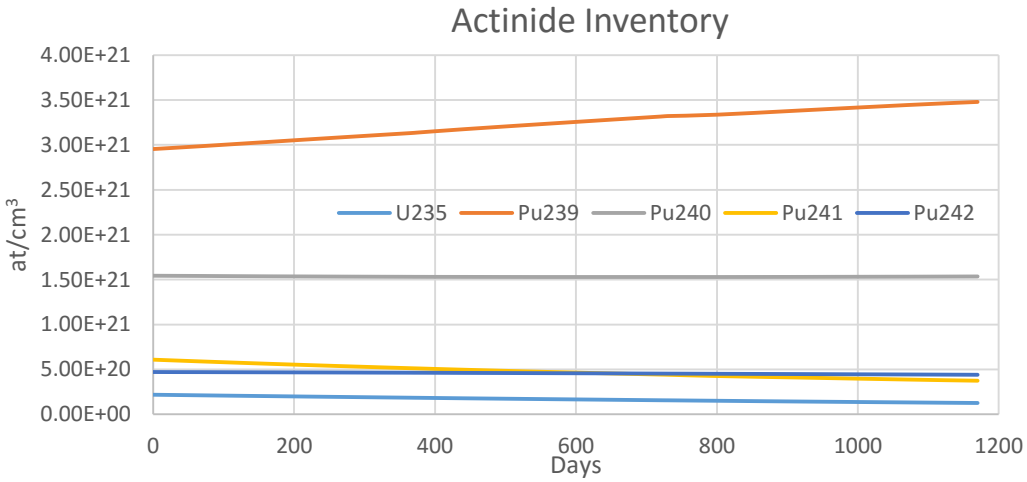

FIGURE 6.10. Actinide Inventory for the oxide-fueled design and reshuffling scheme 2

6.2.2. Metallic fueled ASTRID-like reshuffling analysis

In this section the reshuffling schemes of the metallic models are presented and analyzed. The reactivity for the metallic reshuffling scheme 1 is shown in Figure 6.11, where besides the first cycle, the reshuffling schemes are shown. After the first cycle, reshuffling scheme 1 is done and reactivity increases 5177 pcm, and a difference of 3073 pcm is registered between the initial BOL keff value and the reactivity after the first reshuffling. Once the reactivity increased, a supercritical state was achieved during 1007 days, and after this period, reactivity drops near the critical situation. Therefore, a second reshuffling is done and consequently, reactivity rises again, this time 528 pcm greater than the BOL reactivity. After the second reshuffling the reactor remained in supercritical state during 875 days.

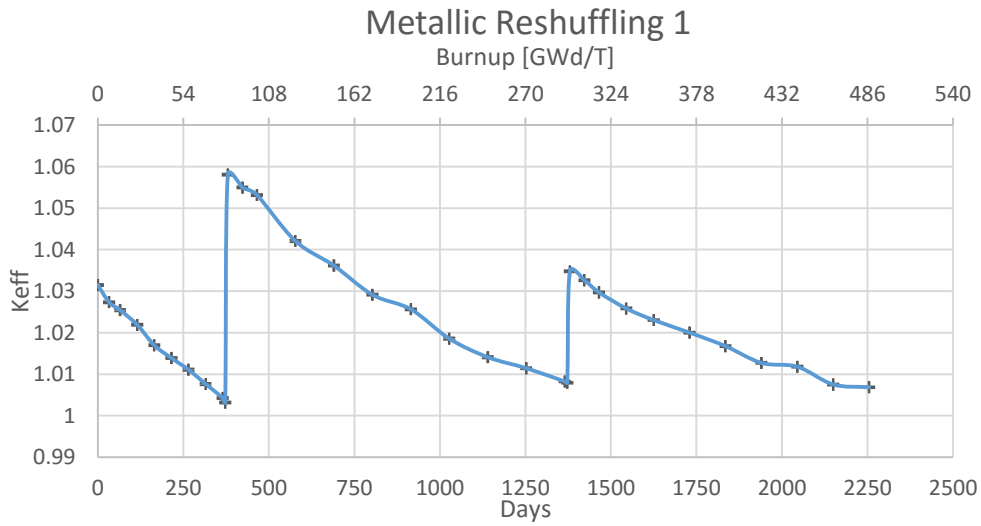

FIGURE 6.11. Keff of the ASTRID-like metallic-fueled model with reshuffling scheme 1

The metallic model with reshuffling scheme 1 could operate for 2255 days, being more than 6 times the first cycle duration. The reactor largely covered the fuel residence time considered in the irradiation program of the ASTRID reactor (1460 days), and even remained in supercritical state during 800 days more. The burnup achieved in this simulation is of 481.89 [GWd/T] which is considerably high. Despite the reactor extended its operation for a large period of time, the reactivity after the first reshuffling in the reactor seems to be very large when compared with the reactivity at BOL.

In Figure 6.12 the actinide inventory of fissile and fertile zones is shown. In the composition of the fissile zone, the isotope ^{239}Pu predominates during the whole simulation. Fissile isotopes; ^{239}Pu and ^{241}Pu are consumed, being the isotope ^{239}Pu the main responsible of the operation of the reactor. In the fertile zone, there are significantly results that prove that the metallic reactors breed is considerably higher than the oxide models. The amount of ^{239}Pu bred in the fertile zone at the end of the simulation is found to be more than the half of the initial concentration of this isotope in the fissile zone, which is considerably higher. Therefore, it can be concluded that supercritical state achieved during the whole simulation is strongly related to the bred amount of ^{239}Pu.

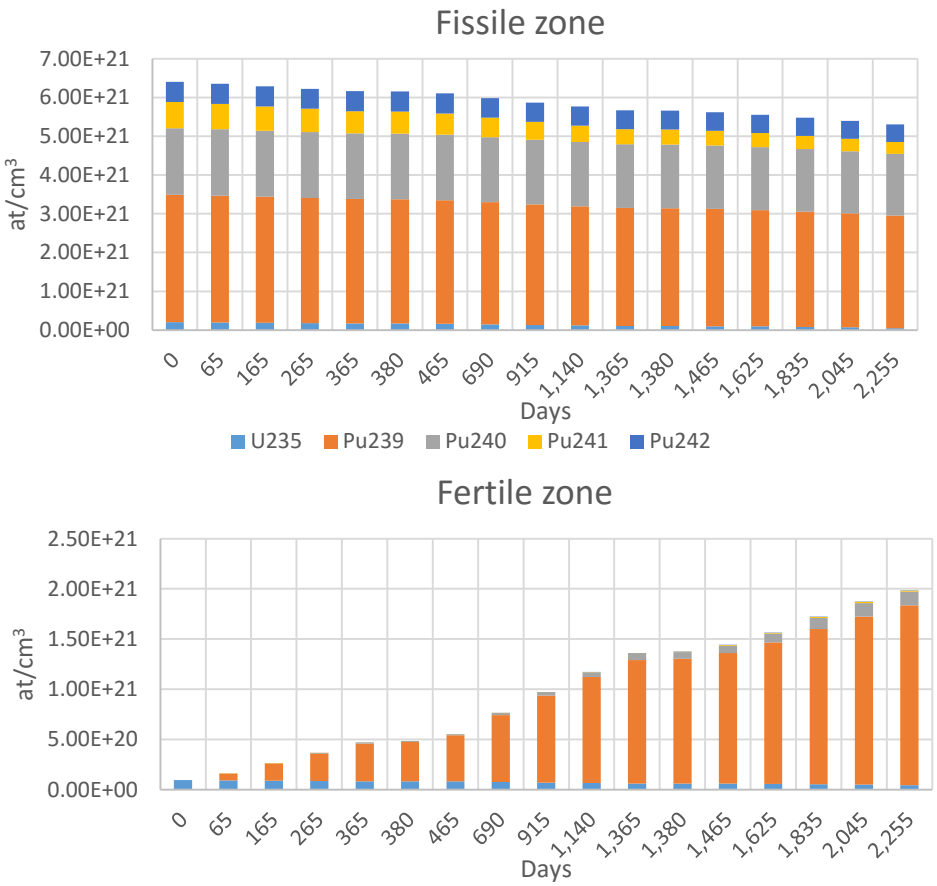

FIGURE 6.12. Actinide inventory of the fissile and fertile zones for the metallic-fueled design and reshuffling scheme 1

Figure 6.13 is shown below, which presents the actinide inventory for the reactor. As expected, ^{239}Pu is produced more than it is consumed, which is bred at higher rate at the beginning of the simulation than at the end of it. While ^{240}Pu remains constant, the fissile isotopes; ^{241}Pu and ^{235}U are consumed and reduced in the reactor inventory.

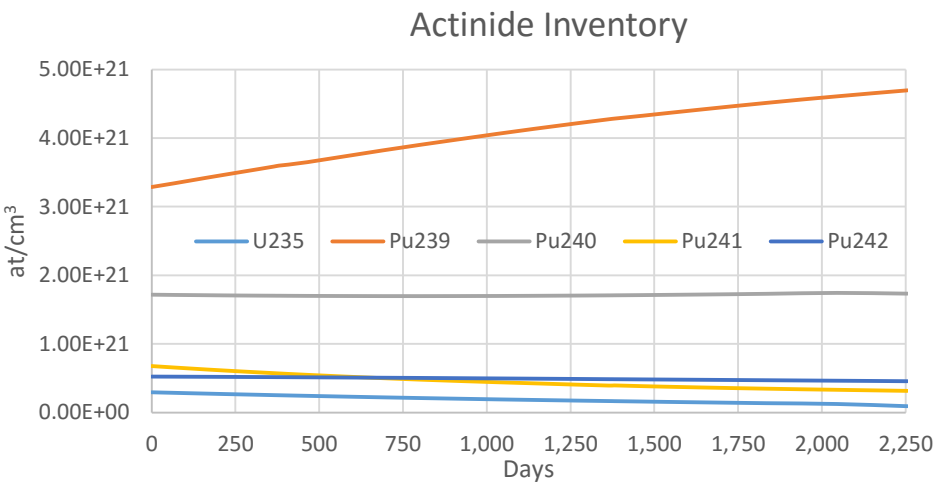

FIGURE 6.13. Actinide Inventory for the metallic-fueled design and reshuffling scheme 1

The reshuffling scheme 2 for the metallic design is analyzed and described in this section. Figure 6.14, shown below, depicts the reshuffling impact on reactivity. After the end of the first cycle, when the reactivity has dropped near the unity, the first reshuffling is done and, consequently, the reactivity increases near to the value at BOL (160 pcm difference). Reactivity then enables the reactor to operate for 615 days, and by then the reactivity is found to be near the critical state, so the second reshuffling in the reactor is done. Once the reshuffling is done, the reactivity increases 3010 pcm, and a slight difference of 8 pcm is obtained when comparing with the reactivity at BOL.

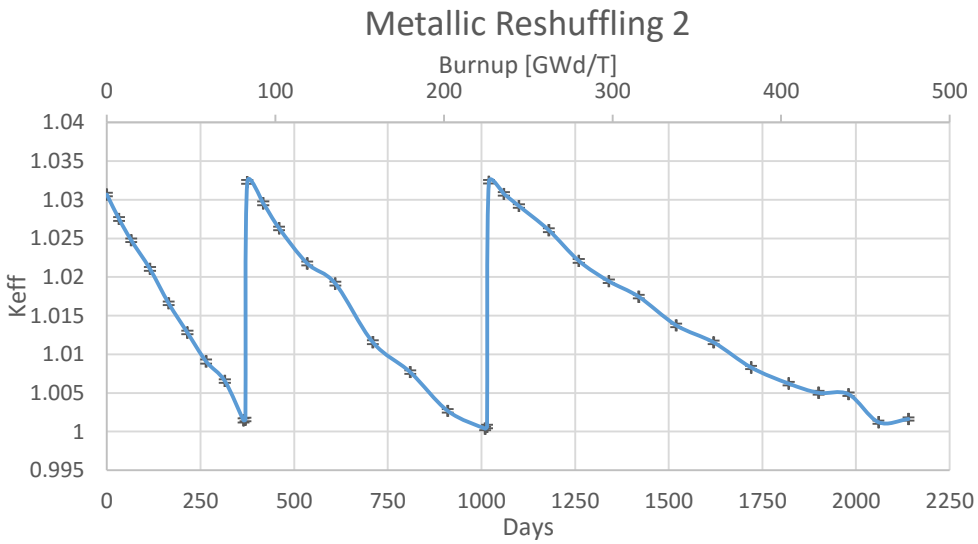

FIGURE 6.14. Keff of the ASTRID-like metallic-fueled model with reshuffling scheme 2

The reactor could extend its operation for 1775 more days, for a total of 2140 days, that is 5.86 times the first cycle duration. The fuel residence time considered in the ASTRID program may be covered by this reactor under the reshuffling scheme 2 without refueling, which is a great advantage. Despite it achieved less days of operation that the metallic reshuffling scheme 1, the reactivity seems to be not as triggered as in that model, which is preferable when controlling the reactor. A burnup of 457 [GWd/T] is achieved at the end of this simulation, which is a not negligible value.

It should be said, that although the reactor could operate during more days, the materials could limit this operation, mainly because of the cladding damage constrains, so the duration of the operation of this reactor directly depends on the material damage resistance.

Figure 6.15 presents the actinide inventory for the fissile and the fertile zones, and, as it was found before, the ^{239}Pu predominates in the concentration of fissile fuel. Fissile isotopes; ^{235}U, ^{239}Pu and ^{240}Pu are consumed as the simulation goes on, while a reduction of the isotopes ^{240}Pu and ^{242}Pu is observed at the end of the simulation. In the fertile zone the breeding of the isotope ^{239}Pu is shown, which is far of being negligible because it reaches more than the half of the initial amount of ^{239}Pu in the fissile zone, which suggest that the great operation extension of the reactor is mainly due to the bred plutonium in the fertile zone.

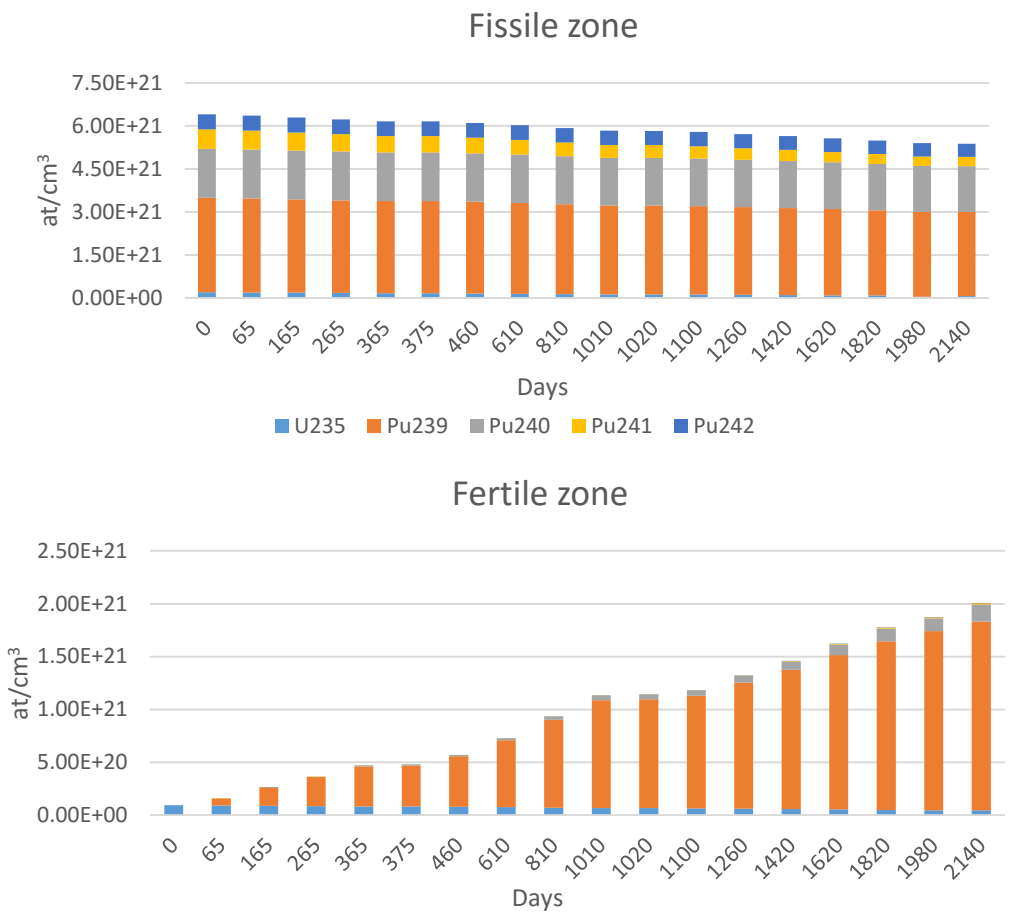

FIGURE 6.15. Actinide inventory of the fissile and fertile zones for the metallic-fueled design and reshuffling scheme 2

Figure 6.16 shows the actinide inventory in the reactor, in which ^{239}Pu increases as the simulation goes on, having more ^{239}Pu at the end of the simulation than at the BOL. Fissile isotopes, such as ^{241}Pu and ^{235}U are consumed in the reactor, and ^{240}Pu remains constant during the simulation.

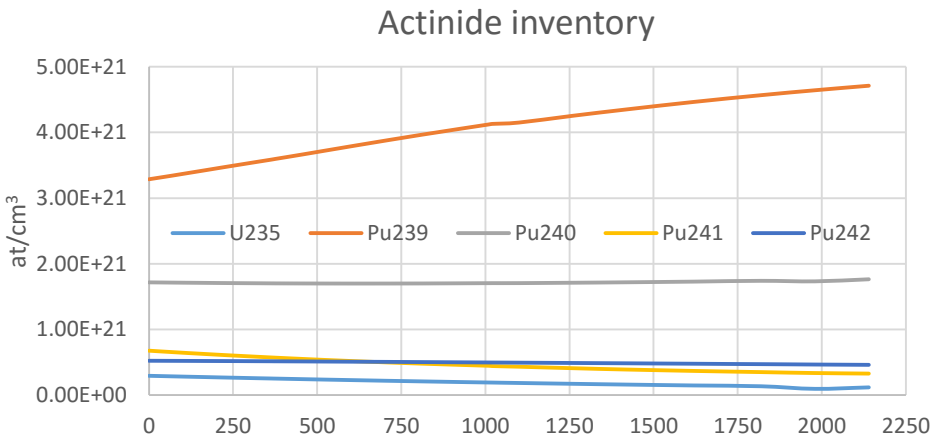

FIGURE 6.16. Actinide Inventory for the metallic-fueled design and reshuffling scheme 2

7. RESULT ANALYSIS AND CONCLUSIONS

The conclusions concerning the developed models and the different analysis are shown in this section. First, the results on the ASTRID-like model validation is provided, having successful results in every neutronic parameter analyzed. Then, results on developed reshuffling schemes for oxide and metallic designs are discussed, in which the reactor operation extension per each model is shown. Finally, the conclusions referring the ASTRID validation and the reshuffling schemes are given in the last section, having positive findings in the research made.

7.1. Results on ASTRID-like validation

The studied ASTRID design was successfully modeled with MCNP6 and validated with reference literature information. Validation of this design took into account three different neutronic parameters: reactivity at EoC, Doppler constants and coolant void worth.

For the obtained neutronic parameters, results had slightly differences in comparison with the European benchmark participants: Reactivity at EoC had less than 100 pcm difference with six of the ten benchmark participants. Doppler constants were within the expected range in three of four cases (5 pcm discrepancy out of range for only one Doppler constant), and coolant void worth registered very closed values to the average reported by benchmark institutions. This let us conclude that the developed model is within the expected values.

A proposed metallic design was compared with the oxide fueled ASTRID validated model. The same three neutronic parameters described before were compared between these two models. An 847 pcm reactivity difference is obtained between these two models at the beginning of cycle, while a 39 pcm reactivity difference is registered at the EoC. The reactivity difference decreases mainly because of the different breeding capability sustained between oxide and metallic designs.

Doppler constants were compared to each other, where it can be noticed that for the metallic design, at higher temperature perturbations a greater impact in the Doppler constant was observed due to the resonances of the ^{90}Zr capture cross section. Finally, coolant void worth was determined for the metallic model, where total voiding in the reactor remained negative and very similar to the oxide fueled design, since this reactivity effect is mainly due to the sodium coolant.

The actinide inventory was depicted for six different isotopes: ^{235}U, ^{238}Pu, ^{239}Pu, ^{240}Pu, ^{241}Pu and ^{242}Pu for oxide and metallic models, where it is possible to observe the consumption of ^{239}Pu in the fissile zone. However, despite the ^{239}Pu consumption in this zone, there is a considerable remaining amount of this isotope that could extend the operation of this rector through a reshuffling scheme.

The ^{239}Pu inventory tracking showed that in the fissile zone the oxide model has a steeper slope than the metallic fueled design. In the fertile zone, it was observed that breeding is higher in the metallic model, with 8.57 % more ^{239}Pu produced than the oxide design. For both models, the amount of ^{239}Pu increases. In the global actinide inventory, the metallic model produced 3% more ^{239}Pu than the conventional design for the first cycle.

It can be concluded that metallic fueled ASTRID design enhances the plutonium management, because the reactor can be sustained in a supercritical state with less initial Pu enrichment. It also produces more ^{239}Pu than it consumes, and in the global actinide inventory, it produces 3% more plutonium than the oxide fueled design.

7.2. Results on the ASTRID-like reshuffling schemes

The ASTRID-like reshuffling schemes were simulated in MCNP6, and it has been proved that the extension of the operation of the reactor without reloading fresh fuel may be accomplished through this strategy, mainly because of the breeding achieved in the fertile zone. The reshuffling scheme strategy would provide an economical advantage by eliminating the reload of fresh fuel.

For the ASTRID oxide-fueled designs the duration of the operation after the first cycle was successfully extended. For the reshuffling scheme 1 the operation of the reactor lasted 1125 days (BU=240.41 GWd/T) while in the reshuffling scheme 2 it lasted 1170 days (BU=250 GWd/T). Besides the second scheme lasted 45 more days, it does not has reactivity peaks, such as in the first reshuffling of the reshuffling scheme 1 where a 707 pcm difference is registered when compared with the BOL reactivity value.

With these reshuffling schemes, it may be possible to save 2.20 tons of plutonium, which is a considerable amount of this material. In both oxide deigns the breeding is successfully accomplished, having in the fertile zones at the end of the simulation one third of the initial concentration of ^{239}Pu in the fissile zone, being not a negligible value.

The metallic-fueled design had the better performance in the simulated reshuffling schemes due to the great operation extension of the reactor. For the reshuffling scheme 1 the extension of the reactor operation achieved 2255 days (BU= 457.32 GWd/T), and for the reshuffling scheme 2 it lasted 2140 days (BU= 481.89 GWd/T). Despite the supercritical state is achieved for 115 more days in the reshuffling scheme 1, a reactivity peak in the first reshuffling in the scheme could complicate the reactor operation (a 3073 pcm difference is registered when compared with the BOL reactivity value).

The metallic design maximized the fuel utilization to the point that it saved up to 5.95 tons of plutonium, which is more than double than oxide designs did. The breeding in the metallic designs was successfully done, achieving more than half of the initial concentration of ^{239}Pu in the fissile zone.

Further work should include the negative coolant void worth value through the different reshuffling proposed configurations in order to maintain the CFV concept. Besides, a thermalhydraulic analysis should be done for the reshuffling schemes with the purpose of knowing the power distribution of the reactor. Finally, a minor actinide inventory should be done in order to analyze the production of neptunium, americium and curium.

7.3. Conclusions

It can be concluded that the defined objectives at the beginning of the research were successfully achieved, by developing an ASTRID-like model based in the existing literature and validating it with different institutions. All neutronic parameters that were analyzed in the validation process showed that the developed model matched with those provided by the international institutions, which led us to the conclusion that the ASTRID-like model was successfully developed.

Then, once that the model was validated, a proposed metallic-fueled design was analyzed and compared with the oxide model, having considerable advantages in the metallic design, in which the less enrichment required for the first fuel cycle in the reactor, and the better breeding performance are remarkable.

A breed and burn strategy was proposed to extend the operation of the reactor, and taking into account the amount of fissile material (mainly ^{239}Pu) after the first cycle, a reshuffling scheme was implemented. Two different reshuffling schemes were simulated in every developed model, having operation extensions of 805 days and 1775 days for the oxide and metallic designs respectively.

The implementation of the reshuffling schemes in the developed models enhanced the fuel utilization and could save 2.20 and 5.96 tons of plutonium for oxide and metallic designs respectively, which has an impact in economic terms. The breeding of ^{239}Pu achieved in the fertile zone of the metallic design reached the half of the initial concentration of the ^{239}Pu in the fissile zone and for the oxide design, the breeding reached one third of the initial concentration of the ^{239}Pu in the fissile zone.

In general, it can be said that the metallic model have better performance than the oxide model, but it should be considered that the operation extension of the reactor is determined by the material radiation damage and mainly by the cladding constrains.

8. BIBLIOGRAPHY

Argonne National Laboratory. (2012, April 5). *Flickr*. Retrieved from Argonne National Laboratory: https://www.flickr.com/photos/argonne/8167914291

Atzberger, P. (2004). *The Monte-Carlo Method.* New York: New York University.

Basak, U. (2009, November 9). *The Abdus Salam International Centre for Theorical Physics.* Retrieved from Joint ICTP/IAEA School on Physics and Technology of Fast Reactors Systems: http://indico.ictp.it/event/a08209/session/46/contribution/27/material/0/0.pdf

Bennett, & Coleman. (2015, December 1). *India plans to construct six more fast breeder reactors*. Retrieved from http://articles.economictimes.indiatimes.com/2015-12-01/news/68688445_1_fuel-loading-prototype-fast-breeder-reactor-pfbr

Bérenger, P. (2012, July 8). *Les différents types de réacteurs*. Retrieved from Réacteur à neutrons rapides, Phénix : Les différents types de réacteurs

Binus, J. (2003, October 6). *The Oregon Historical Society.* Retrieved from Fast Flux Test Facility Hanford: http://oregonhistoryproject.org/articles/historical-records/fast-flux-test-facility-hanford-washington/#.VwPs3Y-cHmJ

Bortot, S., Alvarez-Velarde, F., Fridman, E., Garcia Cruzado, I., Garcia Herranz, N., López, D., . . . Vasile, A. (2015). European benchmark on the ASTRID-like low-void-effect core characterization: neutronic parameters and safety coefficients. *Proceedings of ICAPP*, 668-676.

Brown, F., Kiedrowski, B., & Bull, J. (2013). Verification of MCNP5-1.60 & MCNP6.1 for Criticality Safety Applications. *NCSD* (pp. 1-14). Wilmington: Los Alamos National Laboratory.

Buksha, Y. (1996). Status of Sodium Cooled Fast Reactor. *Institute of Physics and Power Engineering*, 181-208.

CEA. (1967, January 5). *50 ans Cadarache*. Retrieved from HIER: https://cadarache-communication.fr/1967.php

CEA. (2012). *Evaluation complémentaire de la sûreté au regard de l'accident survenu à la centrale nucléaire de Fukushima Daiichi.* Cadarache: Direction de l'energie nucléaire.

CEA. (2012). *The ASTRID Technological Demonstrator.* Saclay.

Chen, Y. (2013). Irradiation effects of HT-9 martensitic steel . *Nuclear Energy Technology Colume 45*, 311-322.

Chenaud, M., Devictor, N., Mignot, G., Variane, F., Vénard, C., & Martin, L. (2013). STATUS OF THE ASTRID CORE AT THE END OF THE PRECONCEPTUAL DESIGN PHASE 1. *NUCLEAR ENGINEERING AND TECHNOLOGY, VOL.45 NO.6*, 721-730.

Cochran, T. B., Feiveson, H. A., Pattersonn, W., Pshakin, G., Ramana, M. V., Schneider, M., . . . Von Hippel, F. (2010). *Fast Breeder Reactor Programs: History and Status.* New Jersey: International Panel on Fissile Materials.

Di Sanzo, C., & Greenspan, E. (2012). A search for the minimum volume of breed and burn cores. *Proceedings of ICAPP*, 1046-1053.

Dravid, H. K. (2010). *Prototype Fast Breeder Reactor.* Chennai: Reactor Technology & Engineering.

Driscoll, M. (2005). *Engineering and Physics Optimization of Breed and Burn Fast Reactor Systems.* Massachusetts: Massachusetts Institute of Technology.

Duderstadt, J. J., & Hamilton, L. J. (1976). *Nuclear Reactor Analysis.* Michigan: John Wiley & Sons Inc.

Dugdale, A. (2010, March 23). *1 Minute Read Technology*. Retrieved from Bill Gates Goes Nuclear With Toshiba's 4S Reactor: http://www.fastcompany.com/1594671/bill-gates-goes-nuclear-toshibas-4s-reactor

Ellis, T. (2011). TerraPower Overview. *NES APS-AAPT-SPS Meeting Plenary* (pp. 1-37). Massachusetts: TerraPower.

Ellis, T., Petroski, R., Hejzlar, P., Zimmerman, G., McAlees, D., Whitmer, C., . . . Myhrvold, N. (2010). Traveling-Wave Reactors: A Truly Sustainable and Full-Scale Resource for Global Energy Needs. *Proceedings of ICAPP*.

ENERGO. (2015, January 14). *Technical design of the BN-1200 Reactor*. Retrieved from http://energo-24.ru/news/7609.html

European Nuclear Society. (2003, March 4). *European Nuclear Society*. Retrieved from Nuclear fission: https://www.euronuclear.org/info/encyclopedia/n/nuclear-fission.htm

Fischer, G. J., & Cerbone, R. J. (1979). *The Fast-Mixed Spectrum Reactor – Initial Feasibility Study.* Georgia: BNL-50976.

Forget, Y. (2007, July 31). *Superphenix Nuclear Power Plant*. Retrieved from Superphenix : https://commons.wikimedia.org/wiki/File:Superphénix_5.jpg

François, J. L. (2008). El método de Monte Carlo para la solución de la ecuación de Transporte. *Análisis de reactores Nucleares*, 1-7.

Fuchs, K., & Hessel, H. (1961). THE POSSIBILITIES FOR THE OPERATION OF A NATURAL URANIUM BREEDER REACTOR WITHOUT FUEL ELEMENT PREPARATION. *Kernenergie*, 15-26.

Gauché, F. (2012). The ASTRID project. *STATUS, COLLABORATIONS, LESSONS FROM FUKUSHIMAACCIDENT*, (pp. 1-14). Tsuruaga.

GEN IV International Forum. (2013, November). *A Technology Roadmap for Generation IV Nuclear Energy Systems*. Retrieved from https://www.gen-4.org/gif/jcms/c_40473/a-technology-roadmap-for-generation-iv-nuclear-energy-systems

Graevemoore, E. (2008, May 12). *Sodium-cooled Fast Reactors*. Retrieved from https://en.wikipedia.org/wiki/Sodium-cooled_fast_reactor#/media/File:LMFBR_schematics2.svg

Greenspan, E. (2012). A Phased Development of Breed-and-Burn Reactors for Enhanced Nuclear Energy Sustainability. *Sustainability*, 2745-2764.

Heard, B. (2011, May 30). *Generation IV Nuclear*. Retrieved from The case against waiting for Generation IV nuclear: http://decarbonisesa.com/2011/05/30/the-case-against-waiting-for-generation-iv-nuclear-and-the-case-for-urgently-bringing-it-to-commercialisation/

Hitachi, & GE. (2007, June 20). *GE Hitachi Nuclear Energy.* Retrieved from PRISM Technical Brief: http://www.uxc.com/smr/Library%5CDesign%20Specific/PRISM/Other%20Documents/Technical%20Brief.pdf

Hozzászólás, N. (2013, October 18). *Atom Energia Info*. Retrieved from BN-800 : http://atomenergiainfo.hu/tudastar/bn-800-ujgeneracios-reaktor

IAEA Nuclear Energy Series. (2011). *STATUS AND TRENDS OF NUCLEAR FUELS TECHNOLOGY FOR SODIUM COOLED FAST REACTORS.* Vienna: IAEA.

International Energy Agency. (2015). *Key World Energy Statistics.* Paris: DESK.

JAEA. (2006, August 14). *Research and Development of Advanced Nuclear System.* Retrieved from Feasibility Study on Commercialized Fast Reactor Cycle Systems : http://jolisfukyu.tokai-sc.jaea.go.jp/fukyu/mirai-en/2006/pdf/1-4.pdf

James, M. R., & McKinney, G. W. (2007). MCNPX - New Features Demonstrated. *13th UK Monte Carlo User Group Meeting* (pp. 1-29). Teddington: Los Alamos National Laboratory.

Japan Nuclear Cycle Development Institute . (2001, February 7). *Fast Breeder Reactors*. Retrieved from Experimental Joyo FBR: https://www.jaea.go.jp/jnc/jncweb/02r-d/fast.html

Japan Nuclear Cycle Development Institute. (2001, February 7). *Fast Breeder Reactors*. Retrieved from Prototype FBR Monju: https://www.jaea.go.jp/jnc/jncweb/02r-d/fast.html

Jesudasan, D. S. (2013, December 13). *Industry supplies delay PFBR commissioning*. Retrieved from http://www.thehindu.com/news/cities/chennai/industry-supplies-delay-pfbr-commissioning/article7982156.ece

Judd, A. (2014). *An Introduction to the Engineering of Fast Nuclear Reactors.* New York: Cambridge University Press is part of the University of Cambridge.

Judkins, R., & Olsen, A. (1979). *Nuclear fuel fabrication and refabrication cost estimation methodology.* Virginia: U.S. Department of Commerce.

Kim, T. K., & Taiwo, T. (2010). *Fuel Cycle Analysis of Once-Through Nuclear Systems.* Illinois: U.S. Department of Energy.

Koch, L. J. (2008). *Experimental Breeder Reactor-II.* Illinois: Argonne National Laboratory.

M. Goldberg, S., & Rosner, R. (2011). *Nuclear Reactors: Generation to Generation.* Massachusetts: American Academy of Arts and Sciences.

Murray, R. L., & Holbert, K. E. (2015). *Nuclear Energy.* Massachusetts: Elsevier.

Ohira, H., & Uto, N. (2012). Progress on Fast Reactor Development in Japan. *Meeting of the Technical Working Group on Fast Reactors* (pp. 1-37). Illinoise: JAEA.

Ohki, S. (2012). Conceptual core design study for Japan sodium-cooled fast reactor: review of sodium void reactivity worth evaluation. *Technical Meeting on Innovative Fast Reactor Designs with Enhanced Negative Reactivity Feedback Features* (pp. 1-25). Vienna: IAEA TWG-FR.

Oka, Y., Inoue, T., & Yoshida, T. (2013). Plutonium breeding of light water cooled fast reactors. *Japanese Nuclear Science and Technology, Vol. 50 No. 1*, 15-20.

Papadakis, S. M. (2010). Desarrollo de un código de cálculo basado en el método de monte carlo orientado a la realización de correcciones de experimentos neutrónicos. *Universidad Nacional de Cuyo*, 1-129.

Qvist, S. A. (2013). *Safety and core design of large liquid-metal cooled fast breeder reactors.* California: UC Berkeley Electronic Theses and Dissertations.

Raj, B., Chellapandi, P., & Vasudeva, P. (2015). *Sodium Fast Reactors with Closed Fuel Cycle.* Florida: CRC Press.

Rawls, J. (2010). *Implications for Waste Handling of the Energy Multiplier Module.* Massachusetts: General Atomics.

Rogner, H.-H. (2014). Nuclear Power and Climate Change. *Department of Nuclear Energy, IAEA*, 1-11.

Saez, M., Robin, J. C., Riou, B., Villedieu, A., Deprest, D., & Prele, G. (2013). Status of ASTRID nuclear island pre-conceptual design. *IAEA-CN-199*, 1-10.

Saidi, P., Sadeghi, M., & Tenreiro, C. (2013). *Variance Reduction of Monte Carlo Simulation in Nuclear Engineering Field.* Tehran: Islamic Azad University.

Schneider, M. (2009). Fast Breeder Reactor in France. *Science and Global Security*, 36-53.

Shepelev, S. F. (2015). STATUS OF BN-1200 PROJECT DEVELOPMENT. *Nizhny Novgorod* (pp. 1-4). Zarechny: Afrikantov OKBM.

Slesarev, J. S., Stukalov, V. A., & Subbotin, S. A. (1984). Problems of development of fast reactors self-fuel-provision without fuel reprocessing. *Atomkernenergie Kerntechnik*, 58-60.

Sofu, T. (2015). A review of inherent safety characteristics of metal alloy sodium-cooled fast reactor fuel against postulated accidents. *Nuclear Engineering and Technology, Volume 47*, 227-239.

Sorensen, K. (2011, October 4). *Thorium*. Retrieved from Flibe Energy in the UK, Part 4: DECC: http://energyfromthorium.com/2011/10/04/flibe-uk-4/

Teller, E., Ishikawa, M., & Wood, L. (1995). *Completely Automated Nuclear Reactors for Long-Term Operation.* Texas: Lawrence Livermore National Laboratory.

The American Society of Mechanical Engineers. (1979). *Experimental Breeder Reactor I.* New York: The American Society of Mechanical Engineers.

Toshiba Corporation. (2013). *Super-Safe, Small and Simple Reactor .* Tokyo: CRIEPI.

U.S. Department of Energy. (2015). *Sodium-cooled Fast Reactor.* Washington, DC: Office of Nuclear Energy.

Vasile, A. (2012). SFR Core Design Performance and Safety. *European Nuclear Education Network Association – Gen IV* (pp. 1-46). Saint Paul Lez Durance: Commissariat à l'énergie atomique et aux énergies alternatives.

Verhoeff, T. (1993). *The Laws of Large Numbers Compared.* Eindhoven: Faculty of Mathematics and Computing Science.

Waltar, A. E., Todd, D. R., & Tsvetkov, P. V. (2012). *Fast Spectrum Reactors.* New York: Springer.

Weaver, K., & et al. (2009). Extending the Nuclear Fuel Cycle with Traveling-Wave Reactors. *Proceedings of Global*.

Weaver, K., Gilleland, J., Ahlfeld, C., Whitmer, C., & Zimmerman, G. (2010). A Once-Through Fuel Cycle for Fast Reactors. *Journal of Engineering for Gas Turbines and Power*, 1-6.

World Nuclear Association. (2013, April). *Greenhouse gas emissions avoided through use of nuclear energy*. Retrieved from http://www.world-nuclear.org/nuclear-basics/greenhouse-gas-emissions-avoided.aspx#.UXbWv7V956k

World Nuclear Association. (2014, November). *Climate Change – The Science*. Retrieved from http://www.world-nuclear.org/information-library/energy-and-the-environment/climate-change-the-science.aspx#.UXbYOLV956k

World Nuclear Association. (2015, October). *Fast Neutron Reactors*. Retrieved from http://www.world-nuclear.org/information-library/current-and-future-generation/fast-neutron-reactors.aspx

World Nuclear Transport Institute. (2012, November 29). *Nuclear Transport Facts*. Retrieved from What are back end materials?: http://www.wnti.co.uk/nuclear-transport-facts/what-is-transported-how/back-end-materials.aspx

Yang, W. S. (2011). Fast Reactor Physics and Computational Methods. *Purdue University School of Nuclear Engineering*, 177-199.

Appendix

The present is a developed code in Matlab to obtain the Actinide Inventory from an output of MCNP6. Two files should be provided, the time steps required and the desired isotopes that constitute the actinide inventory. This code is able to provide the concentration of the desired isotopes at different time steps, and it takes less than 10 seconds to process more than 20000 output lines.

```
clc
clear all
global status;
status=0;
s='salida_';
prompt={'Ingres nombre del archivo:'};
nombre=inputdlg(prompt);
fid=fopen(cell2mat(nombre),'r');
s=strcat(s,nombre);
fil0=fopen(cell2mat(s),'wt');
d = fgetl(fid);
fit=fopen('Times.txt','r');
i=1;
while(status==0)
    time = fgetl(fit);
    tps=time(1:9);
    ti{i}=tps;
    status = feof(fit);
    i=i+1;
end
can=i-1;
status=0;
fin=fopen('Nuclides.txt','r');
i=1;
while(status==0)
    nuclide = fgetl(fin);
    nde=nuclide(1:5);
    ac{i}=nde;
    status = feof(fin);
    i=i+1;
end
cant=i-1;
l=0;
i=1;
k=1;
out=1;
status=0;
while(status==0)

    k=1;
    while(numel(d)==0)
    d = fgetl(fid);
    end
```

```
    qi=cell2mat(ti(i));
    if
(d(2)=='a'&&numel(d)>70&&d(62)==qi(1)&&d(64)==qi(3)&&d(65)==qi(4)&&d(66)=
=qi(5)&&d(69)==qi(8)&&d(70)==qi(9))
        w=d(36);
        fprintf(fil0, '   Mat ');
        fprintf(fil0, w);
        fprintf(fil0,'\n');
        while (k<cant+1)
            qj=cell2mat(ac(k));
            if
(numel(d)>10&&d(7)==qj(1)&&d(8)==qj(2)&&d(9)==qj(3)&&d(10)==qj(4)&&d(11)=
=qj(5))
                di=d(14:22);
                fprintf(fil0,qi);
                fprintf(fil0,'\t');
                fprintf(fil0,qj);
                fprintf(fil0,'\t');
                fprintf(fil0,di);
                fprintf(fil0,'\n');
                qi;
                qj;
                l=l+1;
                k=k+1;
            end
            d = fgetl(fid);
            if (k>1&&numel(d)<1)
                while (k<cant+1)
                    qj=cell2mat(ac(k));
                    fprintf(fil0,qi);
                    fprintf(fil0,'\t');
                    fprintf(fil0,qj);
                    fprintf(fil0,'\t');
                    fprintf(fil0,'0.000E+00');
                    fprintf(fil0,'\n');
                    k=k+1;
                end

                k=cant+1;

            end
        end
        i=i+1;
        if (i==can+1)
            i=1;
        end
    end
    d = fgetl(fid);
    status = feof(fid);
end
```